Rif1 maintains telomeres and mediates DNA repair with its N-terminal alpha-helical repeat

Inauguraldissertation

zur
Erlangung der Würde eines Doktors der Philosophie
vorgelegt der
Philosophisch-Naturwissenschaftlichen Fakultät
der Universität Basel
von

Julia Katrin Reinert

aus Deutschland

Basel, 2018

Genehmigt von der Philosophisch-Naturwissenschaftlichen Fakultät

auf Antrag von

Prof. Dr. Susan M. Gasser
Dr. Nicolas H. Thomä
Prof. Dr. Wei Yang

Basel, den 14. November 2017

_____

Dekan
Prof. Dr. Martin Spiess

Summary

Rif1 plays a central role in genome maintenance ranging from telomere length regulation in budding yeast, to DNA double-strand break (DSB) repair pathway choice in mammals, and replication timing regulation in both organisms. In yeast, Rif1 controls telomere length by inhibiting telomerase and checkpoint signaling at chromosome ends. In mammals, RIF1 has emerged as a critical regulator of genome stability, mediating DSB repair pathway choice by attenuating DNA end resection. RIF1 thereby inhibits homologous recombination and promotes non-homologous end joining (NHEJ). In contrast, the involvement of Rif1 at DSBs in budding yeast remains controversial. The N-terminal domain (NTD) is the most conserved and largest folded domain within Rif1 and is predicted to form an alpha-helical repeat. Although Rif1 has been studied extensively, our molecular understanding remains limited, and it is puzzling how an alpha-helical repeat may fulfill such a wide range of functions. In my Ph.D. research, I examined the Rif1-NTD in budding yeast and human using structural, biochemical, and biophysical approaches to shed light on their structure and function at the molecular level and to characterize their interactions with binding partners.

In the first part of my doctoral studies (Chapter 2), we determined the crystal structure of the conserved 125 kDa budding yeast Rif1-NTD. Our structure revealed an extended architecture spanning 238 Å in length that consists of an irregular alpha-helical repeat. Using biochemical approaches, we identified Rif1-NTD as a high-affinity DNA-binding protein and determined the co-crystal structure of Rif1-NTD in complex with dsDNA. The co-crystal structure shows that a 16 bp DNA footprint is encased by the Rif1-NTD concave surface and that Rif1-NTD forms a figure-8-shaped head-to-tail dimer in the presence of DNA. This arrangement was confirmed by negative stain electron microscopy. Site-directed mutagenesis at the Rif1 DNA-binding interface reduced the binding affinity *in vitro*. *In vivo*, tight DNA association proved essential for checkpoint control and telomere length regulation. Surprisingly, Rif1-NTD also bound to uncapped telomeres and DSBs, thereby inhibiting end resection and promoting NHEJ in budding yeast. Decreasing the DNA binding affinity caused a loss of function phenotype for the inhibition of resection and DSB repair pathway choice. Thus, the direct association of the Rif1-NTD with DNA is required for DSB repair pathway choice in budding yeast. This finding demonstrates that the role of Rif1 in DSB repair pathway choice is conserved from yeast to human and provides first insights into the function of the Rif1-NTD at the molecular level.

In the second part of my doctoral studies (Chapter 3), we turned our attention to the human RIF1-NTD. While localization to DSBs is mediated by the direct interaction with DNA in budding yeast,

human RIF1 recruitment to DSBs is strictly dependent on phosphorylated 53BP1. When recruitment of RIF1 is hampered, DSBs are not protected from resection and NHEJ cannot occur. However, it remained elusive whether RIF1 and 53BP1 interact directly or whether they require a mediator protein that may be able to distinguish between the different 53BP1 phospho-states. Unexpectedly, we found that the 53BP1-Rif1 interaction is direct, that it is mediated by the RIF1-NTD, and that complex formation is strictly dependent on a phosphorylated 53BP1 motif. This finding is remarkable because RIF1-NTD is an alpha-helical repeat and does not contain a domain known for phospho-specific interactions. Our biophysical data dissect RIF1 recruitment to 53BP1 at the molecular level and will inform future structural and functional characterization of the 53BP1-RIF1 complex, which is required to block DNA end resection and trigger NHEJ.

In summary, we have shown that the Rif1-NTD forms an elongated alpha-helical repeat and that Rif1-NTD maintains telomeres and mediates DSB repair pathway choice in budding yeast. Rif1-NTD accomplishes these functions through its direct interaction with DNA thereby blocking DNA end resection. In human, RIF1-NTD also blocks DNA end resection, and we have shown that RIF1-NTD directly interacts with 53BP1 in a phosphorylation dependent manner. Although Rif1 uses different mechanisms across species, Rif1 blocks DNA end resection in budding yeast and human – a conserved function mediated by its N-terminal alpha-helical repeat.

Table of Contents

Thesis Overview

This thesis consists of five chapters. Collaborations are listed at the beginning of each chapter, if applicable. This Ph.D. thesis is based on of published and unpublished work. The work presented in this thesis was performed at the Friedrich Miescher Institute for Biomedical Research, Basel, Switzerland, under the supervision of Dr. Nicolas H. Thomä.

- Chapter 1 is an introduction to telomere protection and DNA double-strand break repair pathway choice with a particular focus on Rif1 in yeast and human.
- Chapter 2 and 3 are experimental chapters.
- Chapter 2 investigates the role of budding yeast Rif1 N-terminal domain in telomere protection and DNA double-strand break pathway choice. It contains published and additional unpublished data based on the manuscript:

Mattarocci, S.*, Reinert, J.K.*, Bunker, R.D.*, Fontana, G.A.*, Shi, T., Klein, D., Cavadini, S., Faty, M., Shyian, M., Hafner, L., Shore D., Thomä N.H., Rass U. (2017). Rif1 maintains telomeres and mediates DNA repair by encasing DNA ends. Nat Struct Mol Biol *24*, 588-595. (*equal contribution)

- Chapter 3 examines the interaction between human RIF1 N-terminal domain and 53BP1. This chapter is unpublished.
- Chapter 4 comprises the materials and methods for Chapter 2 and 3
- Chapter 5 is a discussion of the structural and biochemical findings described in chapter 2 and 3. It integrates the findings into our current understanding of yeast telomere protection and DNA double-strand break repair.
- All references, the list of abbreviations, the acknowledgments, and my curriculum vitae can be found after chapter 5.
- The Appendix contains the published manuscript listed above.

1 INTRODUCTION

1.1 Protection of DNA ends – Telomeres and DNA double-strand breaks

1.1.1 DNA ends occur as telomeres and after DNA double-strand breaks

The eukaryotic genome is made up of chromosomes (3 in *Schizosaccharomyces pombe* (*S.pombe*), 16 in *Saccharomyces cerevisiae* (*S.cerevisiae*) and 23 in human (*Homo sapiens*)) that store the genetic information. Maintaining genomic integrity is a key task to ensure that the genetic information is present in all cells and that it is accurately passaged to the next generations. Chromosomal ends are comprised of DNA repeat sequences (TG_{1-3} in *S.cerevisiae*, T_2AG_3 in *S.pombe* and human) and form 3D-fold back structures (de Bruin et al., 2000; de Bruin et al., 2001; Griffith et al., 1999; Strahl-Bolsinger et al., 1997). Chromosome ends - also called telomeres - are not just distinct because of their repetitive sequence but they are packaged into a protein meshwork, making the DNA sequence and particularly the DNA end inaccessible to other proteins.

DNA damage can be caused by a variety of endogenous and exogenous sources. Endogenous sources can be by-products of the cells own metabolism causing oxidations, deaminations, or alkylations of the DNA as well as replication errors (Iyama and Wilson, 2013). Exogenous sources can be environmental exposure to ionizing radiation (IR), other chemical agents, or ultraviolet light (UV) (Jackson and Bartek, 2009). It is estimated that each eukaryotic cell faces tens of thousands of lesions per day, out of which the vast majority are single-strand lesions ranging from base lesions, intra-strand crosslinks, DNA-protein crosslinks and single-strand breaks. Additionally, double-strand breaks (DSBs) and inter-strand crosslinks occur less frequently (Hoeijmakers, 2009; Lindahl, 1993; Lindahl and Barnes, 2000). However, both strands of the DNA double-helix break in a DSB and they are thought to be the most dangerous to the cell because they pose an immediate risk to genome integrity. DSBs can be caused pathologically when the double-helix is broken by an exogenous source such as IR (Ward, 1988), when at least two single-strand breaks occur in close proximity, or when the DNA replication machinery meets a single-strand break (Jackson and Bartek, 2009). So even if there is no exogenous threat to the genome, spontaneous DSBs can be generated during replication of the genome (Syeda et al., 2014). It is estimated that there is about is about one spontaneous DSB per replicated 10^8 base pairs (bp) in budding yeast (Mehta and Haber, 2014). This number is a lot higher, if cells are exposed to exogenous threats. In addition to pathologic DSBs, metazoan cells can also undergo programmed DSBs in meiosis ensuring the correct chromosome

segregation in the first meiotic division, and at immunoglobulin genes ensuring receptor diversity and antibody class-switching. Particularly the DSBs induced for immunoglobulin class-switch recombination (CSR) rely on the same DSB repair machinery as the pathological DSBs do (Chapman et al., 2012; Dudley et al., 2005).

Taken together, DNA ends occur as telomeres at the end of chromosomes or arise after DSBs. Even though they resemble each other, they have to be handled in a completely different manner – the former being covered by a natural meshwork for protection while the latter require repair.

1.1.2 DNA double-strand break repair in yeast and human

1.1.2.1 There are two main pathways of DNA double-strand repair

The first insight into how DSBs can be repaired was the observation that an induced DSB on a plasmid containing a budding yeast sequences leads to a homologous recombination (HR) with the budding yeast genome (Orr-Weaver et al., 1981). The authors transformed budding yeast with genes on a circular or linear plasmid and found that the linear fragments are far more recombinogenic than the circular ones. This would point towards the idea that DSBs are repaired by copying the homologous sequence in the genome. However, an analogous experiment performed by DNA microinjection of the rabbit beta-globin gene into mouse oocytes did not lead to the same result. Rabbit beta-globin was neither integrated into the beta-globin gene nor was it expressed in erythroid cells but it was integrated at abnormal chromosomal positions (Lacy et al., 1983). This experiment was the first indication, in contrast to what was previously reported in yeast, that a non-homologous integration takes place in mammalian cells. More direct evidence confirmed the initial observation that transfected linear DNA fragments are integrated into the genome but do not integrate into the homologous locus of the genome, and the authors speculated that there is a non-homologous end-to-end-joining mechanism (Wake et al., 1984). Today it is clear that DSBs can be repaired by two major pathways: non-homologous end-joining pathway (NHEJ), or homologous recombination (HR) (Daley and Sung, 2014). Eukaryotic cells possess two main pathways to repair DSBs, which could indicate that they evolved in parallel to ensure reliable repair of DSBs, even if one pathway becomes compromised. Eukaryotic cells can commit to one or the other pathway to repair a DSB lesion, a process that depends on the extent of resection, the phase of cell cycle, and the organism itself. In fact, pathway preference significantly differs between yeast and human. While 80% of DSBs are repaired by NHEJ in mammalian cells based on ionizing radiation-induced breaks and enzymatically induced DSBs experiments (Beucher et al., 2009; Shahar et al., 2012), most DSBs in budding yeast are repaired by HR (Aylon and Kupiec, 2003).

Moreover, it is only partially clear how the pathway choice is made and how this process differs between yeast and human.

1.1.2.2 DNA double-strand break repair in budding yeast

Genome integrity is achieved by immediate repair of DSBs in budding yeast. DSBs are readily detected and trigger the DNA Damage Response (DDR). The DDR is a signaling and genome-maintenance network, which recruits mediators and activates effectors (Jackson and Bartek, 2009). A major component of the DDR is the checkpoint response. Checkpoints were originally described as a signaling network ensuring that the cell-cycle proceeds in a sequential manner having each step completed before starting the next (Hartwell and Weinert, 1989). DSBs activate the checkpoint, arrest the cell cycle, and trigger the repair of the break (Harrison and Haber, 2006) The central checkpoint kinases are Mec1 and Tel1 in bussing yeast (ATR and ATM in human)(Harrison and Haber, 2006). Weinert and Hartwell provided the first line of evidence that irradiated budding yeast cells are arrested prior to mitosis, identifying Radiation sensitive 9 (Rad9) as one gene necessary for DNA damage-induced arrest (Weinert and Hartwell, 1988). This indicates that it is not the DSB itself, which causes the cell cycle to stop but the signaling cascade triggered upon damage. Later it was shown that a single unrepaired DSBs is enough to cause a cell cycle arrest in budding yeast (Sandell and Zakian, 1993). It is estimated that 90% of DSBs are channeled into HR in budding yeast (Paques and Haber, 1999). After a DSB in budding yeast, the heterodimer yKu70/80 detects the DNA ends of the DSB and slows down end resection of the DSB (see Table 1.1 for DSB repair protein overview in yeast and human) (Lee et al., 1998). The key three HR processing machineries, which resect the DSB to generate a 3' overhang are (1) the nuclease complex MRX (Mre11-Rad50-Xrs2, MRN in human), which acts together with Sae2 (homologue of CtIP in human), (2) the exonuclease Exo1, and (3) the helicase exonuclease Sgs1-Rmi1-Top3-Dna2 (Cannavo and Cejka, 2014; Garcia et al., 2011; Lengsfeld et al., 2007; Mimitou and Symington, 2008; Williams et al., 2009; Zhu et al., 2000; Zhu et al., 2008). MRX-Sae2 (1) perform the first short-range resection of DSB. Exo1 and Sgs1-Rmi1-Top3-Dna2 (2 and 3) act in sync to carry out subsequent the long-range resection over kilobases. The short range resected 3'tail of ssDNA is readily bound and protected by RPA (Zou and Elledge, 2003). The RPA coat is bound by the Mec1-Ddc2 complex (ATR-ATRIP in human) and activates the G2/M checkpoint (Paciotti et al., 2000; Rouse and Jackson, 2002). Once MRX localizes to the DSB via its interaction with RPA, MRX and Cohesin tether the DNA ends together for repair (Lisby et al., 2004; Seeber et al., 2016; Uhlmann et al., 1999). These machineries resect the DSB to prepare it for the search of a homologous DNA sequence. If Sae2, Sgs1, and Exo1 are deleted, the formation of ssDNA upon the induction of a DSB is no longer detectable (Mimitou and Symington, 2008). Mec1 phosphorylates histone tail H2A on serine 129 (gamma-H2A), which is a mark for DSBs.

Rad9 (often considered to be the homolog of 53BP1) localizes to gamma-H2A and acts as a mediator to allow Mec1 to further phosphorylate downstream kinases, Rad53 (CHK2 in human) and Chk1 (Sanchez et al., 1999; Sun et al., 1998; Usui et al., 2009). The signal is further amplified so that the cell arrests with an anaphase block in the cell cycle (Harrison and Haber, 2006). Rad51 replaces RPA and assembles a nucleoprotein filament around the ssDNA. This process starts the Rad51-mediated homology search with a sister chromatid, with a homologous chromosome or an ectopic site strand. Having found a homologous region, strand invasion, initiation of new DNA synthesis and completion of repair resolve the DSB by HR (Haber, 2016).

Around 10% of DSBs are repaired by NHEJ in budding yeast (Valencia et al., 2001). Classical (or canonical) NHEJ (c-NHEJ) is a direct ligation of the two blunt DNA ends independently of sequence homology. C-NHEJ *per se* is not an error-prone process assuming the DNA ends do not need to be processed. The model for c-NHEJ in budding yeast best understood is an endonuclease-induced DSB in the mating-type (MAT) locus. In most cases, the DSB is repaired by HR using one of the two silent donors of mating-type information HML or HMR, an ectopic site. However, in yeast strains impaired in HR by the deletion of a key factor such as Rad51 or by the deletion of the HML and HMR homology regions, DSBs are repaired by NHEJ (Kramer et al., 1994; Moore and Haber, 1996). The key proteins required for NHEJ in budding yeast are yKu70/80, Dnl4-Lif1, XRCC4-like Lif1, the MRX complex and Nej1 (see Table 1.1 for DSB repair protein overview in yeast and human) (Kegel et al., 2001; Moore and Haber, 1996; Valencia et al., 2001). After the DSB has occurred yKu70/80 detects the DSB and is loaded on top of the DSB using its ring-like structure. In doing so, the resection of the DSB is inhibited in order to prevent the generation of ssDNA stretches (Clerici et al., 2008; Mimitou and Symington, 2010). If yKu70/80 is deleted, budding yeast cells with a deletion of the homologous HMR/HML loci cannot survive an induced DSB in the MAT locus (Boulton and Jackson, 1996; Mages et al., 1996; Siede et al., 1996). Even though yKu70/80 is not an essential gene in budding yeast, it is the core factor of NHEJ and recruits the other NHEJ factors Dnl4-Lif1, and Nej1 to the DSB site. The ATP-dependent ligase Dnl4 (LIG4 in human) is one of three DNA ligases in budding yeast, it strongly associates with Lif1 and is strictly required for NHEJ break ligation (Herrmann et al., 1998; Wilson et al., 1997). Apart from ligation of the DSB, Dnl4-Lif1 stabilizes the assembly of the repair complex consisting of Dnl4-Lif, yKu70/80 and Nej1 and helps yKu70/80 to block resection (Zhang et al., 2007). After yKu70/80 binding, MRX also localizes to the DSB and it is required for NHEJ in budding yeast, albeit the mechanism of action of MRX in NHEJ is not entirely clear.

	S.cerevisiae	*Human*	*Function*
Pathway choice regulators	gamma-H2A	gamma-H2AX	Phosphorylated histone H2A or H2AX variant, chromatin mark formed by DSB signaling
	-	MDC1	Reads gamma-H2AX chromatin mark, promotes RNF8 ubiquitylation activity
	-	RNF8	E3 ubiquitin ligase, ubiquitylates for example histone 1 linker
	-	RNF168	E3 ubiquitin ligase, ubiquitylates for example H2AK15ub
	-	53BP1	Adaptor protein, promotes NHEJ
	Rif1? (functional conservation remains to be shown)	RIF1	Co-localizes with 53BP1, blocks resection, promotes NHEJ
	-	PTIP	Co-localizes with 53BP1 and helps to block resection
	-	BRCA1	Competes with 53BP1, promotes HR
DSB detection	yKu70/80	KU70/80	DSB recognition
	Mre11-Rad50-Xrs2 (MRX)	MRE11-RAD50-NBS1	DSB recognition, protein recruitment, and initial resection
Effector kinases	Mec1	ATR	Recruited to various lesions including RPA coated ssDNA
	Tel1	ATM	Recruited by NBS1 to DSBs
	-	DNA-PKcs	Recruited by Ku80 to DSBs
DSB processing for HR	Mre11-Rad50-Xrs2 (MRX)	MRE11-RAD50-NBS1	DSB recognition, protein recruitment, and initial resection
	Sae2	CtIP	Support resection
	Exo1	EXO1	Long range resection of DSBs
	Sgs1	BLM	Long range resection of DSBs
	Dna2	DNA2	Resection of DSBs
HR specific proteins	Rad51	RAD51	Strand invasion of homologous duplex
	RPA	RPA	Coating ssDNA
	Rad9	RAD9	Cell cycle checkpoint control protein
	-	BRCA2	Regulate homologous repair
	-	PALB2	Works together with BRCA2
NHEJ specific proteins	Dnl4 (Lig4)	DNA Ligase IV (LIG4)	DNA-ligase
	Nej1	XLF	Scaffolding protein
	Lif1	XRCC4	Scaffolding protein
		Artemis	DNA end processing in NHEJ in humans

Table 1.1 – DSB proteins in budding yeast and human. Partially adapted from (Chapman et al., 2012) and extended

It is thought that MRX bridges the two DNA ends and tethers them together to facilitate ligation and stimulates the Dnl4-Lif1 ligation activity (Chen et al., 2001). *In vitro,* NHEJ has been shown to be possible in the absence of MRX as shown by the DNA end bridging structure of Dnl4-Lif1 (Grob et al., 2012). However, the absence of MRX subunits causes a striking decrease in NHEJ (Moore and Haber, 1996). After (1) DSB detection and blocking of the resection by yKu70/80, the next steps of NHEJ are (2) strand annealing, for which the whole NHEJ complex (Dnl4, Lif1, and Nej1) has to assemble and (3) ligation catalyzed by Dnl4 (Kegel et al., 2001; Teo and Jackson, 2000; Wilson et al., 1997). In addition to c-NHEJ, there are other end-joining pathways, called alternative NHEJ (alt-NHEJ), which generally occurs when there is no sister chromatid available and repair by HR is not an option. Alt-NHEJ pathways are less well defined and more error-prone than c-NHEJ. One of these mechanisms is microhomology-mediated end-joining (MMEJ) and it causes deletions of 5-20 bp over the repaired site, illustrating its mutagenic potential (Emerson and Bertuch, 2016).

1.1.2.3 DNA double-strand break repair in human cells

In contrast to budding yeast, it is estimated that more than 80% of irradiation-induced DSBs in human cells are repaired by NHEJ, and only a minority is repaired by HR in unsynchronized cells (Beucher et al., 2009). Despite this striking difference in pathway choice, the key players of HR and NHEJ are homologous and function in a similar way. In HR, the heterodimer Ku70/80 binds to the DSB within one second and the Mre11-Rad50-Nbs1 (MRN) complex is loaded within 30 seconds after the DSB introduction (see Table 1.1 for DSB repair protein overview in yeast and human) (Hartlerode et al., 2015). It is clear that Ku70/80 and MRN bind DSBs independently; it is, however, unclear whether they can bind to a DSB at the same time. *In vitro* data argues that MRN alone cannot outcompete Ku 70/80 from as DSB (Sun et al., 2012). The NBS1 protein of the MRN complex associates and activates the key DSB effector kinase ATM (Tel1 in budding yeast). MRN associates at the break with CtIP (Sae2 in budding yeast) and CtIP stimulates the nuclease activity of MRN to bi-directionally resect the DSB over a short range (Anand et al., 2016; Huertas and Jackson, 2009; Sartori et al., 2007). A key regulator of effective resection in mammalian cells is BRCA1. BRCA1 interacts with CtIP and together with MRN forms a complex (Chen et al., 2008a; Sartori et al., 2007). When BRCA1 is missing, mammalian cells repair more of their DSBs via NHEJ (Huen et al., 2010; Sartori et al., 2007). In order to resect the DSB over a long range, the combined action of MRN, CtIP, EXO1 and BLM (Sgs1 in budding yeast) is required (Chen et al., 2008a; Gravel et al., 2008; Nimonkar et al., 2008). Single-stranded 3' overhang DNA is first bound by RPA, which is subsequently replaced by RAD51 in order to form the nucleoprotein filament, analogously to what is observed in budding yeast. The recombinase activity to search for the homologous sister chromatid in human is assisted

by BRCA1, PALB2, and BRCA2 (Park et al., 2014; Roy et al., 2011). When homology search, strand invasion, and DNA synthesis occurred, DSB repair by HR is completed.

In contrast to HR, NHEJ is a template and homology-independent process. It was previously thought that it is an error-prone process, but NHEJ is mostly error-free as recent studies show (Betermier et al., 2014). The error rate depends on the nature of the DSB rather than the NHEJ machinery itself (Betermier et al., 2014). Analogously to budding yeast, mammalian cells have the well-investigated classical-NHEJ (or canonical) pathway, which proceeds through the following steps: (1) DSB recognition followed by recruitment of the NHEJ complex; (2) Bridging of the DNA ends; (3) DNA end processing by Artemis, if necessary; and (4) Ligation of the broken ends (Davis and Chen, 2013). DSBs are detected by the KU70/80 heterodimer and a member of the phosphatidylinositol-kinase–related kinase (PIKK) family - the DNA dependent protein kinase catalytic subunit (DNA-PKcs). Upon DNA binding, the KU70/80 heterodimer changes conformation supplying it with a much higher affinity to DNA-PKcs compared to the DNA unbound state (Lieber, 2010). DNA-PKcs contains a catalytic kinase subunit and heavily phosphorylates itself and other c-NHEJ protein targets upon recruitment (Chiruvella et al., 2013). Ku70/80 also triggers the recruitment of the other members of the NHEJ complex are recruited: the ligase complex consisting of DNA Ligase IV (LIG4), X-ray cross-complementing protein 4 (XRCC4), XRCC4-like factor (XLF) (DNA ligase IV-XRCC-XLF), and Aprataxin-and-PNK-like factor (APLF) as well as a recently identified stabilizing factor PAXX (Ochi et al., 2015).

After the detection of the break by KU70/80 and the recruitment of DNA-PKcs, the NHEJ complex (DNA ligase IV-XRCC-XLF-APLF- PAXX) is assembled so that all members of the complex stabilize each other by multiple protein-protein interactions. KU70/80 and DNA-PKcs are building the center of the complex encircling and tethering the DNA ends (Graham et al.). If necessary, Artemis is recruited by DNA-PKcs and cleaves off potentially overhanging DNA nucleotides with its nuclease activity. Stabilized and stimulated by XRCC and XLF, LIG4 ligates both strands of the DNA molecules, so that the DSB is resolved (Lieber, 2010).

1.1.2.4 DNA double-strand break repair pathway choice in mammalian cells

DSB pathway choice is a complex process in mammalian cells and it is dictated by many factors: stage in the cell cycle, the surrounding chromatin context, and the extent of resection. Even though this has been a field of extensive research, it is still not clear how one pathway is promoted over the other on a molecular level. The key difference between c-NHEJ and HR is that c-NHEJ requires the ends to be blunt ends, whereas HR needs 3` overhangs to perform homology search. Thus, it is thought that the initiation or blocking of resection is the decisive step in mammalian DSB pathway

choice. If the DSB is resected by the MRN complex and CtIP (around 20bp) to a small extent and then extensively resected over kilobases by helicases and exonucleases (DNA2, BLM, EXO1, WRN, and CtIP), the DSB is committed to repair by HR (Huertas and Jackson, 2009; Sturzenegger et al., 2014). Therefore, the regulation of end resection seems to be the critical trigger to favor one pathway over the other.

DNA end resection is promoted by CDK activity and thus favored in late S/G2-phase compared to G1 (Jazayeri et al., 2006). It was first observed in budding yeast that decreased 'DNA end stability' favors HR over NHEJ (Frank-Vaillant and Marcand, 2002). DNA end resection requires Cdk1 activity in budding yeast (Aylon et al., 2004; Ira et al., 2004). When Cdk1 activity is perturbed in G2 arrested cells, no resection of DSBs can be detected in budding yeast (Ira et al. 2004). CDK1 activity increases with the entry into S-phase of the cell cycle, during which CDK1 phosphorylates CtIP on residue Thr847, which in turn is crucial for its resection activity (Huertas and Jackson, 2009). CDK1 also phosphorylates EXO1 and NBS1 and thus increases their end processing activity (Falck et al., 2012; Tomimatsu et al., 2014; Wohlbold et al., 2012). If EXO1 phosphorylation is impaired, resection and HR is reduced, whereas NHEJ is increased upon damage (Tomimatsu et al., 2014). Other factors in the machinery were also shown to be phosphorylated in a CDK dependent manner including, CTIP (Sae2 in yeast) and DNA2 (Huertas and Jackson, 2009; Ira et al., 2004). Additionally, other post-translational modifications of Sae2, Mre11, Sgs1 or Exo1 were also shown to promote (sumoylation) or inhibit (acetylation) end resection in budding yeast (Robert et al., 2011; Sarangi et al., 2015). Taken together, the cell cycle and the activity of CDKs influence DSB pathway choice by promoting resection through a range of post-translationally modified players. In doing so, the players are silenced or activated in different stages of the cell cycle.

Cell cycle dependent promotion of resection is one aspect of the DSB repair pathway choice. Additionally, mammalian cells evolved more mechanisms to tightly control pathway choice. DSB repair pathway choice also involves mechanisms upstream of resection and there are many players involved in mammalian cells. A DSB is readily detected by KU70/80 and/or the MRN complex (analogously to yeast) and they recruit DNA-PKcs or ATM, respectively. DNA-PKcs, ATM, and ATR are the three members of the phosphatidylinositol 3-kinase (PI3K)-related kinases (DNA-PK) that share a very similar architecture. DNA-PK proteins all contain an N-terminal HEAT repeat (see also 1.2), a C-terminal kinase domain, and a FAT region (FRAP-ATM-TRRAP domain) folding around the kinase domain (Blackford and Jackson, 2017). While ATR is activated in response to a wide range of DNA damage types, including single-strand lesions and replication fork lesions, ATM and DNA-PKcs are activated upon DSBs. ATM and DNA-PKcs shape the outcome of a break significantly because they are recruiting different factors to repair the break. DSBs detected by KU70/80-DNA-PKcs are

committed to NHEJ. In contrast, DSBs detected by the MRN-ATM can be repaired by NHEJ or HR depending on the activity of the downstream targets and the state in the cell cycle. This poses an as of yet unresolved question of what distinguishes breaks repaired via the activity of DNA-PKcs or ATM. It has been shown that ATM is not required for the resolution of most irradiation induced DSBs, but is required for repair of DSBs located in heterochromatin (Beucher et al., 2009; Goodarzi et al., 2008). It has been suggested that DNA-PKcs and ATM fulfill complementary and non-overlapping functions in DSB repair because DSBs cluster within DSB repair foci in the nucleus, which is a process dependent on ATM (Caron et al., 2015). Additionally, ATM inhibition was reported to cause more inaccurate repair outcomes, which implies that ATM is crucial for correct DSB repair at some DSBs (Caron et al., 2015). This suggests that they act in different chromatin contexts and different nuclear locations. Thus, DSB repair pathway choice could be not just dependent on the state in the cell cycle but also on the nature and local environment of the DSB.

When DSBs are detected by the MRN complex, Nbs1 recruits ATM in an analogous manner as KU80 recruits DNA-PKcs (Falck et al., 2005). In G2-phase and the end of S-phase, ATM triggers a cascade activating BRCA1 and CtIP in order to start the resection of the DSB (Schlegel et al., 2006; Yun and Hiom, 2009). In G1-phase and the beginning of S-phase, ATM phosphorylates the histone variant H2AX on Ser139 (gamma-H2AX) and gamma-irradiation causes spreading of this histone mark over megabases away from the DSB (Figure 1.1) (Lukas et al., 2011; Rogakou et al., 1998). The gamma-H2AX chromatin mark links the DSB with the repair machinery through multiple signaling proteins (see Table 1.1 for DSB repair protein overview in yeast and human). The key sensor of the gamma-H2AX mark is a mediator of DNA damage checkpoint protein1 (MDC1). MDC1 transiently tethers ATM to the locus and helps together with the MRN complex to phosphorylate more H2AX variants to spread the histone mark (Polo and Jackson, 2011; Stucki et al., 2005). MDC1 is also phosphorylated by ATM on its TQxF motifs, which recruits the E3 ubiquitin ligase RNF8 (Huen et al., 2007; Kolas et al., 2007). Together with UBC13, RNF8 ubiquitylates the histone linker H1, which promotes the recruitment of another E3 ubiquitin ligase RN168 by reading out the RNF8 ubiquitin mark (Doil et al., 2009; Thorslund et al., 2015). RNF168 catalyzes the ubiquitylation of histone H2A at lysine position 15 (H2AK15ub), which is in turn read out specifically by p53 binding protein 1 (53BP1). H2AK15ub is one of the histone marks that serves as a landing platform for 53BP1 (Figure 1.1) (Fradet-Turcotte et al., 2013). The other chromatin mark required for 53BP1 binding is the

Figure 1.1

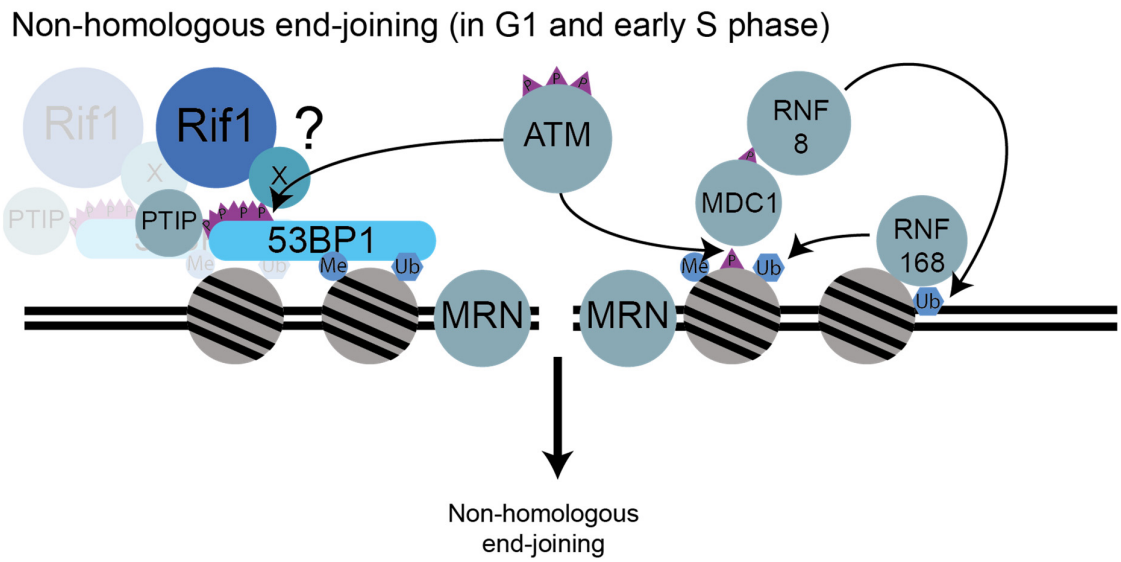

Figure 1 - Cartoon representation of DSB detection and blocking of DNA end-resection in mammalian cells. Signaling cascade detecting the DSB is depicted on the right side. The MRN complex detects the DSB, NBS1 recruits and activates the ATM effector kinase. ATM phosphorylates Ser139 on the histone variant H2AX, a recruitment mark for MDC1. MDC1 also gets phosphorylated by ATM and recruits the E3 ubiquitin ligase RNF8, through phosphorylation. RNF8 ubiquitylates the histone linker H1 and thereby recruits the E3 ubiquitin ligase RNF168. RNF168 ubiquitylates H2AK15, the chromatin mark 53BP1 specifically binds to. Once 53BP1 localizes to H2AK15ub and H4K20me2 chromatin marks, RIF1 co-localizes with 53BP1 and attenuates DNA end-resection (adapted and changed from Blackford et al.,2017 and Hustedt and Durocher, 2016).

more constitutively present H4K20me2 (Botuyan et al., 2006). The H4K20me2 modification is highly abundant throughout the genome (Schotta et al., 2008). H4K20me2 has also been implicated as a chromatin compaction mark and no increase in the modification could be detected upon DNA damage induction in fibroblasts (Hartlerode et al., 2012; Lu et al., 2008; Pesavento et al., 2008).

In contrast, the H2K15ub mark is specifically laid down upon DNA damage via the RNF8 dependent recruitment of the RNF168 E3 ubiquitin ligase while the binding to the H4K20me2 is regulated via a competition with other binding partners. It has been suggested that H4K20me2 becomes selectively accessible for 53BP1 around DSBs by competing with L3MBTL1 and JMJD2A (Acs et al., 2011; Mallette et al., 2012). Additionally, the TIRR complex was shown to regulate the action of 53BP1 by binding to its tandem-Tudor domain (Tudor). TIRR renders 53BP1 inactive when there is no DNA damage (Drane et al., 2017). When the two histone modifications are present and accessible, 53BP1 is recruited and serves as a recruitment platform for downstream effectors. Rap1-interacting factor 1 (RIF1) has been identified as the key downstream effector of 53BP1 (Di Virgilio et al., 2013; Escribano-Diaz et al., 2013; Feng et al., 2013; Zimmermann et al., 2013). When RIF1, and particularly its N-terminal helical repeat, is deleted, RIF1 cannot co-localize with 53BP1 and NHEJ cannot be completed. The 53BP1 binding mode to the H2AK15ub and H4K20me2 modified

nucleosome has recently been structurally analyzed while the structure of the RIF1 N-terminal domain remains elusive (Wilson et al., 2016).

1.1.3 Telomeres in yeast and human

1.1.3.1 Telomeric sequence

Most eukaryotes have evolved very similar mechanisms to protect the chromosome ends in order not to be mistaken as a DSBs. Telomeres were first functionally described by Hermann Muller and Barbara McClintock working in fruit flies and maize, respectively. Both found that telomeres are specially protected from rearrangements compared to the rest of the genome when exposed to X-rays (McClintock, 1931; Muller, 1938). Muller named the ends of chromosomes "telomeres" based on ancient Greek for "telos" meaning "end" and meros meaning "part". Forty years later, Blackburn elucidated that the DNA sequence of telomeres in the ciliated protozoan *Tetrahymena thermophile* is formed by a repetitive motif TTGGGG (Blackburn and Gall, 1978) and together with Szostak she showed that a linear DNA fragment flanked by repeats of this motif is sufficient to stabilize the DNA fragment within *S.cerevisiae* (Szostak and Blackburn, 1982). Albeit budding yeast and *Tetrahymena* thermophile both harbor a repetitive G-rich repeat at their telomeres, the type of repeat differs: The *S. cerevisiae* telomere is formed by an irregular $TG_{1\text{-}3}$ repeat whereas the *Tetrahymena* thermophile telomere is formed by a regular TTGGGG. This means that over a wide range of organisms G-rich repeats are employed to mark chromosomal ends (Zakian, 1989). In fact, most eukaryotes have regular G-rich repeats at their telomeres. Exceptions from the genera *Candida*, *Drosophila melanogaster* and potentially other flies (Biessmann and Mason, 1994). Interestingly, budding yeast also forms an exception because while keeping the G-rich nature of telomere, it forms an irregular repeat having uneven repetitions of TG, TGG, and TGGG motifs compared to a simple repetition of a six nucleotide motif (TTGGGG in holotrichous ciliates, TTAGG in many insects, TTAGGG in vertebrates, and TTTAGGG in flowering plants) (Biessmann and Mason, 1994; Zakian, 1989). Taken together, most eukaryotes have a G-rich sequence at the end of their chromosomes, which usually is comprised of a regular six-nucleotide repeat sequence. Across most eukaryotes, this repeat sequence is very similar arguing for a slow evolution of how telomeres are maintained across organisms.

1.1.3.2 Telomere end replication in yeast an human

Replication of the genome requires 5'to 3' directional DNA polymerases copying the DNA sequence based on the template strand. This means that the 3' ends of each chromosome shorten after every completed cell cycle and it causes a loss of genetic material. Greider and Blackburn investigated the end replication problem and discovered a reverse transcriptase, telomerase, which adds telomeric

repeats to the 3' ends of each chromosome. Telomerase maintains the original length of the telomere and does not require a chromosomal DNA template (Greider and Blackburn, 1985, 1987). Originally discovered in *Tetrahymena*, telomerase is present in most eukaryotes including yeast and human with the exception of *Drosophila melanogaster,* which uses an alternative mechanism and may have lost telomerase during evolution (Blackburn et al., 2006). In order to preserve the genetic information, retain DNA sequence at the telomere, and not to elongate the telomere artificially, the enzymatic activity of telomerase needs to be tightly regulated. Telomerase is active stochastically in budding yeast, elongating short telomeres more often rather than long telomeres (Chang et al., 2007; Teixeira et al., 2004). It is thought that there is a balance between activating and repressing signals for the activity of telomerase and that the balance is tipped based on the length of the telomere. An activating signal due to a short telomere length is, for example, the phosphorylation of Cdc13 (one of the proteins covering the budding yeast telomere) by Tel1, which recruits telomerase (Bianchi and Shore, 2007).

In human, the resultant loss of telomeric DNA after replication is used as a key tumor suppressive mechanism. Telomerase is only active in continuously dividing cells such as germ cells, stem cells, and many cancer cells whereas all other cell types enter replicative senescence or programmed cell death when telomeres become critically short (Shay and Wright, 2011; Stewart and Weinberg, 2006).

In summary, most eukaryotes solve the end protection problem by an enzyme – telomerase -, which has to be tightly regulated in order to keep the chromosomal ends at its original length.

1.1.3.3 Protecting the telomere end in yeast and human

Telomeres are chromosome ends and resemble a DNA end and thus could be easily mistaken as a DSB. It was already observed in the 80s that linear DNA is unstable in budding yeast cells and quickly recombines with the genome (Orr-Weaver et al., 1981). Thus, telomeres must be protected from the DDR. Using the distinct telomeric repeat sequence as a specific interaction partner, eukaryotes evolved different protein complexes, which protect the telomere in order not to be mistaken as a DSB.

In budding yeast, three different protein complexes contribute to the protective telomere cap: yKu70/80, the Cdc13-Stn1-Ten1 (CST) complex, and the Rap1-Rif1-Rif2 complex (Figure 1.2A). yKu70/80 is telomere-bound, helps to keep telomeres at their native length, and protects telomeres from recombination (Gravel et al., 1998; Polotnianka et al., 1998). The CST complex specifically

Figure 1.2

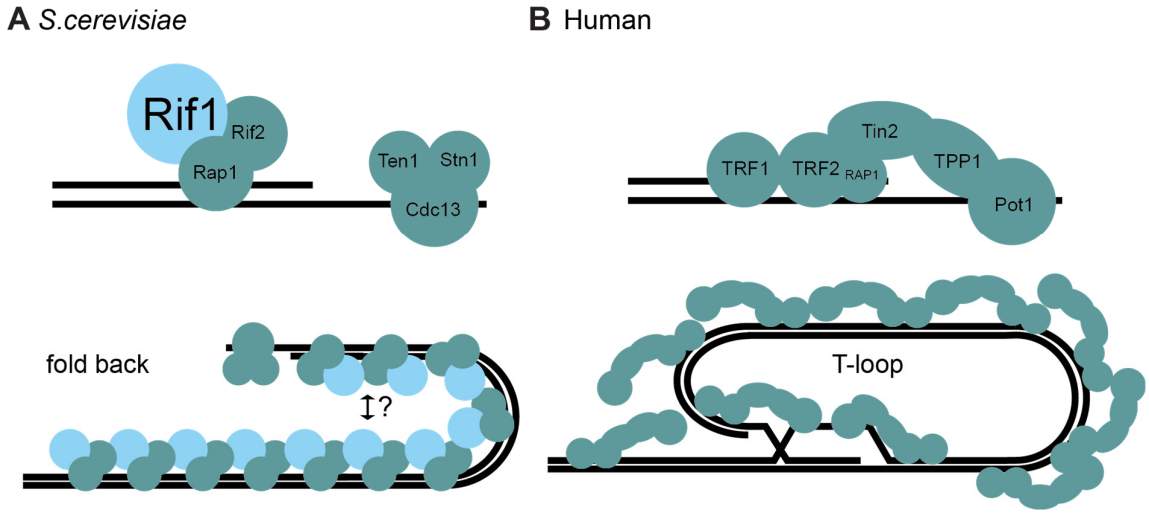

Figure 1.2 – Yeast and human use different protein complexes to protect the telomere. A, Rif1-Rif2-Rap1 cover the dsDNA while Cdc13-Stn1-Ten1 cover the ssDNA portion of the budding yeast telomere. Budding yeast adopts fold-back structures mediated by an uncharacterized protein network. B, Shelterin proteins TRF1, TRF2, TIN2, TPP1, RAP1, and POT1 cover the human telomere and adopt a protective t-loop structure.

binds and protects the single-stranded telomeric 3'-overhang present at the end of telomeres (Grandin et al., 2001; Grandin et al., 1997; Nugent et al., 1996). Temperature sensitive (ts)-lethal mutations in CST component genes lead to G2/M arrest at the non-permissive temperature due to extensive C-strand degradation in the telomeric regions illustrating the protective role of the CST complex (Garvik et al., 1995; Grandin et al., 2001; Grandin et al., 1997). Temperature sensitive (ts)-lethal mutations in CST exemplify a tool to study compromised or uncapped telomeres. Inactivation of Cdc13 causes resection of the telomere, resulting in 3´overhang ssDNA (Garvik et al., 1995). The aberrant ssDNA is readily detected by RPA and Mec1 (ATR in human) and activates the G2/M checkpoint (Hirano and Sugimoto, 2007). Within the Rap1-Rif1-Rif2 complex, Rap1 binds directly to double-stranded DNA (dsDNA) $TG_{1\text{-}3}$ repeat sequences (Konig et al., 1996). Rap1 recruits Rif1 and Rif2 through protein-protein interactions. Together they form a protein meshwork that gives rise to a functional telomeric architecture (Feeser and Wolberger, 2008; Hardy et al., 1992; Shi et al., 2013; Wotton and Shore, 1997).

Rif1 and Rif2 also help to cap the telomere together with the CST complex. Rif1 and Rif2 make specific, independent contributions to capping at telomeres. Rif2 has a prominent role in preventing the association of Tel1 (ATM in human) and the MRX (MRN in human) complex with telomeres. Thus, Rif2 helps to block the consequent resection of telomeric 5'-ends (Bonetti et al., 2010; Hirano et al., 2009) and inhibits NHEJ at telomeres (Marcand et al., 2008). (Role of Rif1 described in more detail in paragraph 1.3)

The Rap1-Rif1-Rif2 complex forms a tightly-bound protein meshwork on the double-stranded TG_{1-3} repeat sequences at telomeres in budding yeast (Shi et al., 2013), where it plays a key role in several central aspects of telomere homeostasis (Wellinger and Zakian, 2012). While Rap1 binds directly to the repeats through its Myb domains (named after the retroviral oncogene v-myb where it was first described), it is thought that Rif1 and Rif2 are recruited there by multiple interactions with the C-terminus of Rap1 (Feeser and Wolberger, 2008; Hardy et al., 1992; Shi et al., 2013; Wotton and Shore, 1997).

Rif1 and Rif2 use the same motif, the Rap1 binding motif (RBM), to directly interact with Rap1. This 3D assembly allowing interlinking between the different Rifs and Rap1 complexes was described as the molecular ”Velcro” model (Shi et al., 2013). The cooperative binding of Rif1, Rif2, and Rap1 coupled to multivalent long- and short-range interactions, which gives rise to functional properties that are more than the sum of their parts. This “Velcro” Rap1-Rif1-Rif2 complex regulates telomere length through an inhibitory effect on the recruitment of telomerase. This inhibition increases with increased TG tract length and results in preferential telomerase action at short telomeres (Bianchi and Shore, 2007; Sabourin et al., 2007; Teixeira et al., 2004). Shortened telomeres display decreased binding of Rap1 and Rif2 proteins (McGee et al., 2010), with a probable reduction of the “Velcro” stabilization. Surprisingly, shortened telomeres do not show a similar decrease in Rif1 binding (McGee et al., 2010; Sabourin et al., 2007). Additionally, budding yeast telomeres are thought to form fold-back structures as an additional layer of telomere protection (de Bruin et al., 2000; de Bruin et al., 2001; Strahl-Bolsinger et al., 1997). However, it is so far unclear which proteins mediate these fold back structures (Figure 1.2A).

Mammals evolved different telomeric repeat binders compared to budding yeast. In mammals, the telomeres are protected by a six-membered complex called shelterin, which is comprised of TRF2, TRF1, RAP1, TIN2, TPP1 and POT1 (Figure 1.2B) (de Lange, 2009). TRF2 and TRF1 bind to double-stranded TTAGGG repeats while POT1 binds to the single-stranded sequence repeat overhang. Because they are the only proteins known in mammals binding to this sequence repeat, shelterin accumulates at all telomeres in a mammalian cell and protects the telomere. The telomeric repeat sequence spans over several kilobases and the telomere is not just protected by the shelterin complex itself, but the shelterin coated telomeric sequences forms a loop structure called t-loop, where the 3’ overhang invades into double-stranded telomeric DNA providing a protective 3D-meshwork (Figure 1.2B) (de Lange, 2004; Griffith et al., 1999).

Taken together, even though eukaryotes evolved different telomeric repeat sequences, while most are regular arrays of repeats and some are irregular repeats, the underlying principle of evolving a

G-rich sequence, which can then be coated by dedicated protein complexes, is conserved. While budding yeast evolved two different complexes to cover the double-stranded and single-stranded part separately, shelterin protects the double-stranded and single-stranded part in human. These seemingly striking difference still serves the same purposes of protecting the telomeres from being detected as a DSB and blocking the activation of the DNA damage response. While in yeast cells, the telomere length is also maintained by these complexes through granting access of telomerase to the telomere, only stem cells or germ cells employ this mechanism of telomere maintenance while the telomeres of somatic cells are not elongated by telomerase in mammals.

1.2 Helical repeat proteins in telomere biology and DNA repair

1.2.1 Helical repeat proteins - HEAT and ARM repeats

Tandem repeats of protein motifs, including alpha-helical and beta-strand repeats, are ubiquitous in eukaryotes and account for at least 14% of all proteins in the genome (Marcotte et al., 1999). Alpha-helical repeats can be found in a wide variety of molecular processes in all kingdoms and are generally widespread (Brunette et al., 2015). Helical repeat proteins fulfill a wide variety of role including molecular recognition, signaling, and scaffolding (Marcotte et al., 1999). Depending on how many helices are contained within a helical motif and depending on the number of residues per helix, they belong to different subfamilies. Two very prominent helical repeats present in eukaryotic cells are HEAT and ARM repeats (Groves and Barford, 1999). The name “HEAT” is an abbreviation for four proteins containing this type of repeat: Huntingtin, elongation factor 3, the A subunit of protein phosphatase 2A (PP2A), target of rapamycin 1 (TOR1). ARM repeats are named after the *Drosophila* segment polarity protein armadillo where this type of repeat was first described (ARM) (Peifer et al., 1994).

HEAT repeats consist several stacked HEAT motifs. A HEAT motif is comprised of two alpha helices forming a helical hairpin connected by a short linker so that the helices pack in an anti-parallel fashion (Figure 1.3A) (Groves and Barford, 1999). One HEAT motif contains 30 to 40 amino acids and the helices are amphiphilic, pointing the hydrophobic side chains towards the antiparallel helix, while the other side is mostly hydrophilic and surface exposed (Yoshimura and Hirano, 2016). The number of repeat motifs in HEAT repeats is variable. Even though the amino acid sequences making up HEAT motifs can be diverse, the tertiary protein structure is overall conserved (Andrade et al., 2001).

Figure 1.3

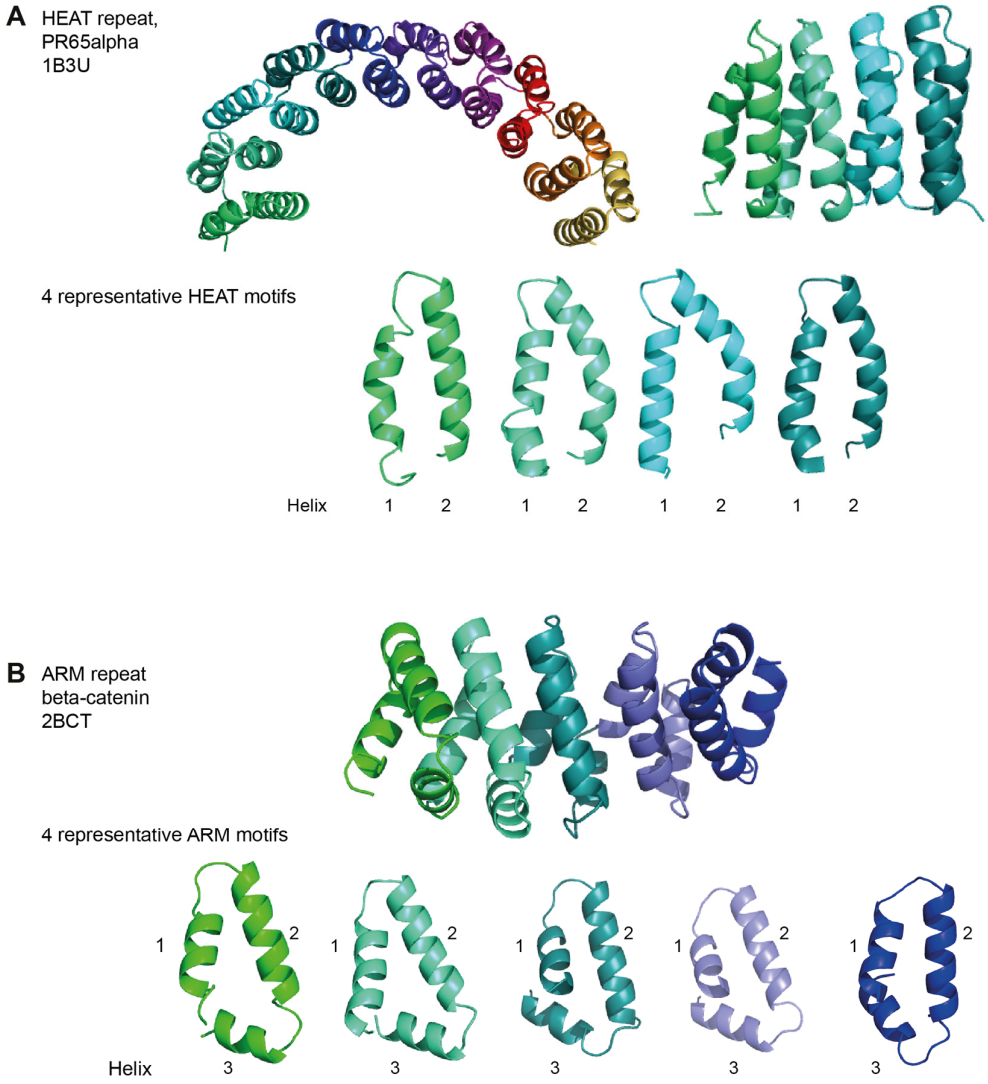

Figure 1.3 – Representative HEAT and ARM repeats. A, Regulatory domain of human PP2A, PR65alpha (1B3U) is depicted as representative HEAT repeat. The first four HEAT motifs are shown in close-up view. B, Murine beta-catenin (2BCT) is depicted as representative ARM repeat. The four ARM motifs are shown in close-up view

The overall fold of a HEAT repeat is an arch-like shape while the first helix per turn lines the outside (convex) surface and the second helix lines the inner (concave) surface of the arch. The interactions between adjacent HEAT motifs define the overall shape and curvature of the HEAT repeat (Brunette et al., 2015).

ARM repeats were first structurally identified and analyzed in the ARM repeat of the *Drosophila* segment polarity protein armadillo (Peifer et al., 1994). The ARM motif consists of three helices per turn, a short helix and two longer helices (Figure 1.3B). The two longer helices fold in an antiparallel fashion and the short helix is approximately perpendicular to the two long helices (Andrade et al., 2001). Each ARM motif has roughly 40 amino acids distributed over the three helices and ARM motifs also stack on top of the neighboring ARM motif. The overall architecture of ARM repeats is similar to HEAT repeats, even though, one more helix per turn is required. Additionally, ARM repeats tend to be more elongated arches or even linear super-helices (Reichen et al., 2014). ARM repeats have been found to play a role in signaling, nucleo-cytoplasmic transport and cell adhesion (Tewari et al., 2010).

Individual HEAT or ARM motifs stack in order to form a HEAT or ARM repeat, respectively (Figure 1.3). HEAT and ARM repeats are stabilized by hydrophobic interactions between the helices. In this arrangement, the first, second, and potentially third helices pack on top of their respective neighbor. Helical repeats often show a high degree of flexibility (Groves et al., 1999; Lee et al., 2005; Sibanda et al., 2010). One example where the molecular flexibility within helical repeats has been systematically analyzed are beta-importins consisting of HEAT repeats (Conti et al., 2006). While there is no crystal structure available of beta-importin in isolation, it has been crystallized together with four different binding partners revealing a different conformation with respect to the HEAT-repeat curvature and opening of the arch (Cingolani et al., 1999; Lee et al., 2005; Lee et al., 2003; Liu and Stewart, 2005).

1.2.2 Are helical repeats involved in telomere biology and DNA repair?

All members of the shelterin complex (TRF2, TRF1, TIN2, TPP1, RAP1, and POT1) are between 400-500 amino acids in size and most individual structured domains are structurally determined (Figure 1.4B). Members of the shelterin complex consist unstructured parts and of the following protein folds: Myb domains, TRF-homology domains, and OB folds (oligonucleotide/oligosaccharide-binding folds) (Chen et al., 2017; Chen et al., 2008b; Fairall et al., 2001; Wang et al., 2007).

Figure 1.4

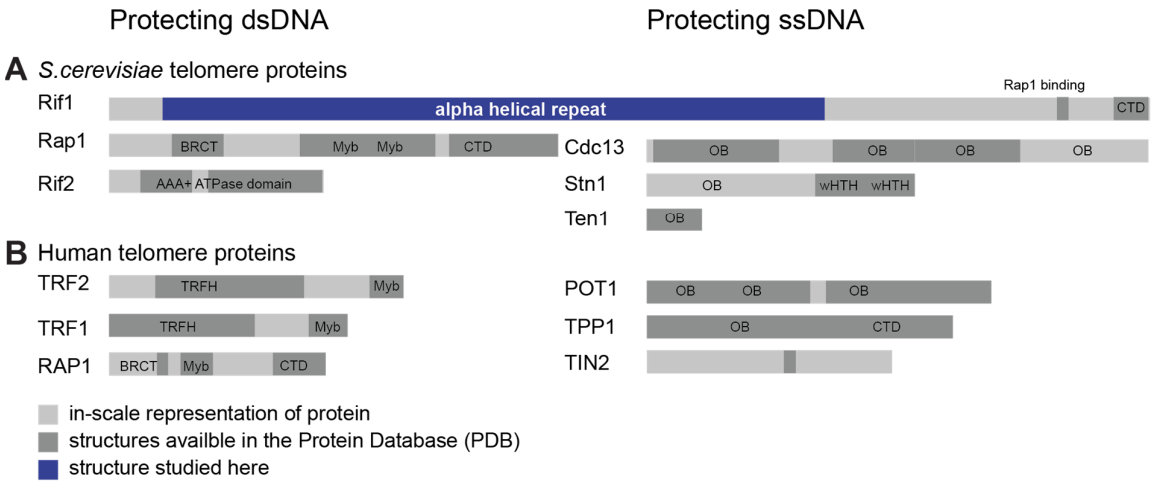

Figure 1.4 – To scale representation of budding yeast and human telomere proteins. Protein size is depicted to scale by light gray bars of budding yeast (A) and human (B) telomeric proteins. Structures available in the PDB are indicated with dark grey bars. Proteins are listed by size within each group. Protein folds predicted or solved are denoted; Myb: named after the retroviral oncogene v-myb where it was first described, TRFH: TRF-homology domains, OB: oligonucleotide/oligosaccharide-binding folds, wHTH: winged helix-turn-helix motif, BRCT: named after BRCA1-C-terminal domain where it was first described, AAA+ ATPase domain. A, The C-terminal domain (CTD) of Rif1 is a tetramerization domain; the Rap1-CTD forms a seven-helix structure. B, The RAP1-CTD forms an eight helix structure, the TPP1 C-terminal domain interacts with POT1 and TIN2, there is no fold predicted for TIN2.

Moreover, the CST complex, Rap1, and Rif2 contain unstructured regions as well as, OB-folds, winged helix-turn-helix (wHTH) motifs, a BRCT domain, a seven alpha-helices unrecognized fold, and an AAA+ ATPase domain (Figure 1.4A) (Bryan et al., 2013; Feeser and Wolberger, 2008; Mason et al., 2013; Mitchell et al., 2010; Mitton-Fry et al., 2002; Shi et al., 2013; Sun et al., 2011; Sun et al., 2009; Yu et al., 2012). In contrast to CST, Rap1, Rif2, and shelterin, Rif1 contains a large N-terminal alpha-helical repeat of around 1000 amino acids in yeast and human (Figure 1.4). This is quite surprising because the function of the alpha-helical repeat within Rif1 is not known. While telomeres and DSB responses have been extensively studied in yeast and human cells, our understanding on a molecular basis is far less advanced. In mammalian cells, we have a limited molecular understanding of the entire shelterin complex, because only parts of the shelterin proteins have been structurally determined such as the structure of POT1 in complex with ssDNA (Lei et al., 2002; Lei et al., 2003). The molecular assembly of the shelterin complex remains largely elusive on a structural level.

Out of the budding yeast telosome proteins, a few have been structurally analyzed. The KU70/80 heterodimer in complex with a hairpin dsDNA was solved by X-ray crystallography (Walker et al., 2001). It is a circular structure threading the DNA through its channel. Additionally, Cdc13 contain four OB-folds of which three were determined by X-ray crystallography or by solution NMR (Mason et al., 2013; Mitchell et al., 2010; Mitton-Fry et al., 2002; Mitton-Fry et al., 2004). Budding yeast

structures of the Stn1 wHTH motifs and the Ten1 OB-fold were determined to atomic resolution and structures of the Stn1-Ten1 complex were solved from fission yeast or human homologs by X-ray crystallography (Bryan et al., 2013; Gelinas et al., 2009; Sun et al., 2009). Out of the Rif1-Rif2-Rap1 complex, the structure of Rif2, all structured individual domains of Rap1 (BRCT domain, Myb domains, C-terminal domain), and the interaction between the Rif proteins and Rap1 were analyzed by X-ray crystallography or NMR (Feeser and Wolberger, 2008; Le Bihan et al., 2013; Shi et al., 2013; Zhang et al., 2011). However, the largest structured part of Rif1 is the Rif1-N-terminal domain (NTD), it spans around 1000 amino acids, and is predicted to be an alpha-helical repeat. The Rif1-NTD was so far not structurally analyzed.

When looking at proteins in DNA double-strand repair, there are several alpha-helical repeats being the same size or even larger than Rif1. The most prominent alpha-helical repeat proteins in DNA DSB repair are members of the phosphatidylinositol-kinase–related kinase (PIKK) family, Ser/Thr protein kinases, in particular, the subfamily of DNA-PK: ATR, ATM, and DNA-PKcs. ATM and ATR harbor an N-terminal 1900 amino acid helical repeat and DNA-PKcs' helical repeat even has 2700 residues. While DNA-PKcs and ATM were determined to an atomic resolution very recently by X-ray crystallography or cryo-EM, the atomic resolution structure of ATR still remains to be determined (Baretic et al., 2017; Sibanda et al., 2017). ATM and DNA-PKcs form a large HEAT repeat cradle. For ATM and DNA-PKcs, it is thought that double-stranded DNA might directly bind to them but both structures were not determined in the presence of DNA, and DNA binding is so far only modeled onto them. It is controversial whether ATM and DNA-PKcs interact with DNA mostly via their associated proteins, the MRN complex and Ku70/80, respectively, or whether the DNA interaction is mediated directly through the helical repeat.

Some other DNA repair proteins such as DNA glycosylases adopt helical repeats. DNA glycosylases initiate the DNA base-excision repair pathway by catalyzing the excision of positively charged alkylated purine bases from DNA (Krokan and Bjoras, 2013). Glycosylases are structurally diverse and fall into six structural classes (Brooks et al., 2013). One of these classes is the ALK-family, of which AlkD is the best characterized member. The bacterial glycosylase AlkD consists of pairs of antiparallel helices stacked on top of each other and they adopt a left-handed turn very similar to HEAT repeats (Rubinson et al., 2008). Interestingly, the structure of AlkD was determined in complex with double-stranded DNA harboring an N3-methyladenine analog as alkylation lesion (Rubinson et al., 2010). AlkD forms a positively charged concave surface, in which the double-stranded DNA is wedged into. Engaging with the DNA through a HEAT-like repeat was unprecedented (Rubinson and Eichman, 2012; Rubinson et al., 2010).

Thus, helical repeat proteins are present in many different aspects of DNA repair and they can function as scaffold proteins, protein-protein interaction surfaces and recently identified also as DNA binding interface. Strikingly, none of the shelterin proteins is predicted to be a helical repeat, which leaves Rif1 as the only helical repeat protein among the telomeric proteins in budding yeast or human. This may already point to a broader function of Rif1 outside of budding yeast telomeres.

1.3 The role of Rif1 in DNA end protection

1.3.1 Rif1 regulates telomere length, helps to cap the telomere and blocks the checkpoint activation in budding yeast

Across organisms, Rif1 participates in a multitude of seemingly unrelated genome maintenance processes ranging from replication to DNA repair and telomere integrity. Some of these functions are shared between yeast and mammalian cells (Mattarocci et al., 2016). Rif1 was originally identified for its interaction with Rap1 (Rap1 *i*nteracting factor 1) and the budding yeast telomere showed a telomere elongation phenotype when Rif1 was deleted (Hardy et al., 1992; Wotton and Shore, 1997). Rif1 has the ability to inhibit the recruitment of telomerase (Bianchi and Shore, 2007). Telomerase-mediated lengthening occurs stochastically and the frequency can be increased by short telomeres (Teixeira et al., 2004). Rif1, together with Rif2, decreases the frequency at which telomere lengthening occurs via telomerase (Teixeira et al., 2004). A possible explanation for this phenotype could be that the amount of Rif1 molecules decreases when the telomere shortens after cycles of replication and that the decrease of Rif1 protein is sensed by telomerase. However, short and native telomeric repeats (around 150bp and 300bp) were reported by Chromatin immunoprecipitation (ChIP) to bind the same amount of Rif1 proteins while the number of Rif2 proteins decreased with a shortening of the telomere (McGee et al., 2010). This suggests that the length of telomeric DNA is not sensed by the amount of Rif1 protein. It is possible that unidentified post-translational modifications of Rif1 contribute to the signaling of the short telomeres, which would explain the increase in the frequency of telomerase extensions at short telomeres (Teixeira et al., 2004).

In order to study the role of Rif1 at telomeres further, destabilizing the telomere cap by temperature-sensitive-lethal mutants of the CST complex is a powerful approach. CST mutants exhibit progressive loss of the 5'-terminated strand (Garvik et al., 1995) and depend on Rif1 for viability. Where Cdc13 capping is compromised, Rif1, but not Rif2, is important to maintain viability in cells (Anbalagan et al., 2011). Using the hypomorphic allele *cdc13-1*, it has been shown that Rif1, but not Rif2, is able to cover the end of chromosomes and attenuate the arrival of RPA, the ssDNA

binding protein, which activates the checkpoint process through MRX-Mec1-Ddc2 (Xue et al., 2011). In these cells, Rif1 appears to bind ssDNA/dsDNA hyper-resected junctions, moving away from chromosome ends and deep into internal regions devoid of Rap1 binding sites, where it serves to dampen the DNA damage checkpoint response (Anbalagan et al., 2011; Xue et al., 2011).

Similarly, Rif1 also contributes to silence the DNA damage checkpoint response at artificial telomeres, particularly at short TG-tracts. This was shown by single-cell analysis of G2/M checkpoint activation in cells where a DSB is generated at a site flanked by short, 80 bp, telomeric repeat tracts TG80 (Ribeyre and Shore, 2012). Interestingly, Rif1 contributes to the protection of telomeres, and inhibits checkpoint activation, even if the Rap1 binding motif of Rif1 is deleted, suggesting a role of Rif1 in protection of the telomere beyond the interaction with Rap1 (Xue et al., 2011). Moreover, Rif1, but not Rif2, is able to partially inhibit telomerase-dependent elongation of telomeres even in the absence of its Rap1-binding modules (Shi et al., 2013). This finding argues that the N-terminal alpha-helical repeat may play a crucial role in blocking DSB sensors including the MRX complex. The mechanism underlying Rif1 localization to a DNA end and the mechanism by which repair and signaling proteins are displaced at these sites remained elusive.

1.3.2 RIF1 is responsible for blocking resection of DSBs in mammalian cells – is there an analogy to budding yeast?

Compared to the crucial role of Rif1 in budding yeast at telomeres, RIF1 only binds to aberrant telomeres in human cells upon inducible TRF2 deletion together with NBS1, ATM, and 53BP1 (d'Adda di Fagagna et al., 2003; Silverman et al., 2004). Aberrant telomeres in mammalian cells can be studied by fluorescent microscopy and are found to cause foci, which are comparable to DNA damage-induced foci (Silverman et al., 2004). RIF1 focus formation at aberrant telomeres in mammalian cells is strictly dependent on 53BP1 (Silverman et al., 2004). RIF1 foci are also formed upon DNA damage treatment such as ionizing radiation or UV-treatment throughout the genome (Silverman et al., 2004). Testing ATM and ATR inhibitors revealed that IR and UV damage can activate the ATR and ATM kinases. However, RIF1 focus formation is dependent on ATM phosphorylated 53BP1 while ATR inhibitors did not show an effect on RIF1 focus formation (Silverman et al., 2004). Mouse embryonic fibroblasts (MEFs) depleted of RIF1 show an even more increased sensitivity to IR causing cell death compared to the treatment of ATM inhibitors or the depletion of 53BP1 (Silverman et al., 2004). This suggests a key role of RIF1 in DSB repair. Co-immunoprecipitation experiments in Xenopus egg extracts showed that RIF1 directly interact with ATM and NBS1 and it is so far not clear how Rif1 mediates this interaction or what the functional relevance is (Kumar et al., 2012). Thus, RIF1 is a key player in 53BP1 and ATM dependent DSB repair.

Growing evidence suggests that the cell cycle dependent DSB pathway choice between NHEJ and HR is a competition between BRCA1/CtIP dependent resection and 53BP1-RIF1 mediated blocking of resection (Chapman et al., 2013; Escribano-Diaz et al., 2013; Feng et al., 2013; Sartori et al., 2007; Zimmermann et al., 2013). 53BP1 binding to post-translationally modified nucleosomes (Fradet-Turcotte et al., 2013; Wilson et al., 2016) is the not sufficient to block resection of DSBs and RIF1 was identified to be the key downstream effector to block resection of a DSB in order to promote NHEJ over HR (Chapman et al., 2013; Di Virgilio et al., 2013; Escribano-Diaz et al., 2013; Feng et al., 2013; Zimmermann et al., 2013). Moreover, this role goes beyond DNA damage repair because NHEJ is also the DNA end-ligation mechanisms required for Class switch recombination (CSR) where RIF1 was also identified to be essential (Chapman et al., 2013; Di Virgilio et al., 2013). 53BP1 recruits RIF1 by N-terminal S/TQ phosphorylation sites on 53BP1. However, whether the interaction of 53BP1 and RIF1 is of direct nature or whether there is a mediator protein between them remains elusive because mechanistic studies are so far based on co-localization and cellular extract pull-downs. Additionally, there are 28 possible ATM phosphorylation targets in the 53BP1 N-terminus and it is so far not clear which sites are required for the RIF1 co-localization. Additionally, it was determined that it is the N-terminal helical repeat of RIF1 (1-967), which is required for the co-localization with 53BP1 (Escribano-Diaz et al., 2013). 53BP1 has another ATM-phosphorylation dependent interaction partner, Pax Transactivation Domain- Interacting Protein (PTIP). RIF1 and PTIP block resection of the DSB together, are recruited independently (Callen et al., 2013) and the phosphorylation sites that interact with PTIP are defined (S6, S13, S25, S29) (Lottersberger et al.). The molecular understanding of the 53BP1-RIF1 interaction remains to be defined and how RIF1 promotes NHEJ on a molecular level remains elusive.

Considering that RIF1 plays such a crucial role in DSB pathway choice in mammalian cells, it raises the question of whether RIF1 functions similarly in budding yeast. Initially, Rif1 was not detected at induced DSBs by ChIP (Xue et al., 2011). However, Martina et al. detected Rif1 at DSB in G1-and G2-phase and assessed the degree of resection upon an induced DSB by a Southern Blotting-based assay (Martina et al., 2014). In cells lacking Rif1, the authors see an increase in resection in the G1-phase upon 2 to 6 hours of DSB induction. The authors propose that Rif1, in contrary to mammalian RIF1, promotes resection (Martina et al., 2014). This was a quite surprising finding particularly because they could not detect an increase in RPA binding to the DSB upon resection. However, the role of Rif1 in DSB repair in budding yeast is still poorly defined and awaits further research.

1.3.3 Rif1 - shared roles across organisms in DNA end protection

Only recently Rif1 has been found to be a key member of DSB pathway choice and we are only beginning to understand this mechanism on a molecular level. So far there are only vague hints in the literature about common roles of Rif1 in DNA end protection in yeast and human. The Maringele lab noted that Rif1 contributes to the capping of telomeres when the Rif1-C-terminus was deleted (Xue et al., 2011). This is a quite puzzling result considering that the C-terminus contains the Rap1 binding sites to recruit Rif1 to telomeres. This indicates that the N-terminal helical repeat of Rif1 may be the functional domain for telomere capping when telomeres become compromised. Additionally, it is the RIF1 N-terminal helical repeat, which is required for the co-localization with 53BP1 in mammalian cells further supporting the idea of the helical repeat being the functional domain for DNA end protection in DSBs (Escribano-Diaz et al., 2013). Although Rif1 has been detected at DSBs in yeast (Martina et al., 2014), it is currently unclear whether DSB repair pathway choice occurs analogously to mammalian cells.

While RIF1 is not part of the mammalian telosome, murine RIF1 has recently been implicated in protecting telomeres from hyper-resection when the TPP1-POT1 complex, which provides CST-like functions in mammalian cells, is compromised (Kibe et al., 2016). These experiments mimic the *cdc13-1* phenotypes where Rif1 is able to protect telomeres when CST integrity is compromised. However, the detailed role of yeast and mammalian Rif1 at aberrant telomeres and DNA breaks remains elusive and it is presently unclear whether a general capacity to modulate the processing of DNA ends might underlie diverse Rif1 functions.

1.4 Roles of Rif1 outside of end protection

If co-localization with DSBs and aberrant telomeres in mammalian cells is fully dependent on 53BP1 and ATM, RIF1 should not have more severe phenotypes than the deletion of 53BP1 or ATM. However, deletion of RIF1 is embryonically lethal in mice while deletion of 53BP1 and ATM is not (Buonomo et al., 2009). This points towards a function of RIF1 in embryonic development. Additionally, mouse embryonic fibroblasts show a high sensitivity to Hydroxyurea (HU), a treatment depleting cellular nucleotides resulting in stalled replication forks (Buonomo et al., 2009). RIF1 co-localizes with stalled replication forks while it does not co-localize with native replication forks. Co-localization is dependent on 53BP1 but independent of ATM. Treating murine embryonic stem cells with the ATR inhibitor caffeine still did not interrupt the 53BP1-Rif1 co-localization to stalled replication forks, which could imply that Rif1 can be recruited by other means (Buonomo et al., 2009). Interestingly, Rif1 co-localizes to stalled replication forks with similar kinetics as the Bloom

Syndrome RecQ Like Helicase (BLM), which is recruited to stalled replication forks and is required for efficient recovery of the stalled forks (Xu et al., 2010). Mass spectrometry analysis of BLM binding partners revealed that RIF1 interact with each other and that the binding is strictly dependent on the C-terminal domain of Rif1 (Xu et al., 2010). Interestingly, RIF1 recruitment to stalled replication forks is delayed in BLM-deficient cells, which suggests that BLM could recruit RIF1 to stalled replication forks and not 53BP1, as is the case in DSB repair (Xu et al., 2010). This is in line with the finding that replication fork stabilization is not dependent on 53BP1 in B-cells upon HU treatment whereas replication forks were equally resected in cells devoid of *BRCA1, RIF1* or both genes (Ray Chaudhuri et al., 2016). Additionally, Rif1-deficient B-cells show increased chromosomal aberrations in response to replication poisons such as PARP inhibitors, HU, and cisplatin pointing to a crucial role of Rif1 in resolving replication stress resolving (Ray Chaudhuri et al., 2016). In budding yeast, Rif1 lacks parts of the C-terminal domain shown to interact with BLM in human. The yeast ortholog, Sgs1, was so far not reported to directly interact with Rif1. Also, *sgs1Δ*, *rif1Δ* or *sgs1Δ rif1Δ* double mutants are not epistatic showing additive effects to the sensitivity to HU or methyl-methanesulfonate treatment (an alkylating agent causing replication stress), which suggests that these genes act in separate pathways during DNA replication stress in budding yeast (Xu et al., 2010).

Compared to seemingly different roles of Rif1 in replication stress, Rif1 is a key regulator of replication timing in yeast and mammalian cells (Cornacchia et al., 2012; Hayano et al., 2012; Peace et al., 2014; Yamazaki et al., 2013; Yamazaki et al., 2012). RIF1 was shown to alter the replication program shown by genome-wide profiling in mammalian cells leading to a change in replication timing in over 40% of the replication domains. Replication timing is governed by a local compartmentalization into chromatin domains that replicate simultaneously, known as replication timing domains. The physical definition of these replication domains and the temporal order of activation is altered upon RIF1 deletion throughout the genome (Foti et al., 2016). Additionally, the timing of early and late origins changed in mouse embryonic fibroblasts and in mouse embryonic stem cells upon RIF1 deletion (Cornacchia et al., 2012; Foti et al., 2016). In yeast, the Rif1 replication timing function depends on interactions with the protein phosphatase PP1/Glc7 and similar models have been suggested in mammalian cells (Dave et al., 2014; Hiraga et al., 2014; Mattarocci et al., 2014). In yeast Rif1, a KSVAF/SILR amino acid motif (abbreviated as RVxF/SILK) (Hendrickx et al., 2009; Sreesankar et al., 2012) recruits and targets PP1/Glc7 to parts of the replication machinery, including the Mcm4 subunit of the replicative helicase, whose phosphorylation drives origin firing (Hiraga et al., 2014; Sheu and Stillman, 2006). Rif1 has further been proposed to fulfill architectural functions, establishing the three-dimensional organization of late-replicating chromatin domains in

mammalian cells and fission yeast (Foti et al., 2016; Kanoh et al., 2015a). This poses the question whether Rif1 is spatially tethered to subnuclear structures such as the nuclear periphery. RIF1 co-localizes and co-immunoprecipitates with Lamin B1 in mammalian cells and thus Rif1 could have a chromatin-organizing function during replication timing definition (Foti et al., 2016). In budding yeast, Rif1 has been shown to be palmitoylated and that this lipidation may link telomeres to the nuclear periphery via Rif1 (Park et al., 2011). Whether palmitoylation is the direct link in budding yeast to tether Rif1 to the nuclear periphery remains elusive.

Taken together, this shows that Rif1 plays important roles outside of DNA end-protection in telomeres and DSBs. All the functions described are within the area of DNA/chromatin homeostasis and it remains to be shown how Rif1 is able to integrate so many diverse roles across many different pathways ranging from telomere protection to 3D organization of the genome.

1.5 The architecture of Rif1 and 53BP1 from yeast to human

1.5.1 Architecture of Rif1 from yeast to human

Even though Rif1 orthologs are highly divergent at the primary sequence level, Rif1 has several conserved and partially characterized domains or motifs. While budding yeast Rif1 comprises 1916 amino acids, fission yeast Rif1 is considerably smaller in size, comprising 1400 residues. In contrast, vertebrate RIF1 spans around 2400 residues (2472 in human, 2419 in mouse, and 2326 in chicken) (Figure 1.5A).

The best-characterized motif is the RVxF/SILK motif, a PP1/Glc7 binding motif. In budding yeast, this motif is located N-terminally with the KSVAF/SILR signature (commonly abbreviated as RVxF/SILK, residues 116-118 and 147-149) while this motif is located C-terminally in vertebrates (Hendrickx et al., 2009; Sreesankar et al., 2012). Rif1 recruits PP1 (Glc7 in budding yeast) to late replication origins and is instrumental in the regulation of DNA replication initiation (Dave et al., 2014; Hiraga et al., 2014; Mattarocci et al., 2014). The functional implications of the different location of the RVxF/SILK motif between yeast and vertebrates are not clear.

Figure 1.5

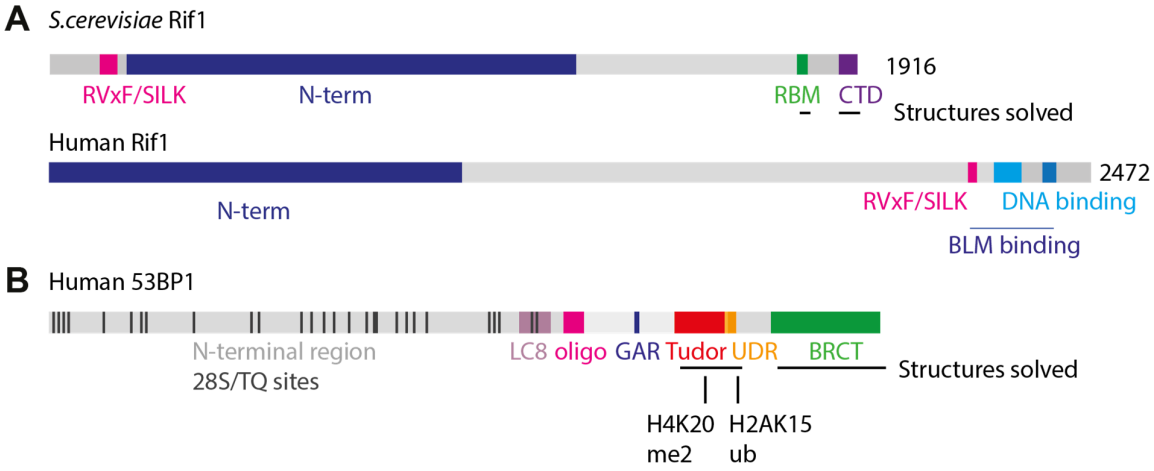

Figure 1.5 – To scale representation of Rif1 and 53BP1. A, Budding yeast and human Rif1 depicted with its described domains: N-terminal domain and RVxF/SILK motif (both conserved); the Rap1-binding motif (RBM), C-terminal domain (CTD) (in part specific to budding yeast); the DNA binding and BLM binding regions (in part specific to mammalian RIF1). B, Human 53BP1 depicted with its characterized domains and motifs: N-terminal region harboring 28 serines or threonine sites (targets of ATM phosphorylation), the dynein light chain binding motif (LC8), the oligomerization domain (OD), the glycine/arginine-rich region (GAR), the tandem Tudor domain (Tudor), the ubiquitin-dependent recruitment domain (UDR) and the BRCA1 C-terminus domain (BRCT). Required histone modifications for 53BP1-nucleosome binding are indicated: dimethylated Histone 4 Lysine position 20 (H4K20me2); ubiquitylated Histone 2A Lysine position 15 (H2AK15). A, B, deposited structures in the PDB are marked (4BJT (Rif1_RBM), 4BJS (Rif1_CTD), 5KGF (53BP1_UDR), 2LVM (53BP1_Tudor), 1KZY (53BP1_BRCT)).

Budding yeast Rif1 contains a well-characterized and structurally determined Rap1-binding motif (RBM, residues 1752-1772) and C-terminal domain (CTD, residues 1857-1916) (Shi et al., 2013). The RBM is thought to be the primary binding site for Rif1 localization to telomeres and the CTD was shown to be a tetramerization module with a low-affinity Rap1 binding site (Shi et al., 2013). While the RBM is restricted to budding yeast species, the CTD is partially conserved from yeast to human.

The vertebrate CTD can be subdivided into three subregions CI, CII, and CIII (I: 2170- 2246, II: 2274-2344, III: 2370-2438 numbers refer to human). CRI contains the RVxF/SILK motif, CRII was shown to have a micromolar DNA binding affinity with a preference for branched structures (Xu et al., 2010). CRI, II and III are required for the BLM helicase recruitment. The sequence of CRII is conserved from yeast to human, has been structurally determined by X-ray crystallography in budding yeast and was shown to form a tetramerization domain (Shi et al., 2013). The tetramerization domain forms two antiparallel dimers, assembling along a pseudo-2-fold symmetry axis (Shi et al., 2013).

In all eukaryotes, Rif1 contains a predicted N-terminal helical domain (NTD) (Sreesankar et al., 2012), while the structure and molecular function of the Rif1-NTD remain largely elusive. In yeast, the NTD is preceded by the RVxF/SILK motif and starts after residue 150, whereas the NTD starts at the N-terminus of the protein in vertebrates. Interestingly, the NTD is always predicted to have a

length of around 1000 residues, even though fission yeast Rif1 is more than 1000 amino acids shorter than the human version. This could suggest that the role of the Rif1-NTD is conserved across organisms. The Rif1-NTD is predicted to be a HEAT/ARM repeat in yeast and human. Within the Rif1-NTD, a core HEAT repeat has been identified. It can be aligned from yeast to human and is also the most conserved part of the protein (Sreesankar et al., 2012).

1.5.2 Architecture of 53BP1

53BP1 is comprised of 1972 amino acids and is a multidomain protein containing six characterized parts: a C-terminal tandem BRCT domain (BRCT1 and BRCT2; named after 'BRCA1 C-terminal domain domain'), a ubiquitylation-dependent recruitment motif (UDR), a tandem Tudor domain (Tudor), a oligomerization domain (OD), a glycine–arginine-rich (GAR) domain, a dynein light chain 8 (LC8) binding motif, and a 1200 amino acid long N-terminal domain (NTD), which contains 28 serine/threonine-glutamine sites (S/T-Q) (Figure 1.5B). BRCT deletion mutants are indistinguishable from wild-type 53BP1 in their ability to localize to DNA damage-induced foci and to block DNA resection. In addition, BRCT deletions fully support physiological DNA end-joining during CSR and NHEJ in the context of DNA repair (Bothmer et al., 2011; Lottersberger et al., 2013). The BRCT domain has been implicated to play a role in DSB repair in heterochromatic regions (Baldock et al., 2015; Lee et al., 2010; Noon et al., 2010) but more evidence suggests that the role of the BRCT domain is separable from DSB pathway choice. The BRCT domain was shown to directly interact with p53 and thereby to enhance the p53-dependent gene activation and repression to trigger cell fate decisions upon stress (Cuella-Martin et al., 2016) and a co-crystal structure of the BRCT1 domain with the p53 DNA-binding domain has been determined, which provides further evidence (Joo et al., 2002).

The UDR domain follows the Tudor domain and they are specifically reading out the two post-translational modifications on the nucleosome upon damage, H2AK15ub and dimethylated lysine 20 on histone 4 (H4K20me2) (Fradet-Turcotte et al., 2013). Point mutations within the Tudor domain abolish DNA damage induced focus formation and render cells incapable of ATM-dependent NHEJ for DNA repair or NHEJ dependent CSR (Bothmer et al., 2011; Botuyan et al., 2006).

Figure 1.6

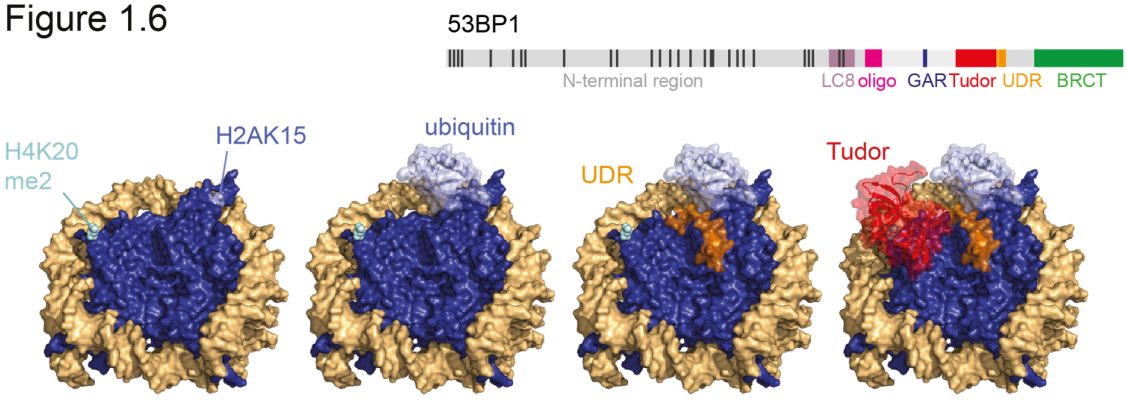

Figure 1.6 – To scale representation and surface representation of 53BP1 binding to the modified nucleosome. Nucleosomes are dimethylated on H4K20 and ubiquitylated on H2AK15. The UDR domain is wedged between the ubiquitin and the acidic patch on the nucleosome (depiction based on cryo-EM structure retrieved from PDB: 5KGF). The Tudor domain is modeled on top of the H4K20me2 based on the crystal structure, PDB: 2LVM.

The UDR specifically locates to H2AK15 ubiquitylated nucleosomes and is engaged between the ubiquitin and the acidic patch of the nucleosome (Fradet-Turcotte et al., 2013; Wilson et al., 2016). The Tudor domain binds to H4 di-methylated lysine 20 and sits on top of the nucleosome, while binding to the unmodified H4 peptide cannot be detected (Wilson et al., 2016). Electron density maps of the UDR and Tudor domain bound to the nucleosome have been determined, elucidating the specific nucleosomal interactions (Figure 1.6) (Wilson et al., 2016).

While the function of the Tudor and UDR domain are well defined, the importance of the OD domain is still puzzling. OD mutants show reduced focus formation upon IR-induced DNA damage (Zgheib et al., 2009), but recruitment of RIF1 and blocking of resection at dysfunctional telomeres is only mildly impaired whereas CSR is completely defective (Lottersberger et al., 2013). Additionally, the OD domain is required for NHEJ in PARP-inhibitor treated cells deficient of BRCA1 (Bothmer et al., 2011). Even though the oligomerization domain was defined early, it is still unclear which oligomer conformation 53BP1 adopts. When the OD was artificially replaced by a tetramerization domain or an inducible dimerization domain, 53BP1 focus formation could be restored to WT levels (Fradet-Turcotte et al., 2013; Zgheib et al., 2009). However, it remains elusive whether this is the natural oligomer and whether dimerization or tetramerization restore the CSR or NHEJ function of 53BP1. Interestingly, 53BP1 oligomerization via the OD domain is not just crucial for NHEJ outcome but also for the 53BP1-dependent p53 regulation (Cuella-Martin et al., 2016). The functional role of the LC8 binding motif and the GAR motif also remains to be determined. Mutation of either site only very mildly affects the processing of dysfunctional telomeres (Lottersberger et al., 2013).

The N-terminus of 53BP1 spans 1220 amino acids, is predicted to be unstructured and contains 28 serines or threonines followed by a Glutamine (S/T-Q), which are ATM targets (Bothmer et al., 2011). Bothmer et al. observed that 53BP1 forms irradiation-induced foci, even if the N-terminus is deleted or if 28 S/T-Q sites in the N-terminus are mutated to Alanine (Bothmer et al., 2011). These mutants are deficient in CSR and blocking of resection at DSBs, assessed by unprotected chromosome ends (Bothmer et al., 2011; Lottersberger et al., 2013). Thus, the 28S/T-Q sites recruit other binding partners to fulfill the function of DSB repair.

An increased mobility of 53BP1 was observed at dysfunctional telomeres and IR induced DSBs to promote DNA repair. Interestingly, the BRCT domain, GAR, and LC8 motifs were dispensable for the mobility phenotype while the Tudor, UDR, NTD, and oligomerization domain were not. The authors suggest that there is an additional domain, which is responsible for the nuclear mobility by association with the LINC complex to the dynamic microtubules within the NTD (Lottersberger et al., 2015). Taken together, 53BP1 has been extensively studied in mammalian cells, several domains are well characterized in terms of their cellular function, and some of their interaction partners. Additionally, we have a molecular understanding of how the Tudor and UDR domains interact with H2AK15ub and H4K20me2 modified nucleosome.

1.5.3 The RIF1-53BP1 interplay in mammalian cells

RIF1 was detected to be the key downstream effector of 53BP1 and its co-localization has also been found to be dependent on the 28 S/T-Q sites (Di Virgilio et al., 2013; Escribano-Diaz et al., 2013; Zimmermann et al., 2013). Considering that RIF1 does not contain a predicted phospho-peptide binding motif such as a BRCT domain or a 14-3-3 domain (name based on migration pattern on DEAE-cellulose chromatography), it is so far not clear how RIF1 mediates this putative interaction. Thus, RIF1 might bind to 53BP1 in an indirect way and may require a mediator protein, which specifically binds to the phosphorylated 53BP1 sites. It has been suggested that the major binding site of RIF1 lies within the 7 more C-terminal S/T-Q sites of 53BP1 (sites 9-15) (Callen et al., 2013). However, other evidence suggests that the Rif1 interaction is mediated between S/T-Q site between 5 and 12 (Lottersberger et al., 2015).

Thus, we are lacking a molecular understanding of 53BP1 apart from the solved UDR motif, Tudor domain, and BRCT domain. The mechanism underlying 53BP1 binding to RIF1 – the key downstream effector - is not understood on the molecular level and it is presently unclear whether they interact directly. Thus, 53BP1 and RIF1 remains loosely understood and deserves further attention.

Aims of this Thesis

Rif1 plays a central role in DNA homeostasis pathways ranging from telomere length regulation in budding yeast, to DNA double-strand break (DSB) repair pathway choice in mammals. In yeast, Rif1 controls telomere length by inhibiting telomerase and checkpoint signaling at chromosome ends. In mammals, RIF1 has emerged as a critical regulator of genome stability, mediating DSB repair pathway choice by attenuating DNA end resection. However, it is unclear how Rif1 can fulfill this range of functions, and which domain is responsible for each function. The Rif1-NTD is predicted to form an alpha-helical repeat, it is the most conserved part of the protein, and it spans over 1000 amino acids in all eukaryotes. Thus, we hypothesized that the evolutionary link is contained within the structured Rif1-NTD.

We aimed to gain a molecular understanding of the Rif1-NTD by initially focusing on budding yeast as a model organism. We expected that a structural and biochemical analysis of the Rif1-NTD would provide first insights into the molecular mechanisms of action of Rif1-NTD in telomere biology and DSB repair. We were particularly intrigued by a previous finding that Rif1-NTD interacts with DNA directly (Tianlai Shi, Thomä laboratory). To our surprise, the co-crystal structure of Rif1-NTD and dsDNA revealed how Rif1 encases DNA with its alpha-helical repeat. *In vivo* analysis further elucidated how Rif1-NTD is recruited to yeast telomeres independently of its Rap1 binding motif and how Rif1 blocks resection at aberrant telomeres and induced DSBs in budding yeast.

The second aim of my thesis was to build on the newly gained structural insights from the budding yeast Rif1-NTD model and to shed light on the question of whether its structure and function are conserved across organisms. In mammals, RIF1-NTD and 53BP1 are at the center of DSB repair pathway choice, with 53BP1 acting as the DSB chromatin mark sensor and the Rif1-NTD as the downstream effector blocking resection being strictly dependent on phosphorylated 53BP1. However, it remained unclear whether RIF1 and 53BP1 interact directly or require a mediator protein. We hypothesized that the RIF1 may interact with phosphorylated 53BP1 in an analogous way as Rif1-NTD interacts with DNA. Thus, we aimed to investigate the Rif1-NTD – 53BP1 interplay biochemically and our data reveal that the RIF1-NTD binds directly and specifically to a phosphorylated motif within 53BP1 *in vitro* and *in vivo*.

2 CHAPTER 2 – RESULTS: THE BUDDING YEAST RIF1-NTD MAINTAINS TELOMERES AND MEDIATES DSB REPAIR BY ENCASING DNA ENDS

This chapter contains published data and additional unpublished data. I planned and performed experiments presented in sections 2.1 – 2.5. Crystallographic data analysis was performed by Richard Bunker (Thomä laboratory, FMI, Basel) and the work is based on initial work from Tianlai Shi (Thomä laboratory). *In vivo* results described in 2.6 – 2.8 were performed by members of the Shore (University of Geneva) or Rass (FMI, Basel) laboratory.

Mattarocci, S.*, Reinert, J.K.*, Bunker, R.D.*, Fontana, G.A.*, Shi, T., Klein, D., Cavadini, S., Faty, M., Shyian, M., Hafner, L., Shore D., Thomä N.H., Rass U. (2017). Rif1 maintains telomeres and mediates DNA repair by encasing DNA ends. Nat Struct Mol Biol *24*, 588-595. doi: 10.1038/nsmb.3420. Epub 2017 Jun 12.

The published manuscript can be found in the Appendix of this thesis.

2.1 Structure of the Rif1-NTD - an elongated, crook-shaped alpha-helical repeat

S. cerevisiae Rif1 is predicted to contain a largely uncharacterized N-terminal domain containing helical repeat elements (Hendrickx et al., 2009; Silverman et al., 2004; Sreesankar et al., 2012) within the first 1400 residues of its 1916 amino acids (Figure 2.1A). This domain is preceded by an RVxF/SILK PP1/Glc7 binding motif (residues 116-118 and 147-149), which is found at varying positions in different Rif1 orthologues (Sreesankar et al., 2012). The remaining C-terminal ~600 resides are specific to the budding yeast protein and contain the primary Rap1-binding motif (RBM; amino acid residues 1752-1772) with a major role in Rif1 telomere localization, and the Rif1 C-terminal domain (CTD; residues 1857-1916), a tetramerization module, and low-affinity Rap1 binding site (Shi et al., 2013).

A Rif1 construct comprising the residues 100-1322 had been recombinantly expressed and analyzed by limited proteolysis previously, identifying an N-terminal domain (NTD) defined by residues 177–1283 (data not shown; Ph.D. Thesis of Tianlai Shi, Thomä laboratory). Rif1-NTD was recombinantly expressed, purified, crystallized, and diffraction data were collected (Figure 2.2A and B). Due to the lack of a search model, phases were determined by using a selenium multiple-wavelength anomalous dispersion approach, where all native methionines in the Rif1_NTD were substituted with the heavy atom labeled seleno-methionine. The model was built manually and refined at 3.95 Å resolution (data analysis and model building was performed by Richard Bunker, Thomä laboratory). Rif1-NTD assumes an extraordinarily elongated, crook-shaped fold 238 Å long (Figure 2.1B) resembling a shepherd's crook. The structure, which is formed entirely by alpha-helices and connecting loops, is composed of 23 irregular α-helical repeat units containing a mixture of two-helix HEAT-like and three-helix ARM-like modules. Rif1-NTD has two distinct regions: *i*) a curved N-terminal region (the 'Hook': helical units 1-12, residues 185-874, HEAT-like), and (*ii*) a straight C-terminal portion (the 'Shaft': units 16-23, residues 976-1272, ARM-like). The boundary between Hook and Shaft is marked by a kink followed by eight helices ('Transition': units 13-16, residues 875-975) oriented perpendicular to the other major helices in the domain. The Hook is decorated by

Figure 2.1

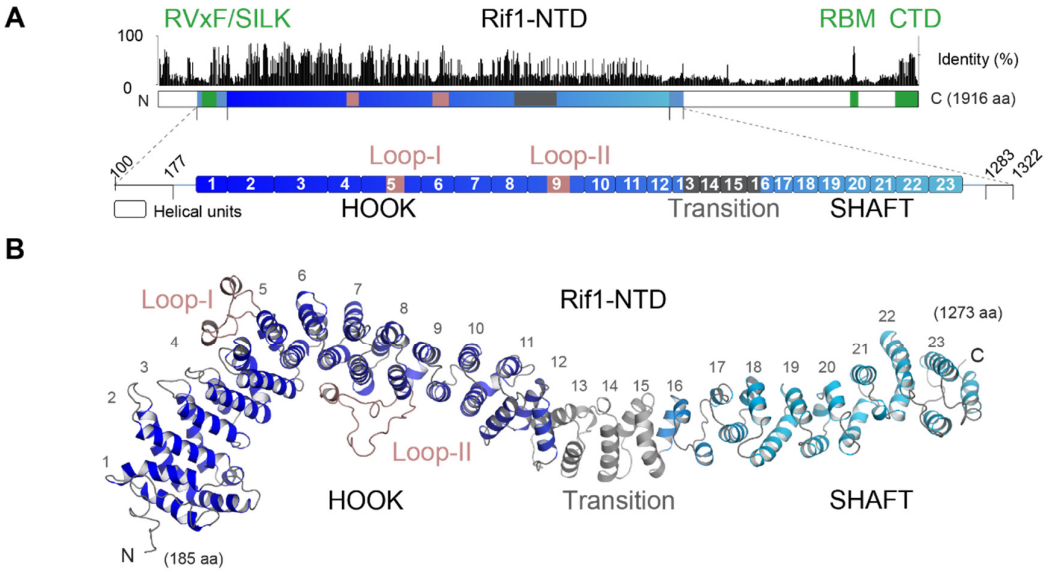

Figure 2.1 – Crystal structure of Rif1-NTD. A, Rif1 domain organization with the RVxF/SILK, Rap1 binding motif (RBM), C-terminal domain (CTD) (green) and Rif1-NTD (blue) functional regions. A sequence identity histogram from a structure-guided sequence alignment of 17 yeast Rif1 orthologs is shown above (details in Figure 2.2). The expanded view shows the organization of the two- and three-helix units (HEAT and ARM) found in the crystal structure. The HOOK region (dark blue), SHAFT region (light blue), insertion loops I and II (mauve), and a transition region (gray) are indicated. B, Rif1-NTD overall fold in cartoon representation (see also Fig. 2.2).

two insertion loops: Loop-I (residues 469-498), emerging from its convex face, and Loop-II (residues 676–715), emerging from its concave face. Overall, Rif1 conservation across yeast species is low, with 22% average pairwise amino acid identity across 17 yeast protein sequences (Figure 2.2C). Despite low amino acid sequence conservation from yeast to human, the Hook contains a signature region (designated Rif1_N (PF12231) in the Pfam database (Finn et al., 2016)) that is most conserved and present in all Rif1s, suggesting it is functionally important (Figure 2.2D).

Figure 2.2

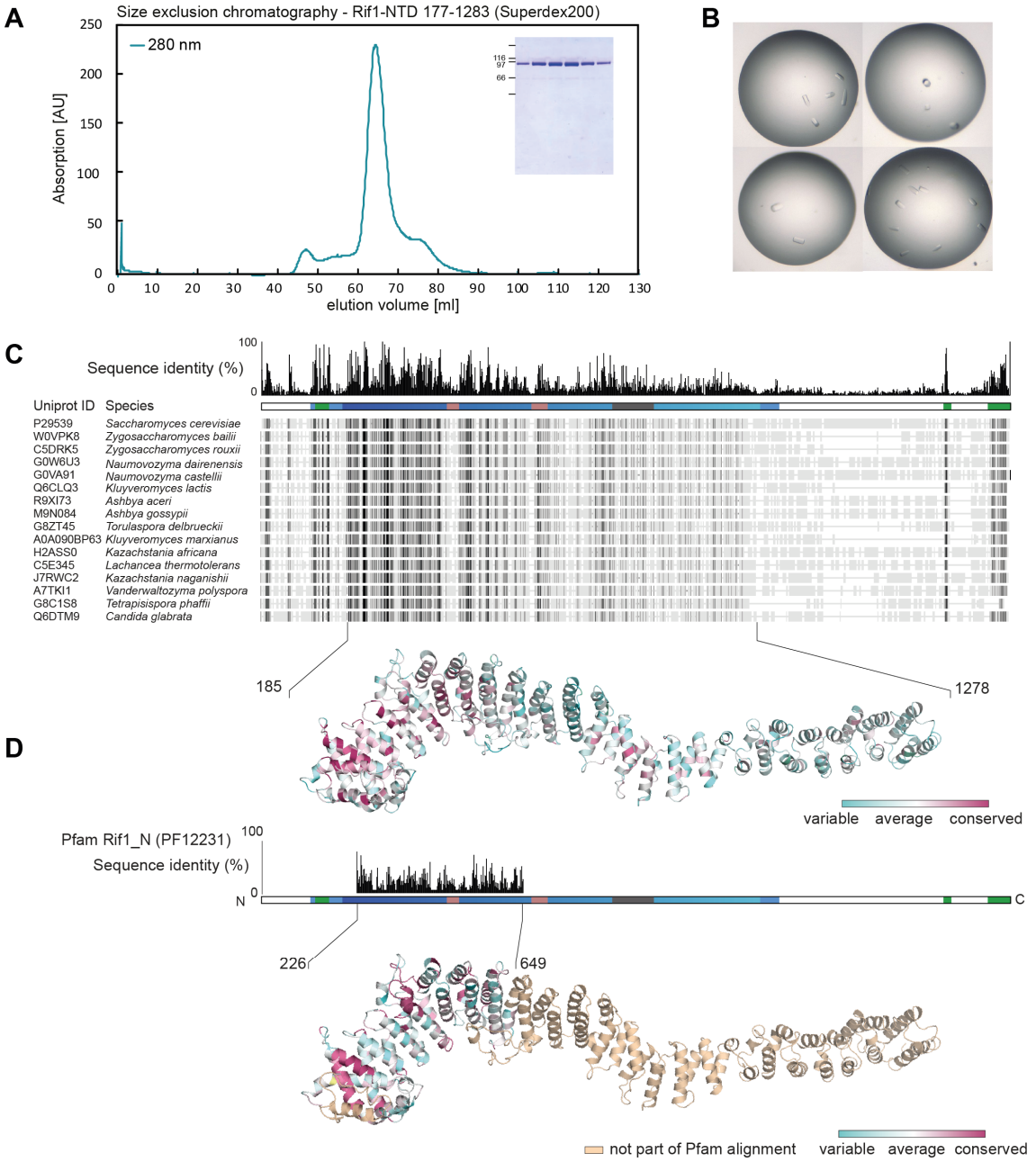

Figure 2.2 – Rif1-NTD protein purification and sequence conservation. A, Purification of scRif1-NTD (177-1283). Size exclusion chromatography profile at 280nm absorption, Coomassie-stained gel analysis of purified scRif1-NTD. B, scRif1 crystal pictures. Crystals were grown in 0.3 M Lithium sulfate and 0.85 M Potassium Sodium tartrate. C, Structure-guided multiple sequence alignment of Rif1 orthologs from 17 yeast species with conservation mapped onto the Rif1-NTD. Regions of highest conservation are the RVxF/SILK motif, Rap1 binding motif (RBM), the C-terminal domain (CTD) (all green), and the Rif1-NTD (blue). The concave face of the Rif1-NTD HOOK domain is the most conserved region within the Rif1-NTD. D, Conservation from the Pfam Rif1_N (PF12231) 70-sequence seed alignment extending from yeast and humans mapped onto the Rif1-NTD model spanning from residues 226-649.

2.2 Rif1-NTD binds DNA with nanomolar affinity

Noting that Rif1-NTD co-purified with nucleic acid from insect cells, we explored a DNA binding role for this domain. Rif1 acts at *S. cerevisiae* telomeres, which carry short 3' ssDNA overhangs (25 nt in S-phase or ~5-10 nt outside S-phase) (Soudet et al., 2014). We thus focused on three potential Rif1-NTD DNA substrates: ssDNA, dsDNA, and 3'-tailed dsDNA (Figures 2.3A and B). We assessed DNA binding by electromobility shift assays (EMSAs) with recombinantly expressed Rif1-NTD comprising residues 100-1322 and poly-T ssDNA, random sequence dsDNA, or duplexes with a poly-T 3' tail. Rif1-NTD bound ssDNA in a length-dependent manner: a 20 nt ssDNA fragment did not interact with Rif1-NTD at concentrations up to 40 nM, whereas Rif1-NTD bound 30 nt under these conditions (Figure 2.3A). As judged by EMSA, Rif1-NTD also bound 30 bp dsDNA and ssDNA/dsDNA junction (15 bp + 15 nt and 30 bp + 30 nt, Figure 2.3B). Quantification of a Rif1-NTD titration with a 30 nt + 30 bp ssDNA/dsDNA junction yielded an apparent K_d of approximately 20 nM (Figures 2.3C). Titration curves appeared non-hyperbolic and were fitted assuming cooperative binding by the Hill equation (see Materials and Methods, Chapter4). EMSAs with 60 nt ssDNA, 60 bp dsDNA or 30 nt + 30 bp ssDNA/dsDNA junction, produced distinct banding patterns, indicating the formation of different Rif1-NTD-DNA oligomeric species (Figure 2.4). Different binding patterns were observed for a plethora of different DNA substrates, showing that Rif1-NTD binds DNA substrates tightly resulting in various oligomeric states (Figure 2.4).

Figure 2.3

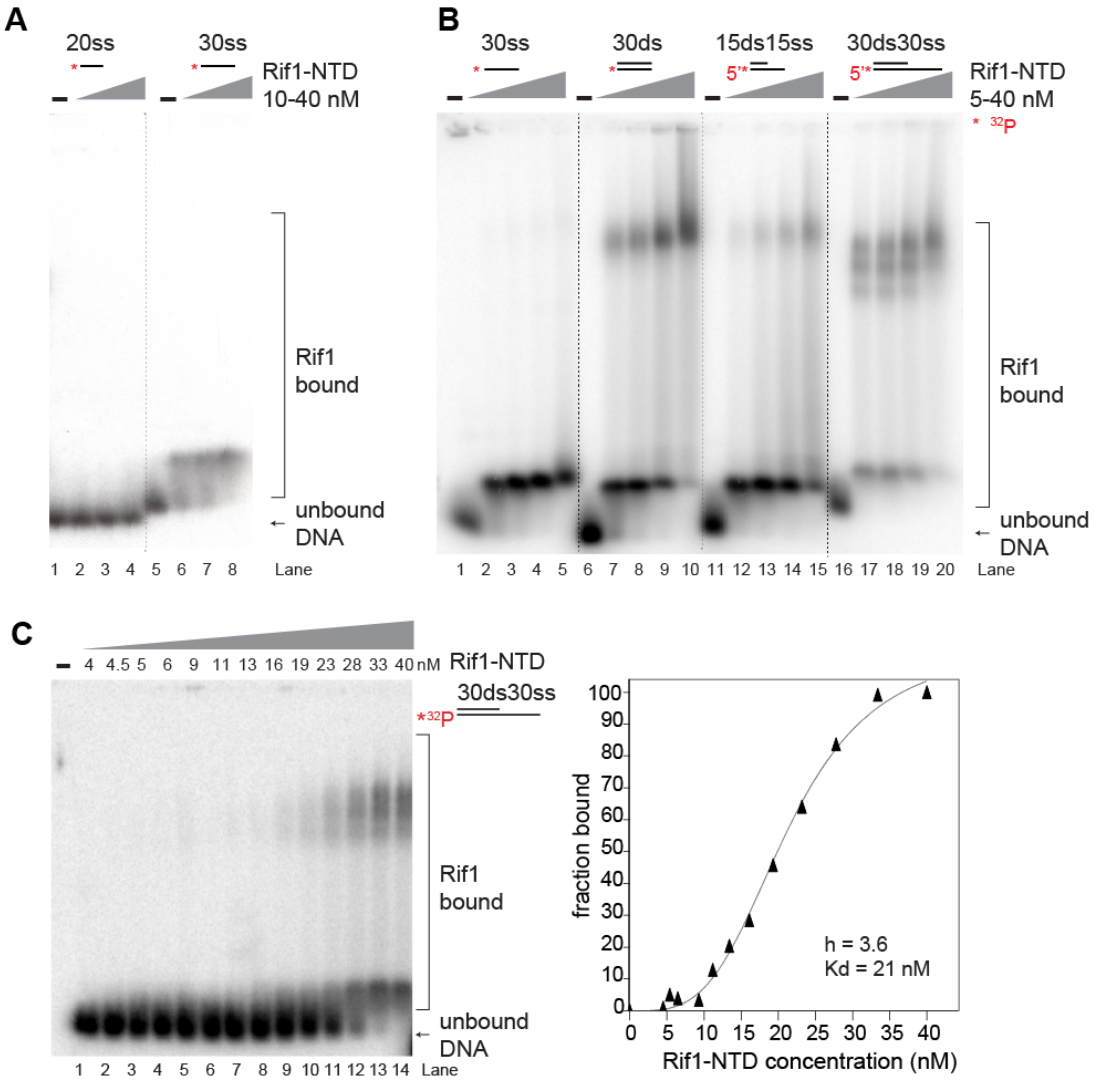

Figure 2.3 – Rif1-NTD binds DNA with nanomolar affinity. A, EMSA analysis using 1 nM ^{32}P-labeled 20ss or 30ss DNA with Rif1-NTD (10, 20 and 40 nM). The Rif1-NTD binds ssDNA in a length-dependent manner with affinity for 30ss. B, EMSA analysis using 1 nM 32P-labeled 30ss, 30ds, 15ds15ss or 30ds30ss substrate titrated with increasing concentrations of Rif1-NTD (5, 10, 20 and 40 nM). All DNA substrates were bound with low nanomolar affinity. C, EMSA analysis using 1 nM of a ^{32}P labeled 3'-tailed 30ds30ss junction DNA as substrate with increasing concentrations of Rif1-NTD (4-40 nM). Rif1-NTD binds 3'-tailed DNA cooperatively with low nanomolar affinity. Band intensities of (C) were quantified relative to total signal in each lane and plotted. The resulting binding curve was best accounted by a Hill slope.

Figure 2.4

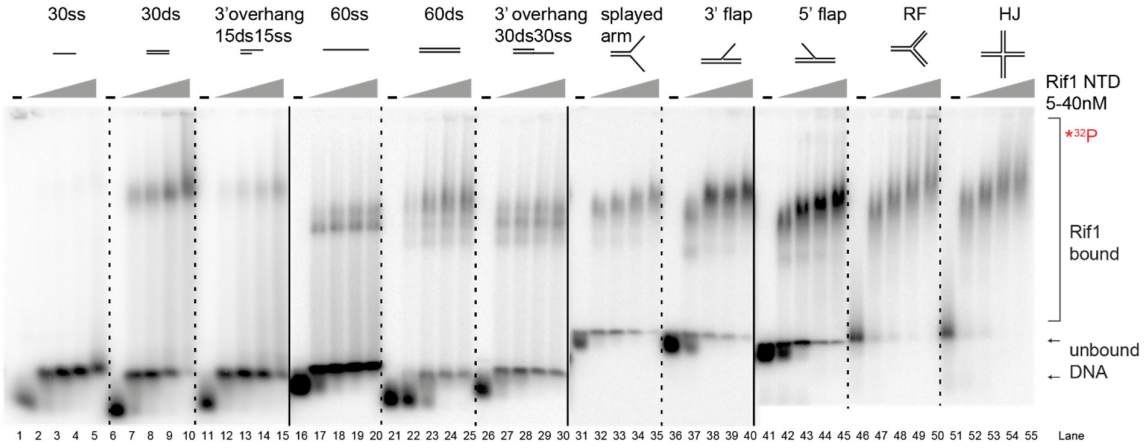

Figure 2.4 – Rif1-NTD binds a plethora of DNA substrates with low nanomolar affinity. EMSA analysis using 1 nM ^{32}P-labeled DNA as indicated titrated with increasing concentrations of Rif1-NTD (5, 10, 20 and 40 nM).Each substrate elicits a different binding pattern.

2.3 Rif1-NTD contains a novel high-affinity DNA binding site

The finding that Rif1-NTD readily binds different DNA substrates with nanomolar affinity, prompted us to explore a DNA-binding role for Rif1-NTD by structural analysis. Following extensive screening with ssDNA, dsDNA, and ssDNA/dsDNA junction substrates, crystals were obtained by mixing a Rif1 construct spanning amino acid residues 100-1322 with a 30 bp dsDNA carrying a 24 nt or 30 nt ssDNA 3' tail. Several hundred crystals were screened, yielding two useful datasets (Rif1-NTD-DNA-1 and -2; Table 2.1, end of the chapter). The crystals belong to space group $P2_12_12_1$ with variable unit cell parameters, containing two conformationally distinct Rif1-NTD protomers and a single DNA duplex in the asymmetric unit (Figure 2.5). The structure was determined by molecular replacement with a Rif1-NTD monomer search model. The two Rif-NTD protomers per asymmetric unit formed several plausible dimer conformations with DNA in the crystal, of which a head-to-tail or head-to-head conformation of the Rif1-NTD were most likely (Figure 2.6A for possible dimer conformations).

Figure 2.5

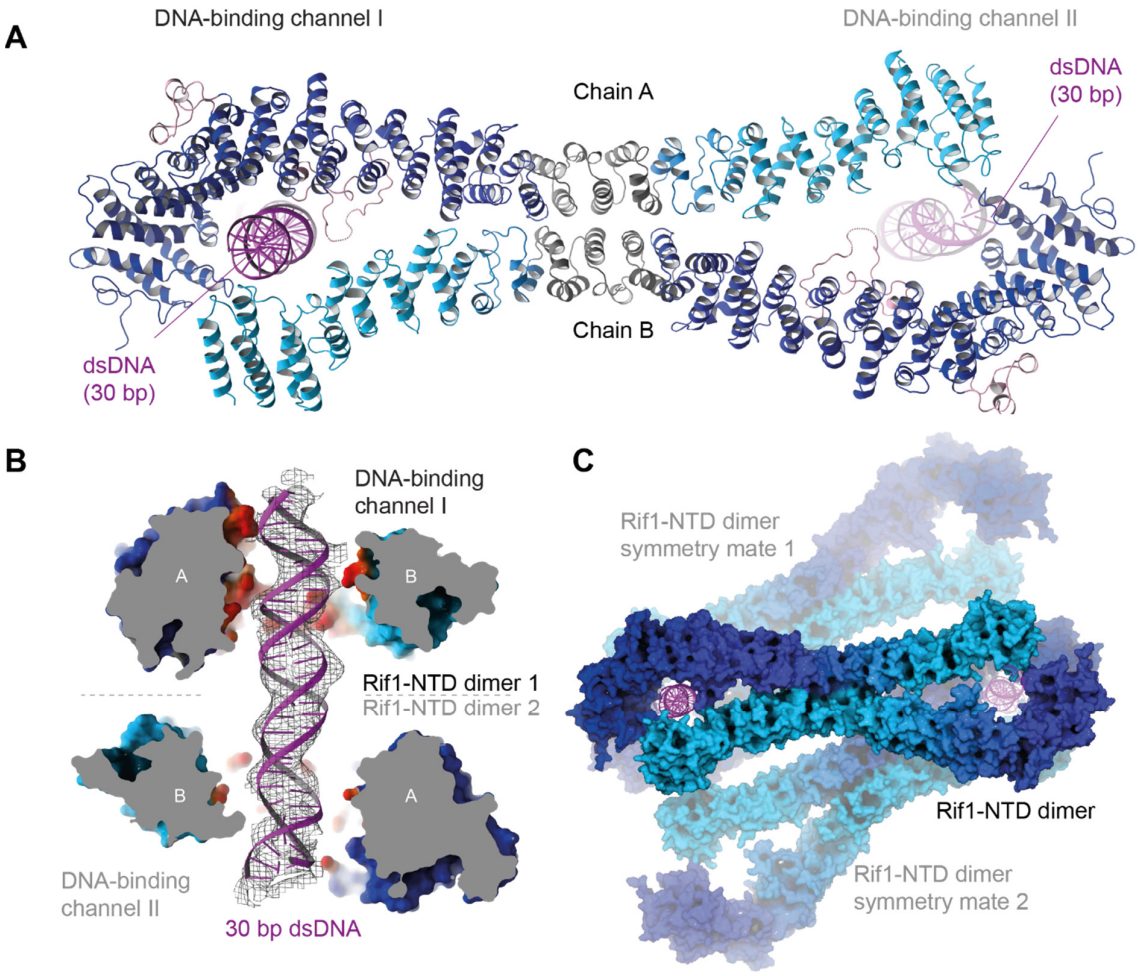

Figure 2.5 – Crystal structure of Rif1-NTD in complex with DNA. A, Cartoon representation of Rif1-NTD in complex with DNA. B, Cross-section of the two Rif1-NTD dimers bound to each 30 bp dsDNA with an unbiased segment of its 2mFo-DFc electron density (gray mesh) contoured at 0.8 r.m.s.d and shown at a 4 Å radius around the DNA. The Rif1-NTD surface within 8 Å of the DNA is shown in red. No interpretable electron density was found for the 30 nt ssDNA 3'-tail of the crystallized dsDNA. C, View of B expanded by crystallographic symmetry showing how multiple Rif1-NTD dimers (blue surfaces) bind the same two DNA molecules in the Rif1-NTD co-crystals with DNA.

Figure 2.6

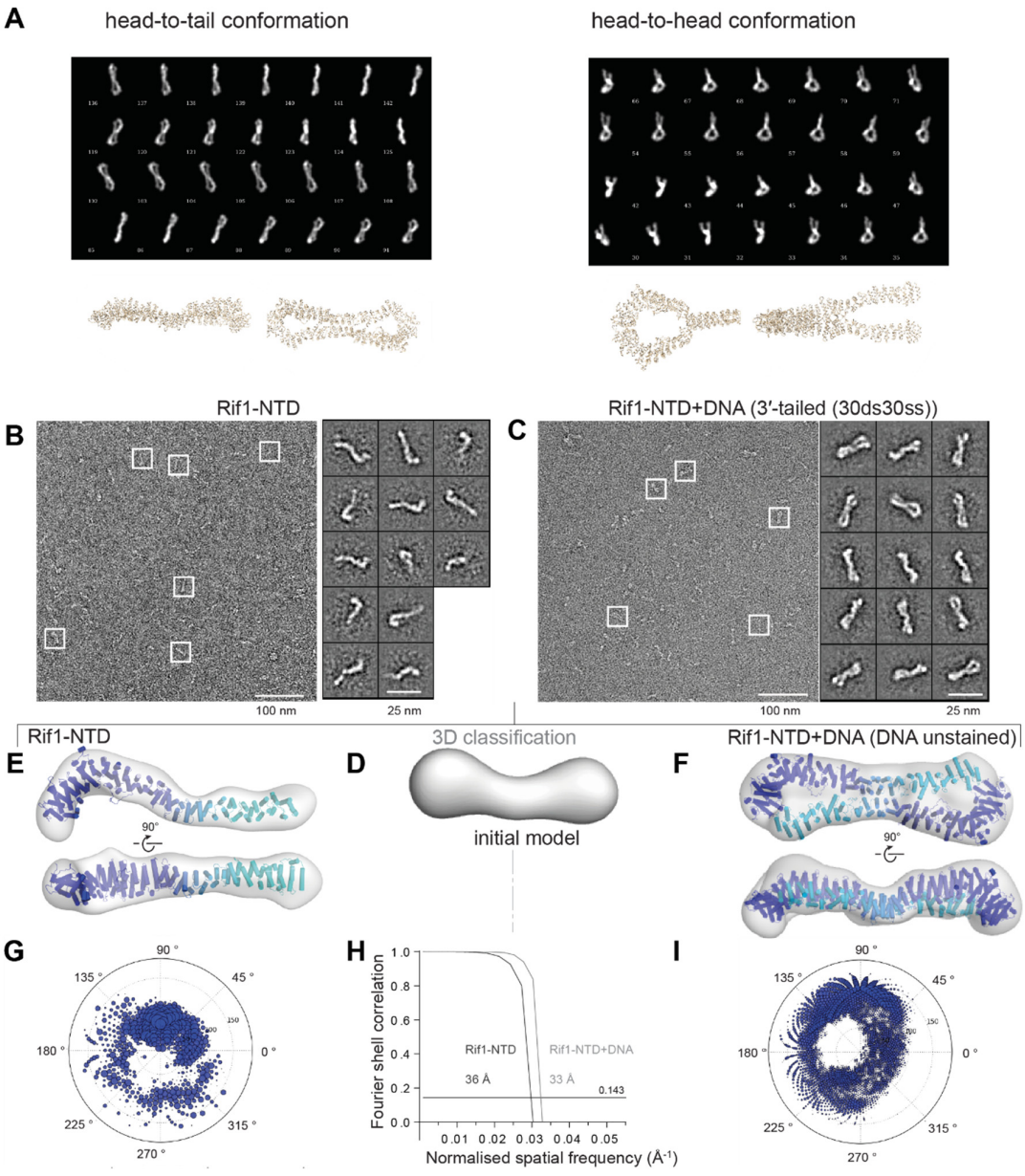

Figure 2.6 – Negative stain electron microscopy of Rif1-NTD with and without DNA. D, Calculated back-projections on the bases of the crystal structure assuming a head-to-tail (left) or head-to-head (right) conformation of the dimer. B-C, Representative negative stain electron micrographs and 2D class averages of Rif1-NTD in absence (B), or presence (C) of 3′-tailed DNA. D, Initial 3D model used for 3D classification. E, Rif1-NTD EM model and cartoon representation of crystallographic model, consistent with a Rif1-NTD monomer conformation. After 3D classification, no dimer species was observed. F, Rif1-NTD+DNA EM model. After 3D classification, the predominant class showed a Rif1-NTD dimer. A monomer class was also observed (data not shown). G, I, Angular distribution plots for Rif1-NTD and Rif1-NTD+DNA, respectively. H, Gold-standard Fourier shell correlation curves.

Seeking independent evidence for functionally relevant Rif1-NTD-DNA configurations, we used negative stain electron microscopy (EM) (Figures 2.6). Two-dimensional class averages and three-dimensional reconstructions confirmed the crook-shaped appearance of monomeric Rif1-NTD (Figures 2.6B and E) and established that Rif1-NTD predominantly forms a figure-8-shaped head-to-tail dimer in the presence of ssDNA/dsDNA junction substrate (Figures 2.6C and F; 2.6A for calculated back-projections). This closely matches one plausible type of dimer – the head-to-tail dimer – formed by Rif1-NTD in the co-crystal with DNA (Figure 2.5), validating the relevance of the assembly found in the co-crystal.

The crystals contained two conformationally distinct Rif1-NTD protomers in a head-to-tail dimer arrangement, with DNA threaded through the two internal channels (designated DNA-binding channel I and II in Figure 2.5). Clear undulating electron density for linear dsDNA was found for Rif1-NTD-DNA-1 and -2 after refinement with an optimized bulk solvent model, enabling the entire 30 bp dsDNA portion of the crystallized construct to be modeled (Figure 2.5B). No interpretable density was found for the single-stranded portion of the DNA (Figure 2.7A).

The dsDNA threads through channel I of one Rif1-NTD dimer and into channel II of a neighboring dimer so that each DNA is bound by two Rif1-NTD dimers (Figures 2.5B and C). Conformational differences between the Rif1-NTD dimer mates influence the architecture of the internal channels, which differ and vary from 34 to 42 Å in diameter (Figures 2.7B). Combined with the periodicity of the DNA and the offset of the two Rif1-NTD dimers bound to the same DNA, this leads to a distinct DNA binding mode in each of the channels. The differences between the two channels are highlighted by plotting DNA proximity onto the surface of Rif1-NTD, which shows that the potential contact surface is more extensive in channel I compared with channel II (Figures 2.7C). Nevertheless, the two channels of the figure-8-shaped Rif1-NTD dimer each completely surrounds duplex DNA and bind with a 16 bp footprint. A common set of positively charged residues lie within 8 Å of the DNA in channel I and II (Figures 2.7C). Bound dsDNA lies across the concave face of the Hook domain in each channel and is closest to helical units 4-8, which are part of the Rif1_N signature region defined by Pfam (helical units 1-8, Figures 2.2C).

Figure 2.7

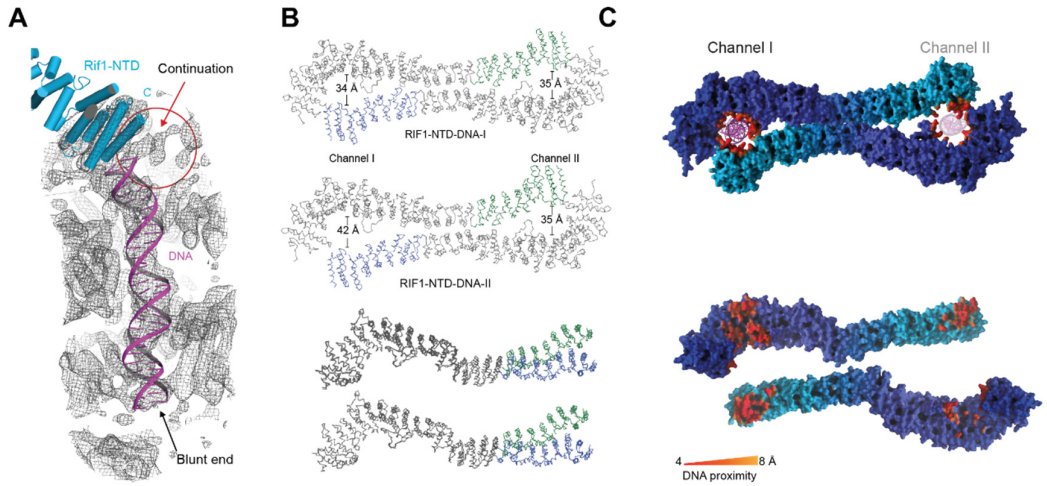

Figure 2.7 – Rif1-NTD DNA binding in the crystal and in comparison to the Rif1-CTD. A, Portion of the 2mFo-DFc electron density map shown in Fig. 2.5 (grey mesh) calculated by CNS-DEN before DNA was added to the model and displayed at a contour level of 0.8 r.m.s.d with a 40 Å radius about the DNA. The 5′ end of DNA is positioned at the blunt end of the tubular DNA electron density (black arrow). Continuation of the electron density at the 3′-tail of the crystallized DNA was visible but not sufficiently ordered to be interpreted (red arrow). Cartoon representations for the 30 bp dsDNA in the final model (magenta) and the C-terminal region of Rif1-NTD chain packing against its end (blue).B, Cα traces of Rif1-NTD–DNA crystals, with the diameter of the DNA-binding channels indicated. Rif1-NTD–DNA crystals show a flexibility in the SHAFT conformation making the two DNA channel non-identical. C, Rif1-NTD–DNA crystal with highlighted DNA contact surface. Right*, an 'open-book' view of the Rif1-NTD dimer with DNA removed, emphasizing the greater extent of the DNA proximity surface in DNA binding channel I compared with channel II. Rif1-NTD residues between 4 Å (red) and 8 Å (orange) of the DNA (magenta) are indicated.*

2.4 Biochemical validation of high-affinity Rif1-NTD-DNA interactions

In the crystal structure, Rif1-NTD binds the dsDNA portion of the 3′-tailed DNA substrate. Consistently, Rif1-NTD EMSAs with a 30 bp dsDNA substrate produced similar binding affinities compared to 30 bp + 30 nt or a 15 bp + 15 nt 3′-tailed ssDNA/dsDNA junction substrates (Figure 2.3B). Given that Rif1-NTD exhibited affinity to ssDNA, dsDNA, and several other DNA substrates (Figure 2.4), we next performed competition experiments to determine the preferred DNA substrate of Rif1-NTD in solution (Figure 2.8A). Rif1-NTD (80 nM) was pre-bound to a labeled 15 bp + 15 nt 3′-tailed ssDNA/dsDNA junction substrate (1 nM) and challenged with increasing amounts (20-320 nM) of unlabeled 30 nt ssDNA, 30 bp dsDNA, an equimolar mixture of 15 nt ssDNA (20-320 nM) and 15 bp dsDNA (20-320 nM), or a 15 bp + 15 nt 3′-tailed ssDNA/dsDNA junction substrate. As judged by the release of labeled DNA in EMSA assays, Rif1-NTD bound the ssDNA/dsDNA junction substrate with higher affinity than either ssDNA (~8-fold lower) or dsDNA (~4-fold lower) of the same length. The mixture of ssDNA and dsDNA, containing the elements of the ssDNA/dsDNA

junction substrate as discrete entities, was bound with >8-fold lower affinity than the intact junction substrate (Figure 2.8A). These competition experiments reveal that Rif1-NTD binds 3'-tailed dsDNA preferentially. Repeating this type of competition experiment with labeled 30 bp + 30 nt 3'-tailed ssDNA/dsDNA junction substrate, as used for the co-crystal structure, and competing with ssDNA, dsDNA or a mixture thereof, gave a similar effect (Figure 2.8B). The resulting binding pattern was more complex, accounting for several Rif1 dimers bound per ssDNA/dsDNA junction substrate.

Additionally, these assays were performed with substrates containing yeast telomeric DNA sequences to test whether Rif1-NTD shows a sequence preference. We found that TG_{1-3} repeats were no more effective in competitive binding than random sequence substrates (Figure 2.8C). It was previously published that the human RIF1-CTD binds DNA *in vitro* showing a preference for Holliday Junctions (Xu et al., 2010). Considering that the Rif1-CTD fragment contains the conserved DNA-binding region present in yeast and human, we compared the budding yeast Rif1-NTD and Rif1-CTD under these conditions. Our EMSA analysis showed similar Kds for the Rif1-CTD as previously published (Xu et al., 2010), revealed that both Rif1 domains bind DNA *in vitro* and that the affinity is roughly 10-fold higher for the NTD compared to the CTD (Figure 2.8D). Taken together, these experiments are consistent with the propensity of Rif1-NTD to crystallize with 3'-tailed ssDNA/dsDNA junction DNAs and to make preferred interactions with the same substrates in solution. Rif1-NTD binds DNA very tightly and in a sequence-independent manner. The detailed structural basis for preferential binding to 3'-tailed DNA remains unclear, as the current crystal structures only reveal dsDNA-Rif1 interactions.

Figure 2.8

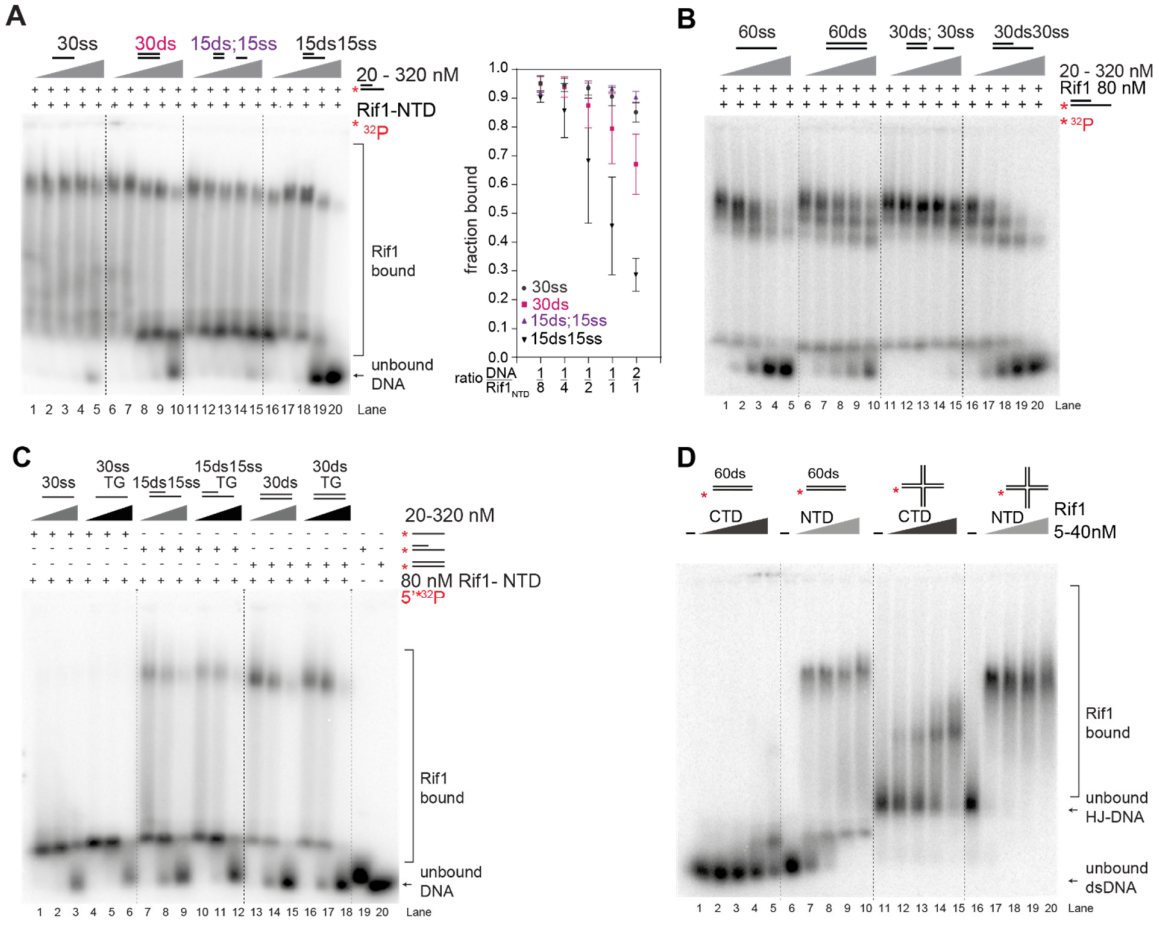

Figure 2.8 – Rif1-NTD exhibits a preference for 3'-tailed DNA. A, EMSA analysis using 1 nM ^{32}P-labeled 3'-tailed 15ds15ss junction DNA and 160 nM Rif1-NTD in all lanes. Unlabeled competitor DNA was added at increasing concentrations (20, 40, 80, 160 and 320 nM; an equimolar mixture of 15 nt ssDNA and 15 bp dsDNA). Quantification of experiments as shown in panel B. Binding to competitor substrates was measured by reappearing unbound DNA. (n = 3; mean ± s.e.m, independent experiments.) B, EMSA analysis (as A) using 1 nM ^{32}P-labeled 3'-tailed 30ds30ss junction DNA and 80 nM Rif1-NTD in all lanes. Unlabeled competitor DNA was added at increasing concentrations (20, 40, 80, 160 and 320 nM; equimolar mixture of 30 nt ssDNA and 30 bp dsDNA). C, Rif1-NTD does not preferentially bind telomeric TG sequences. EMSA analysis with 1 nM ^{32}P-labeled 30 nt ssDNA, 15 nt + 15 bp 3'-tailed DNA or 30 bp ds DNA substrates in lanes 1-6, 7-12 and 13-18, respectively, and 80 nM Rif1-NTD (lanes 1-18). Unlabeled competitor DNA with random or telomeric TG sequence was added at increasing concentrations (20 nM, 80 nM and 320 nM). D, Rif1-NTD binds to dsDNA and Holliday Junctions (HJ) ten-fold tighter than the Rif-C-terminal domain (CTD). EMSA analysis using 1 nM ^{32}P-labeled dsDNA or HJ-DNA titrated with increasing concentrations of Rif1-NTD (5, 10, 20 and 40 nM).

2.5 Site-directed mutagenesis of Rif1-NTD–DNA interaction site

The Rif1-NTD-DNA co-crystal structure shows that the DNA is wedged into the concave face of the Hook by Loop-II emerging from helical unit 9, identifying these regions as predominant protein-DNA interaction sites. In this configuration, the Shaft element of one Rif1-NTD monomer closes like a lid over the DNA buried inside the Hook of the dimer mate, completely surrounding the DNA (Figure 2.3). Plotting DNA proximity onto the surface of Rif1-NTD, we identified clusters of positively charged amino acids as potential protein-DNA contact points (Figure 2.9A and B). Despite differences in DNA binding between dimer mates in the Rif1-NTD head-to-tail dimer arrangement, there is a common set of positively charged residues in the Hook within 8 Å of the DNA (Figure 2.7C). In contrast, the less-conserved Shaft (Figure 2.2C) shows increased flexibility, which places different sets of residues proximal to the DNA in channels I and II across crystals. At the current resolution, this mobility and the resulting conformational disorder make it difficult to pinpoint key residues in the Shaft that might mediate DNA interactions.

On the concave face of the Hook the DNA is bound closest to helical units 4-8, which are part of the Rif1_N signature region defined by Pfam (helical units 1-8, see Figure 2.2D). Twelve positively charged residues in helical units 4-8 are positioned for potential DNA backbone contacts (Lys 406, 437, 451, 452, 514, 518, 563, 570, Arg 401, 565, 573, and His 561), as defined by the DNA proximity surface in (Figure 2.9A and B). These were targeted, and among several mutant versions of Rif1, a protein with amino acid substitutions K437E, K563E, and K570E (designated Rif1-NTD$_{HOOK}$; Figure 2.9A) was generated. Loop-II (residues 677-714) bears a cluster of six positively charged residues (K680, R688, K689, K691, K692, K706, K708), and we mutated two DNA-facing lysine residues (K691E and K692E) to generate a mutant designated Rif1-NTD$_{LOOP}$ (Figures 2.9A and B). Rif1-NTD$_{HOOK}$ and Rif1-NTD$_{LOOP}$ mutants were expressed recombinantly, purified and proved stable for investigation in recombinant form (Figure 2.9C and D). Rif1-NTD$_{HOOK}$ and Rif1-NTD$_{LOOP}$ were tested for DNA binding in EMSA assays using a 30 bp DNA duplex, the portion of the substrate visible in the crystal structure (Figure 2.9E). As shown in Figure 2.9E, DNA binding was compromised compared to wild-type Rif1-NTD, and ~4-fold higher protein concentrations of Rif1-NTD$_{HOOK}$ and Rif1-NTD$_{LOOP}$ were needed to bind the 30ds substrate. Additionally, Rif1-NTD$_{HOOK}$ and Rif1-NTD$_{LOOP}$ mutants were also compared to Rif1-NTD in competition experiments also revealing a less tight association of the Rif1-NTD mutants compared to the Rif1-NTD (Figure 2.9F). These experiments indicate that the regions within the Rif1-NTD involved in duplex DNA interactions in the crystal are also involved in DNA binding in solution.

Figure 2.9

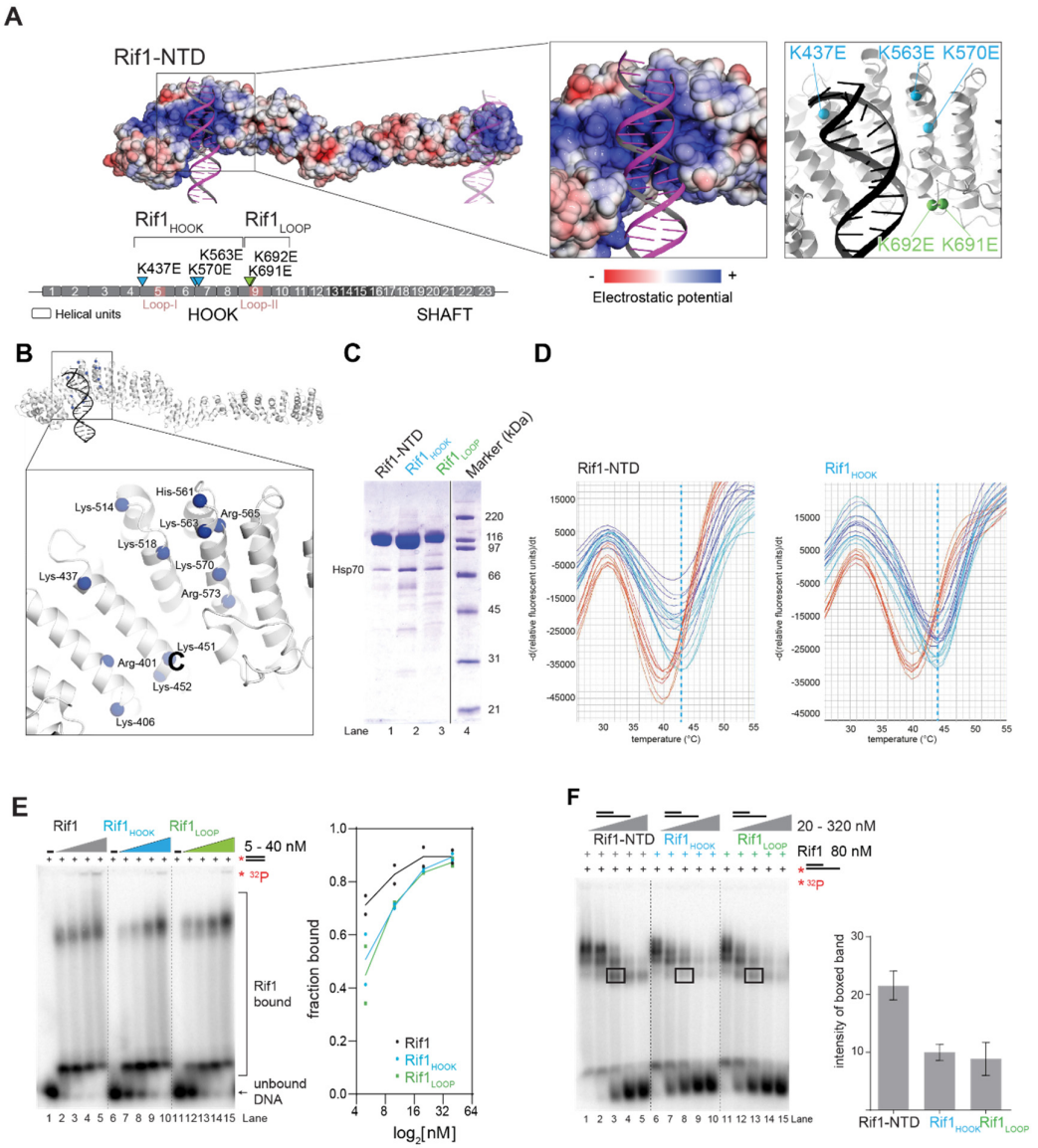

Figure 2.9 – Rif1-NTD mutants can be purified and are DNA binding deficient. A, Rif1-NTD surface electrostatic potential with a close-up view of the Rif1 HOOK domain. Schematic representation of Rif1-NTD (residues 100 to 1322) indicating the location of the Rif1$_{HOOK}$ (blue) and Rif1$_{LOOP}$ (green) mutations and their position in the Rif1 crystal structure relative to the DNA. B, Cartoon representation of Rif1-NTD Hook domain. The Cα positions of positively charged residues are highlighted. C, SDS-PAGE gel of purified Rif1-NTD variants, stained with Coomassie blue. Hsp70 was identified by mass spectrometry. D, Differential Scanning Fluorimetry of Rif1-NTD and Rif1$_{HOOK}$ mutant in three different buffers (100mM NaAc buffer pH5.5 (red), 100mM Bis-Tris pH7 (cyan) and 100mM Tris-HCl pH8 (blue)). The first derivative of the melt curve (peak curve) is shown representing the melting temperature at the peak. Rif1-NTD and Rif1HOOK show a melting temperature of 44 °C in Bis-Tris pH7. E, Rif1$_{HOOK}$ and Rif1$_{LOOP}$ mutants have a lower binding affinity for dsDNA than wild-type Rif1. EMSA analysis using 1 nM 32P-labeled 30 bp dsDNA with increasing concentrations (5, 10, 20 and 40 nM) of wild-type or mutant Rif1-NTD with quantification (individual values plotted and mean values presented, independent experiments). F, Rif1-NTD variants have decreased DNA binding affinity in competition EMSA analysis. EMSA analysis using 1 nM ^{32}P-labeled 3'-tailed 30ds30ss junction DNA and 80 nM Rif1-NTD WT or variants in all lanes. Unlabeled competitor DNA (30ds30ss junction DNA) was added at increasing concentrations (20, 40, 80, 160 and 320 nM). The boxed band was quantified relative to total signal in each lane and plotted and the intensity of the boxed band is reported (Mean values ± s.e.m. are plotted (n = 3)).

2.6 Rif1-NTD is required for telomere length regulation

To assess the *in vivo* functions of the Rif1-NTD and its capacity to bind DNA, we first addressed its potential involvement in telomere length control, the canonical role of Rif1 in yeast. Consistent with previous results (Shi et al., 2013), Rif1 occupancy at native telomeres, measured by chromatin immunoprecipitation (ChIP), was reduced by 97% compared to wild-type Rif1 when the major Rap1 binding site was disrupted ($Rif1_{RBM}$ mutant I1762R, I1764R) (Figure 2.10A, Figure 2.11A for protein expression). The $Rif1_{HOOK}$ DNA-binding mutant reduced the ChIP signal more moderately (~30%; Figure 2.10A). The $Rif1_{HOOK/RBM}$ double mutant further diminished the residual telomere occupancy of $Rif1_{RBM}$, indicating that the Rif1-NTD_{HOOK} and $Rif1_{RBM}$ together anchor Rif1 at telomeres (Figure 2.11B). Unexpectedly though, cells harboring the $rif1_{HOOK}$ allele exhibited a more severe telomere elongation phenotype (gain in length ~250 bp, phenocopying *rif1*Δ cells) than $rif1_{RBM}$ mutant cells (gain in length of ~150 bp) (Figure 2.10B and Figure 2.11C). Cells expressing Rif1-NTD_{LOOP} showed an intermediate telomere elongation phenotype, suggesting that Rif1-NTD_{HOOK} is the more severely compromised Rif1-NTD mutant *in vivo* (Figure 2.11C). Thus, while the Rif1 RBM represents the major means of Rif1 recruitment to telomeres, the DNA-binding Hook region and its ability to properly engage DNA is essential for mediating telomerase inhibition.

2.7 Rif1-NTD mediates the telomeric anti-checkpoint function of Rif1

In addition to inhibiting telomerase at normal-sized telomeres, Rif1 serves an anti-checkpoint function at eroded telomeres. This is evident in a model for critically short telomeres at HO endonuclease-induced DSBs flanked by short (80 bp) telomere repeat tracts (TG80), where Rif1 attenuates a transient DNA damage checkpoint response (Ribeyre and Shore, 2012). We determined cell-cycle restart times following induction of the HO endonuclease and found significant anti-checkpoint defects for cells harboring the $rif1_{HOOK}$ or $rif1_{LOOP}$ mutant alleles (Figure 2.10C). In contrast, $rif1_{RBM}$ mutant cells behaved like *RIF1* wild-type cells, whereas $rif1_{HOOK/RBM}$ double mutant cells displayed a G2/M cell-cycle delay greater than that of either of the single mutants, approaching a *rif1*Δ phenotype (Figure 2.10C).

Figure 2.10

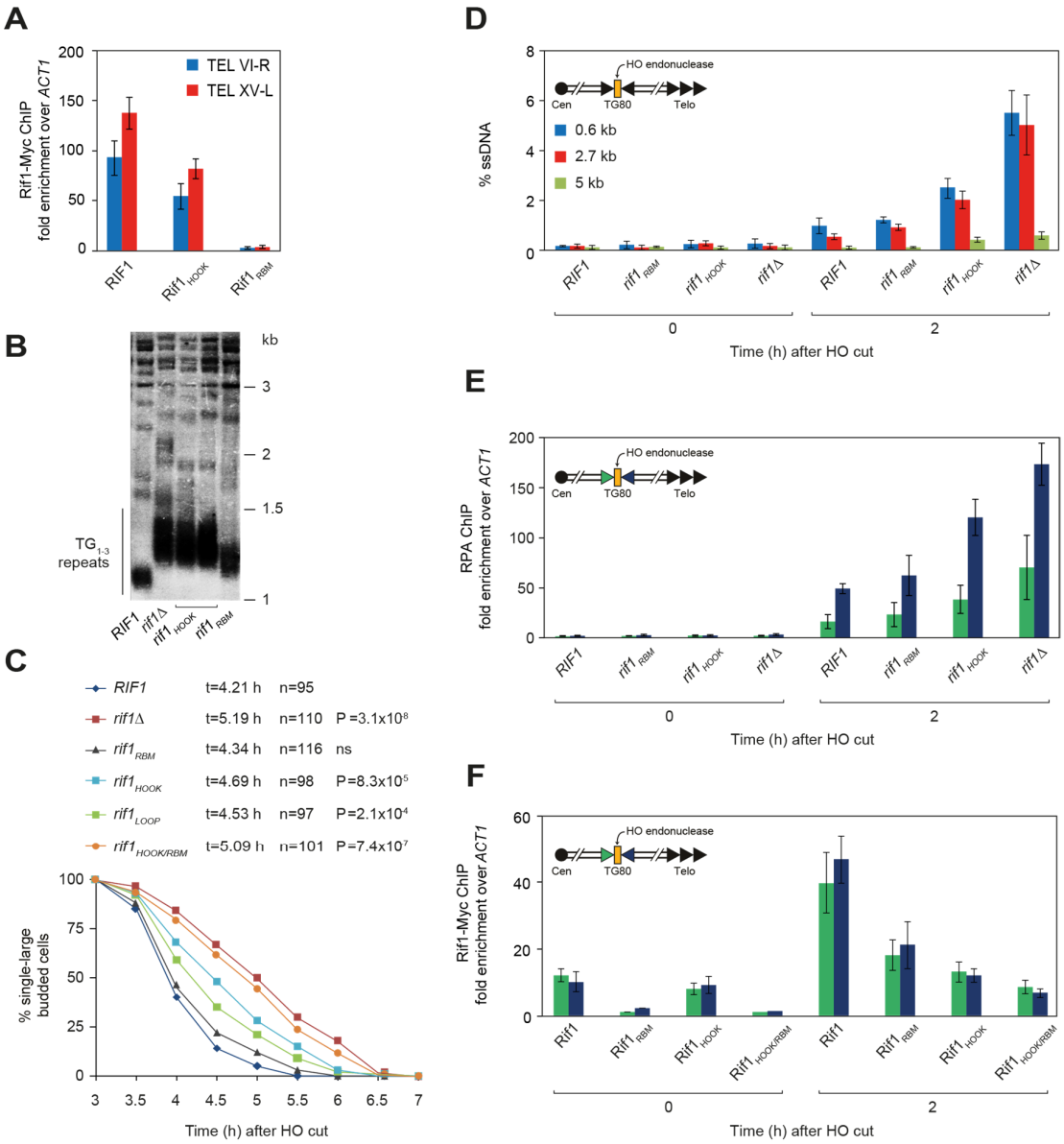

Figure 2.10 – Rif1-NTD is an effector of telomere homeostasis at native and critically short telomeres. A, ChIP analysis of Myc-tagged wild-type Rif1, or the indicated mutants, at native telomeres VI-R (blue) and XV-L (red). Results are reported as average fold-enrichment relative to ACT1 ± s.d. (n = 5). B, Telomere length analyzed at telomeric Y′ elements. Southern blots were performed with genomic DNA digested with XhoI using a radiolabeled TG1-3 repeat probe. C, Percentage of large-budded, G2/M-arrested cells following HO endonuclease induction in wild-type or rif1 mutant cells presented as Kaplan-Meier survival analysis. Average G2/M to G1 transition times (t), number of cells examined for each sample (n) and P-values are indicated. D, Percentage of ssDNA formed at three sites of increasing distance from a TG80-flanked DSB HO cut site, reported as mean values ± s.d. (n = 4). E, ChIP analysis of RPA recruitment at a TG80-flanked DSB in the indicated strains. Results for centromere-proximal (green) and telomere-proximal (blue) RPA accumulation are reported as average fold-enrichment relative to ACT1 ± s.d. (n = 4). F, ChIP analysis at either side of a TG80-flanked DSB of cells expressing Myc-tagged Rif1 wild-type and the indicated mutants before (0 h) and after (2 h) HO endonuclease induction, reported as average fold-enrichment relative to ACT1 ± s.d. (n = 4).

Figure 2.11

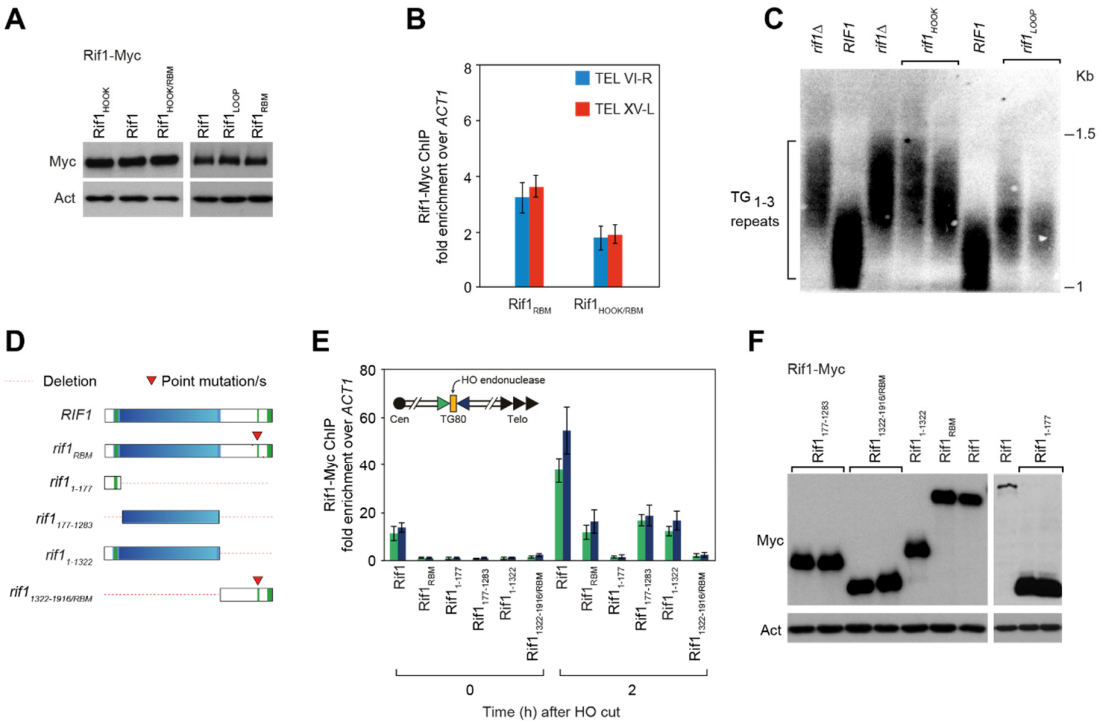

Figure 2.11 – Rif1-NTD is important for telomere length regulation. A, Rif1 mutants used in this study are expressed at levels comparable to wild-type. Western blot analysis of the indicated 13xMyc-tagged Rif1 proteins expressed from the endogenous RIF1 *locus in yeast. Actin (Act) was used as a loading control. B, ChIP analysis of the recruitment of 13xMyc-tagged $Rif1_{RBM}$ and $Rif1_{HOOK/RBM}$ mutants at two native telomeres (TEL VI-R and XV-L). Results are presented as mean values of fold-enrichment relative to* ACT1 *± s.e.m. (*n *= 4). C, Telomere length analysis of the indicated strains, performed as described in Fig. 3.4. D, Schematic representation of wild-type and mutant* RIF1 *forms used for the ChIP and Western blot analyses presented in panels E and F. E, ChIP analysis of 13xMyc-tagged versions of Rif1 at a TG80-flanked HO-induced DSB. Results for the centromere-proximal (green) and telomere-proximal side (blue) of the HO site are reported as mean values ± s.e.m. (*n *= 3). F, Western blot analysis showing the levels of expression of the indicated 13xMyc-tagged Rif1 proteins.*

Checkpoint activation at TG80-flanked DSBs in the absence of Rif1 involves 5′ end resection, generating 3′-terminated ssDNA bound by RPA (Ribeyre and Shore, 2012), which provides the signal for activation of the apical ATR (Mec1) checkpoint kinase. We observed an increase in both ssDNA (Figure 2.10D) and RPA binding (Figure 2.10E) at TG80 ends after HO cut induction in the *$rif1_{HOOK}$* mutant compared to wild-type or the *$rif1_{RBM}$* mutant, despite $Rif1_{RBM}$ and $Rif1_{HOOK}$ exhibiting a similar level of recruitment (Figure 2.10F; Figure 2.11D – F). These findings are consistent with a Rif1 Hook mediated anti-checkpoint effector function.

Figure 2.12

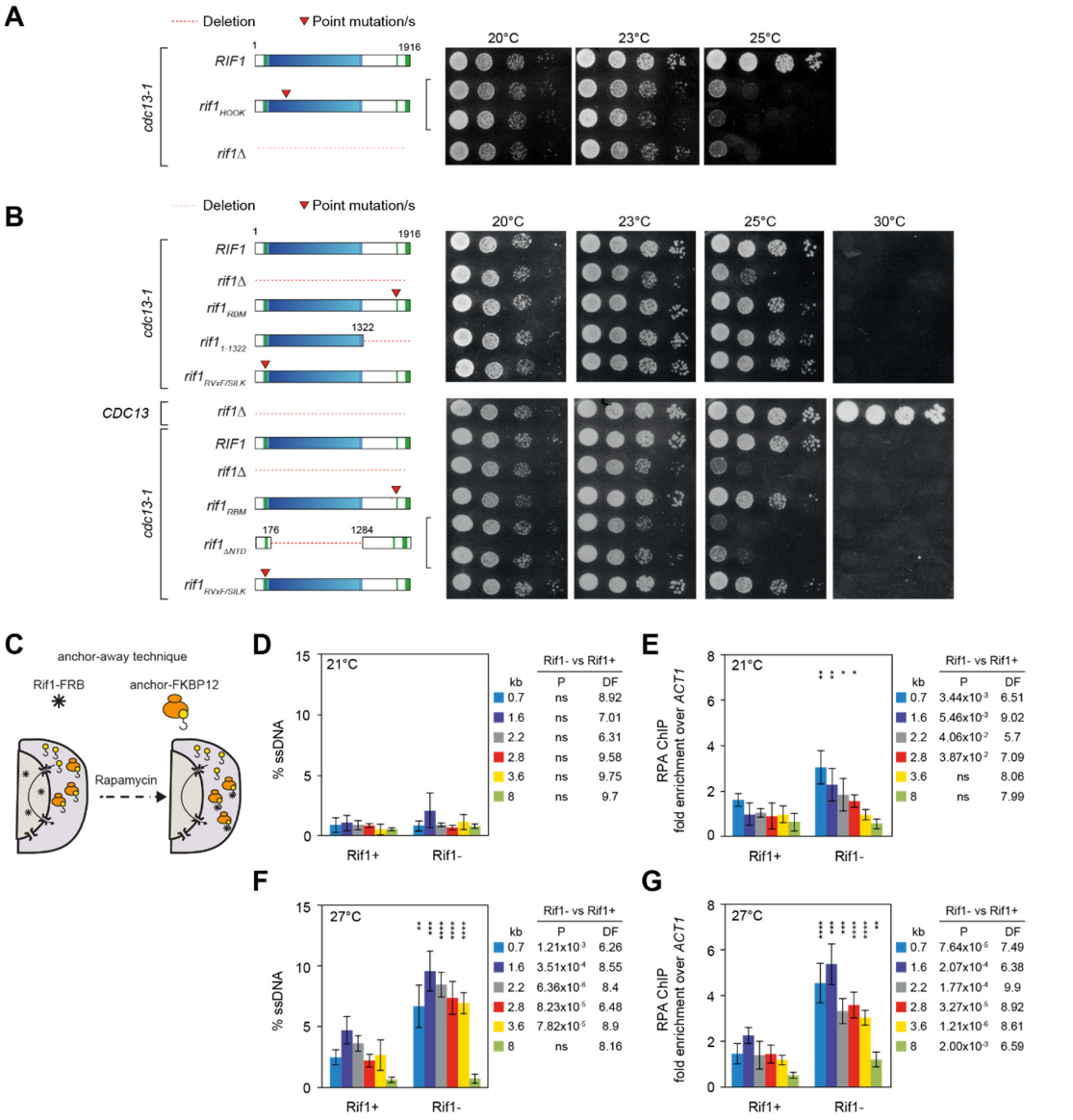

Figure 2.12 - Rif1-NTD prevents resection of uncapped chromosome ends and promotes survival of cdc13-1 cells. A, Rif1-NTD is required for viability of cdc13-1 *cells with uncapped telomeres. Drop assay of* cdc13-1 *cells harboring the indicated* RIF1 *alleles. Serial 10-fold dilutions of cells were spotted on YPAD plates and incubated at the indicated temperatures for 48 h. B, The Rif1-NTD, but not Rap1 or protein phosphatase PP1/Glc7 interactions, is essential for the function of Rif1 in promoting growth when* cdc13-1 *related chromosome uncapping has occurred.* CDC13 *wild-type control cells and isogenic* cdc13-1 *mutants expressing* RIF1 *wild-type or the indicated* rif1 *alleles were spotted on YPAD medium and incubated at the indicated temperatures for 48 h. C, Schematic representation of the anchor-away technique used for rapid depletion of Rif1 from the nucleus (avoiding confounding effects relating to chronic telomere elongation in* RIF1*-deleted cells), using a rapamycin-dependent interaction between FRAP (FRB) and FKBP12. Rif1 was FRB tagged; the ribosomal protein RPL13A (anchor) was tagged with FKBP12. (D-G) Rapid depletion of Rif1 from the nucleus increases resection at uncapped telomeres. Percentage of ssDNA was determined by qPCR or RPA recruitment determined by ChIP at the indicated distances to native telomere VI-R in* cdc13-1 *cells. ChIP results are reported as average fold-enrichment relative to* ACT1*. Cells were mock-treated (Rif1+) or rapidly depleted for Rif1 by rapamycin addition (Rif1-) at the permissive temperature of 21°C, or after a shift to the restrictive temperature of 27°C for 2 h. An unequal variance t-test was used to compare mean values ± s.d of independent biological replicates (*n *= 6) of Rif1+ and Rif1- cultures. P-values, * = P < 0.05; ** = P < 0.01; *** = P < 0.001; **** = P < 0.0001, Degrees of freedom (DF)*

We then used strains carrying *cdc13* temperature-sensitive (ts) mutations, which exhibit no overt telomere abnormalities at the permissive temperature, but show telomere uncapping and synthetic lethality following deletion of *RIF1* (Anbalagan et al., 2011; Xue et al., 2011; Zubko et al., 2004). We found that the Rif1 Hook, but not the Rif1 RBM, is required for viability in *cdc13-ts* strains (Figure 2.12A-B) and that Rif1 attenuates resection of chromosome ends and RPA binding upon depletion from the nucleus (Figure 2.12C-G) (Haruki et al., 2008). Thus, different models of critically short and uncapped telomeres show that the Rif1 Hook domain and its ability to directly engage with its DNA substrate is required to counteract DNA end resection and silence the DNA damage checkpoint.

2.8 An evolutionarily conserved role of Rif1 in DSB repair, mediated by the Rif1-NTD

A Rif1 Hook-mediated mechanism of attenuating DNA end resection at TG80-flanked DSBs and eroded telomeres, independent of Rap1-binding, suggested a possible role of Rif1 at DNA breaks outside telomeric settings, akin to the DNA repair role of mammalian Rif1. We used a reporter strain, in which an HO endonuclease-induced DSB at the *MAT* locus can only be repaired by NHEJ (Figure 2.13A), providing a cell survival-based readout for NHEJ efficiency (Horigome et al., 2016; Lee et al., 1999; Moore and Haber, 1996). Compared to *RIF1* wild-type cells, we observed a ~40% drop in cell survival for *rif1*Δ mutants as measured by colony outgrowth following 2 h or 4 h of transiently induced HO endonuclease expression (Figure 2.13B). Following chronic HO endonuclease expression, which only allows survival through rare imprecise NHEJ events that alter the DNA sequence of the HO cut site (Moore and Haber, 1996), we also observed a significant decrease in viability for *rif1*Δ compared to *RIF1* wild-type cells (Figure 2.14A). As expected, survival under acute or chronic HO endonuclease expression conditions was fully dependent on the core NHEJ factor Ku70 (Boulton and Jackson, 1996; Mages et al., 1996; Siede et al., 1996) (Figure 2.13B, Figure 2.14A). These findings establish Rif1 as a modulator of DSB repair by promoting NHEJ in yeast.

Figure 2.13

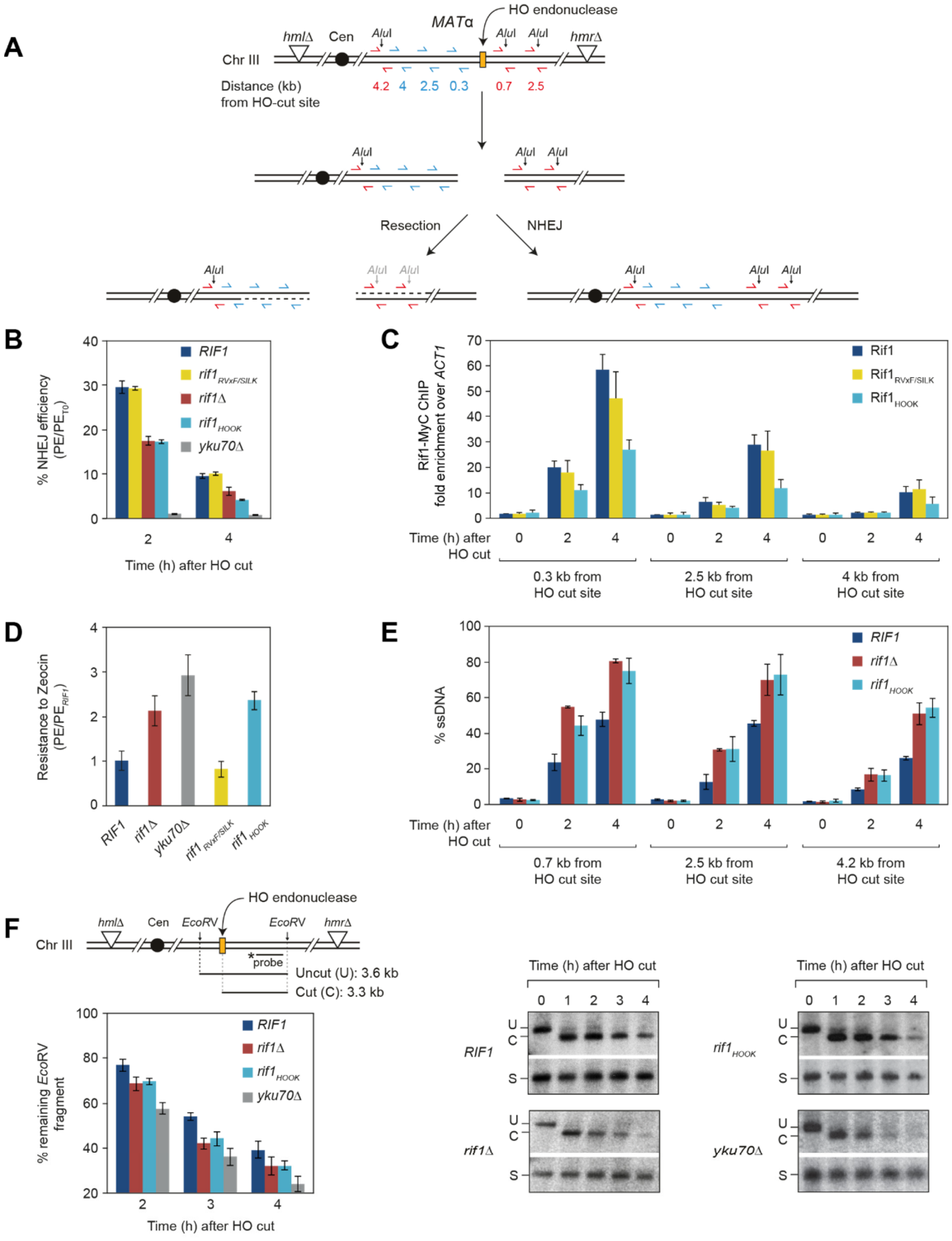
A
HO endonuclease
MATα
hmlΔ
Cen
AluI
hmrΔ
Chr III
Distance (kb) from HO-cut site
4.2 4 2.5 0.3 0.7 2.5
Resection
NHEJ
B
% NHEJ efficiency (PE/PE$_{T0}$)
RIF1
rif1$_{RVxF/SILK}$
rif1Δ
rif1$_{HOOK}$
yku70Δ
Time (h) after HO cut
C
Rif1-Myc ChIP fold enrichment over ACT1
Rif1
Rif1$_{RVxF/SILK}$
Rif1$_{HOOK}$
Time (h) after HO cut
0.3 kb from HO cut site
2.5 kb from HO cut site
4 kb from HO cut site
D
Resistance to Zeocin (PE/PE$_{RIF1}$)
RIF1
rif1Δ
yku70Δ
rif1$_{RVxF/SILK}$
rif1$_{HOOK}$
E
% ssDNA
RIF1
rif1Δ
rif1$_{HOOK}$
Time (h) after HO cut
0.7 kb from HO cut site
2.5 kb from HO cut site
4.2 kb from HO cut site
F
HO endonuclease
hmlΔ
Cen
EcoRV
EcoRV
hmrΔ
Chr III
probe
Uncut (U): 3.6 kb
Cut (C): 3.3 kb
% remaining EcoRV fragment
RIF1
rif1Δ
rif1$_{HOOK}$
yku70Δ
Time (h) after HO cut
Time (h) after HO cut
RIF1
rif1Δ
rif1$_{HOOK}$
yku70Δ
U
C
S

Figure 2.13 – Rif1-NTD attenuates end-resection at chromosome-internal DSBs to promote DNA repair by NHEJ. A, Overview of S. cerevisiae chromosome III harboring the MATα HO endonuclease cut site and deleted for the homologous donor loci (hmlΔ/hmrΔ). HO endonuclease is induced by galactose addition and the resulting DSB can only be repaired by NHEJ. Primer pairs used for ChIP analyses of Rif1-Myc recruitment (blue) and qPCR to study DNA end-resection (red) are indicated. DNA end-resection progressively destroys the annotated AluI restriction sites, leading to increased qPCR product yield, which serves as a measure for the level of ssDNA formation44. B, NHEJ efficiency measured by colony outgrowth after acute HO endonuclease induction. Data are presented as mean values ± s.e.m. (n = 6). PE, plating efficiency, PET0, plating efficiency before HO endonuclease induction. C, ChIP analysis of the recruitment of Myc-tagged wild-type and mutant versions of Rif1 at the MATα HO endonuclease cut site. Results are reported as average fold-enrichment relative to the ACT1 gene ± s.d. (n = 3). D, Cell viability in the presence of 70 µg/mL Zeocin. Data are presented as mean values ± s.e.m. (n = 6). E, ssDNA formed by DNA end-resection as measured by qPCR. Data are presented as mean values ± s.e.m. (n = 4).F, Analysis of DSB ends destabilization by Southern blotting. Top left, Schematic representation of the MATα locus. The location of the Southern probe, the EcoRV restriction sites used for DNA digestion, and the size of the detected bands are indicated. Bottom left, percentage of remaining DNA relative to the 1 h time point. Data are presented as mean values ± s.e.m. (n = 4). Right, representative Southern blots. The SMC2 locus (designated S) served as a loading control and for normalization.

In a structure-function analysis, we found that cells expressing a C-terminally truncated Rif1 missing the Rap1 interaction motifs (RBM and CTD) did not exhibit a NHEJ phenotype (Figure 2.14B). The ability of Rif1 to modulate NHEJ thus resides in its N-terminal region and is independent of Rap1. Expression of $Rif1_{RVxF/SILK}$ also gave no phenotype, demonstrating that recruitment of PP1/Glc7 to DSBs is not required for Rif1 to facilitate NHEJ repair (Figure 2.13B). In contrast, cells expressing the $Rif1_{HOOK}$ DNA-binding mutant were as compromised in survival by NHEJ as *rif1*Δ cells (Figure 2.13B). Consistent with a previous report (Martina et al., 2014), ChIP analyses showed that Rif1 accumulated at chromosome-internal DSBs (Figure 2.13C, Figure 2.14C). Rif1 binding at chromosome-internal sites devoid of telomeric DNA sequences was independent of the RBM Rap1 interaction motif (Figure 2.14C-D). Importantly, however, DSB binding required the Rif1 Hook, and the NHEJ defect of the $Rif1_{HOOK}$ mutant correlated with ~50% reduction in Rif1 protein levels at DSBs at the *MAT* locus and elsewhere in the genome (Figure 2.13C, Figure 2.14C). We conclude that the Rif1-NTD, and its DNA binding ability, is necessary and sufficient for the role of Rif1 in promoting NHEJ at induced DSBs.

We then examined the effect of Rif1 at stochastic breaks. Genetic disruption of NHEJ in yeast does not cause overt DNA damage sensitivity, but instead leads to a survival advantage in the presence of exogenous DSBs, consistent with HR being the preferred pathway for DSB repair under these conditions (Clikeman et al., 2001; Zhang et al., 2007). The contribution of NHEJ to break repair is evident in HR-deficient cells, where loss of NHEJ factors causes increased DNA damage sensitivity (Boulton and Jackson, 1996; Mages et al., 1996; Siede et al., 1996). We found that deletion of *RIF1* increased cell survival upon chronic exposure to the radiomimetic drug Zeocin ~2-fold compared to wild-type cells. This effect was very similar to the phenotype caused by disruption of core end-joining factors such as *YKU70* (Figure 2.13), and was mediated by the Rif1 Hook domain, but

independent from PP1/Glc7 and Rap1 interactions (Figure 2.14E). In HR-deficient cells, which depend on NHEJ for DSB repair, loss of *RIF1* increased sensitivity to Zeocin (Figure 2.14F). These results demonstrate that the Rif1-NTD also functions in NHEJ at stochastic DNA breaks.

We found that loss of Rif1 or introduction of the Hook mutation resulted in a marked increase in ssDNA accumulation compared to *RIF1* wild-type at the HO endonuclease cleavage site near the *MAT* locus (Figure 3.5A, E). Similar results were obtained at the *MNT2* locus (Figure 2.14G). Consistent with these findings, Southern blot analyses showed that the stability of a genomic fragment harboring the *MAT* locus after HO endonuclease cleavage was reduced in *rif1*Δ and $rif1_{HOOK}$ mutant cells compared to *RIF1* wild-type cells (Figure 2.13F). Taken together, these findings show that Rif1 binds DSBs *in vivo* and attenuates DNA end resection, facilitating re-ligation by the NHEJ pathway. The role of Rif1 in DSB repair pathway choice is thus conserved from yeast to human, and the Rif1-NTD DNA-binding domain is required for all functions of Rif1 involving telomeric and non-telomeric DNA ends.

Figure 2.14

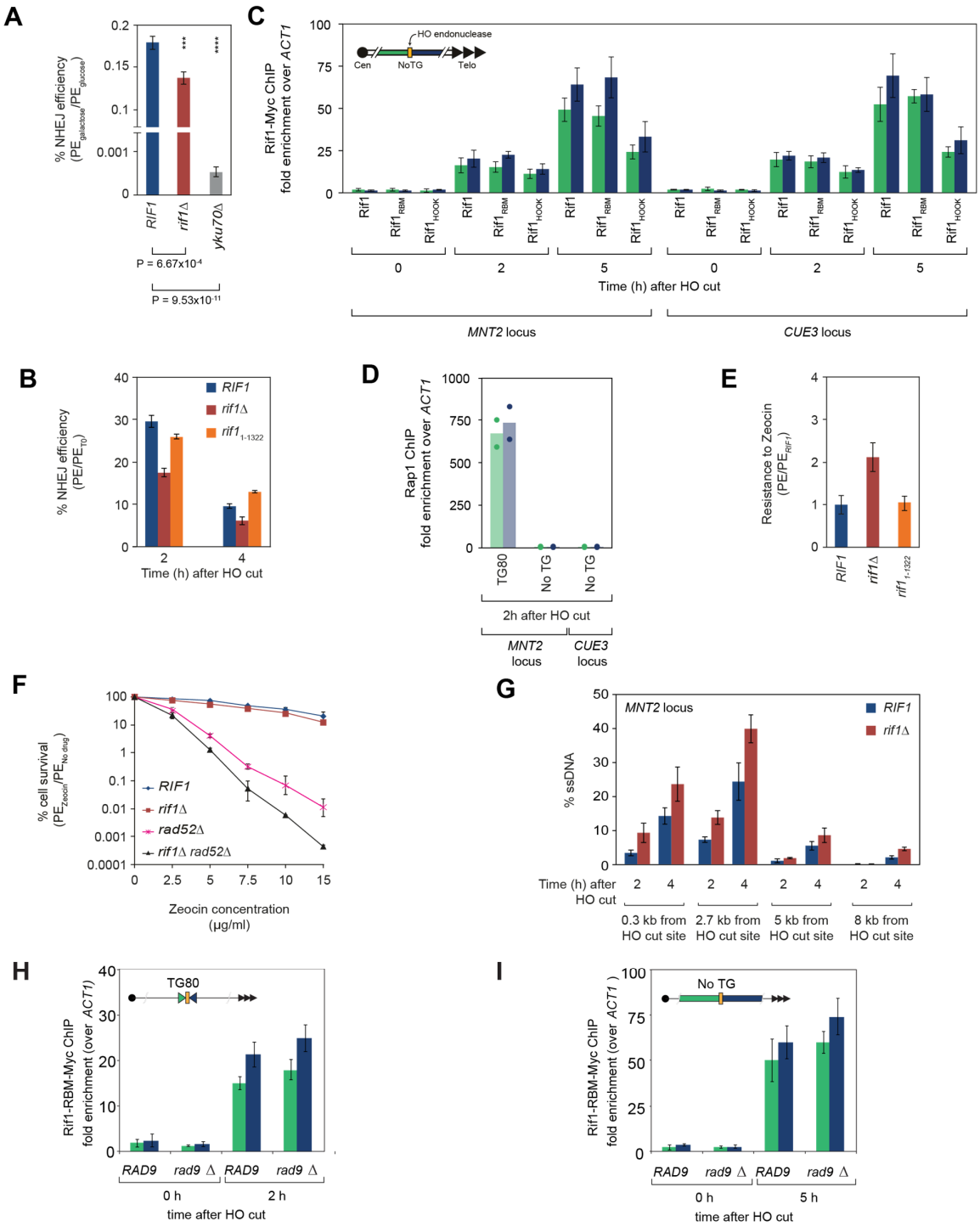

Figure 2.14 – Rif1 is recruited to DSBs at different genomic locations and promotes NHEJ. A, NHEJ efficiency of a DSB at the MATα *locus measured by colony outgrowth under chronic HO endonuclease induction. Results are presented as mean values ± s.e.m. (*n = 6, DF = 15*). Statistical analysis: one-way ANOVA. PE, plating efficiency. P-values, *** = P < 0.001; **** = P < 0.0001. B, The Rif1 N-terminus modulates NHEJ. Transient HO induction as described in Fig. 4b. Results are presented as mean ± s.e.m. (*n = 6*). PE$_{T0}$, plating efficiency without HO induction. C, Rif1 accumulates at DSBs in the absence of*

telomeric repeats and independently of Rap1. ChIP analysis of 13xMyc-tagged wild-type and mutant versions of Rif1 at HO cut sites near indicated loci (No TG, not flanked by telomeric TG_{1-3} repeats). Results for centromere-proximal (green) and telomere-proximal (blue) Rif1 accumulation are reported as average fold-enrichment relative to ACT1 *± s.d. (*n *= 5). D, Rap1 does not associate with No-TG DSBs. ChIP analysis of Rap1 binding in the proximity of No-TG or TG80-flanked HO cut sites near the indicated loci. Results for centromere-proximal (green) and telomere-proximal (blue) Rap1 accumulation are reported as average fold-enrichment relative to* ACT1 *(*n *= 2, mean and individual values plotted). E, Increased Zeocin resistance associated with loss of* RIF1 *is not observed for cells with a Rif1 C-terminal truncation (*$rif1_{1-1322}$*). Cell viability was determined as in Fig. 4d. Results are presented as mean ± s.e.m. (*n *= 4). F, Loss of* RIF1 *in an HR-deficient* rad52Δ *strain further sensitizes cells to Zeocin. Cell viability upon increasing concentrations of Zeocin determined by colony outgrowth and presented as mean values ± s.e.m. (*n *= 4). G, Increased DNA end-resection at an HO cut near the* MNT2 *locus in the absence of* RIF1*. ssDNA levels determined by qPCR and presented as mean values ± s.e.m. (*n *= 3). H, I, Cells with RAD9 or rad9Δ genotype were assessed for* $Rif1_{RBM}$ *recruitment at TG80 or No-TG ends before and after HO cleavage. The* rif_{RBM} *mutant was used to assess the recruitment of Rif1 independently of its binding to Rap1. Deletion of the RAD9 gene does not affect the recruitment of* $Rif1_{RBM}$ *at these ends. Results are presented as mean ± s.e.m. (*n *= 3)*

Table 2.1 Crystallographic data collection and refinement statistics.

	RIF1-NTD-1 (PDB code 5NVR)	RIF1-NTD–DNA-1	RIF1-NTD–DNA-2 (PDB code 5NW5)
Data collection[a]			
Wavelength (Å)	0.9790	1.0000	0.9186
Space group	$P6_522$	$P2_12_12_1$	$P2_12_12_1$
Unit cell (Å)	$a = b = 203.57$, $c = 197.723$	$a = 81.93$, $b = 157.60$, $c = 385.19$	$a = 92.16$, $b = 169.88$, $c = 390.26$
Resolution (Å)[b]	50–3.94 (4.16–3.94)	58.02–4.40 (4.64–4.40)	43.25–6.50 (7.27–6.50)
Unique reflections	21894 (3132)	32678 (4704)	12703 (3529)
Multiplicity	50.6 (42.7)	6.3 (5.8)	11.9 (12.5)
Completeness (%)	100 (100)	99.9 (100)	99.6 (100)
$\langle I/\sigma(I)\rangle$	14.4 (1.3)	5.5 (0.6)	8.0 (0.5)
$CC_{1/2}$ outer shell; no. of pairs	0.497; n =3129	0.172; n =4689	0.142; n = 3529
Resolution (Å) where			
$\langle I/\sigma(I)\rangle > 2.0$ (overall)	4.16	6.10	7.56
$\langle I/\sigma(I)\rangle > 2.0$ (along h)	-	6.11	7.83
$\langle I/\sigma(I)\rangle > 2.0$ (along k)	-	8.10	10.16
$\langle I/\sigma(I)\rangle > 2.0$ (along l)	-	5.25	7.11
$CC_{1/2} > 0.3$ (overall)	3.94	4.96	7.09
$CC_{1/2} > 0.3$ (along h)	-	4.76	7.19
$CC_{1/2} > 0.3$ (along k)	-	7.01	9.91
$CC_{1/2} > 0.3$ (along l)	-	5.25	6.50
R_{meas}	0.234 (4.131)	0.264 (3.294)	0.358 (6.001)
R_{pim}	0.033 (0.629)	0.114 (1.496)	0.101 (1.757)
Wilson B-factor (A^2)[c]	183	220	389
Refinement			
Resolution range (Å)	49.29–3.94 (4.09–3.94)	-	43.25–6.50 (7.15–6.50)
Reflections	21814 (2125)	-	8873 (732)
Reflections (R_{free})	1132 (115)	-	578 (59)
Completeness (%)	100 (100)	-	70.0 (23.9)
Complete to resolution (Å)	3.94	-	9.09
R_{work} / R_{free}	0.2115 / 0.2609	-	0.2529 / 0.2772
No. non-hydrogen atoms	8691	-	18864
Average B-factor ($Å^2$)		-	
Protein / DNA	221 / -	-	316 / 547
R.m.s bonds (Å) / angles (°)	0.003 / 0.54	-	0.015 / 2.12
Ramachandran plot (%)[d]			
Favored	91	-	85.8
Allowed	7.2	-	11.3
Outliers	1.6	-	2.9

[a]All data sets collected from single crystals

[b]Values in parenthesis are for the highest-resolution shell

[c]From *phenix.xtriage*

[d]From *Molprobity*

3 CHAPTER 3 – RESULTS: HUMAN RIF1-NTD BIND TO 53BP1 USING A PHOSPHORYLATED MOTIF

This Chapter contains unpublished data. All experiments were planned and performed by me apart from the *in vivo* analysis (Figure 3.2A-C). The *in vivo* data were obtained by Cristina Escribano-Diaz, Durocher Laboratory (The Lunenfeld-Tanenbaum Research Institute, Toronto, Canada).

3.1 The predicted structure of human RIF1

Human RIF1 has a similar architecture compared to the budding yeast counterpart (Figure 3.1A– B). Being comprised of 2472 amino acids, RIF1 also has an N-terminal domain (NTD) and a C-terminal domain (CTD) containing the RVxF/SILK motif and a region, which was shown to bind DNA biochemically in mammals (Sukackaite et al., 2014; Xu et al., 2010). Multiple sequence alignments for the whole sequence can only be calculated within fungi and vertebrate separately using the sequence conservation server ConSurf (Figure 3.1A and B) (Ashkenazy et al., 2016; Ashkenazy et al., 2010; Celniker et al., 2013). The only part of Rif1, which can be aligned from yeast to human is the Pfam domain within the N-terminal Hook (Pfam: Rif1_N; PF12231) (Figure 2.2D).

The RIF1-NTD spans the first 1000 amino acids of the protein and is predicted to also form an alpha-helical repeat as budding yeast Rif1 (Jones and Cozzetto, 2015; Yang et al., 2015). In contrast to the budding yeast form, the structured domain in RIF1 is predicted to start with the first residues of the molecule based on secondary and tertiary structure predictions (Figure 3.1B and D). It is remarkable that both N-terminal alpha-helical repeats are predicted to span an equal length of residues even though mammalian RIF1 is 1.3- fold more extended.

Having solved the *S.cerevisiae* Rif1-NTD structure (Figure 3.1E), we attempted to model the structure of the RIF1-NTD. Phyre² and RaptorX predict a very similar alpha-helical shape for the N-terminal Hook domain whereas the models do not agree on the Shaft domain (Figure 3.1F) (Kallberg

Figure 3.1

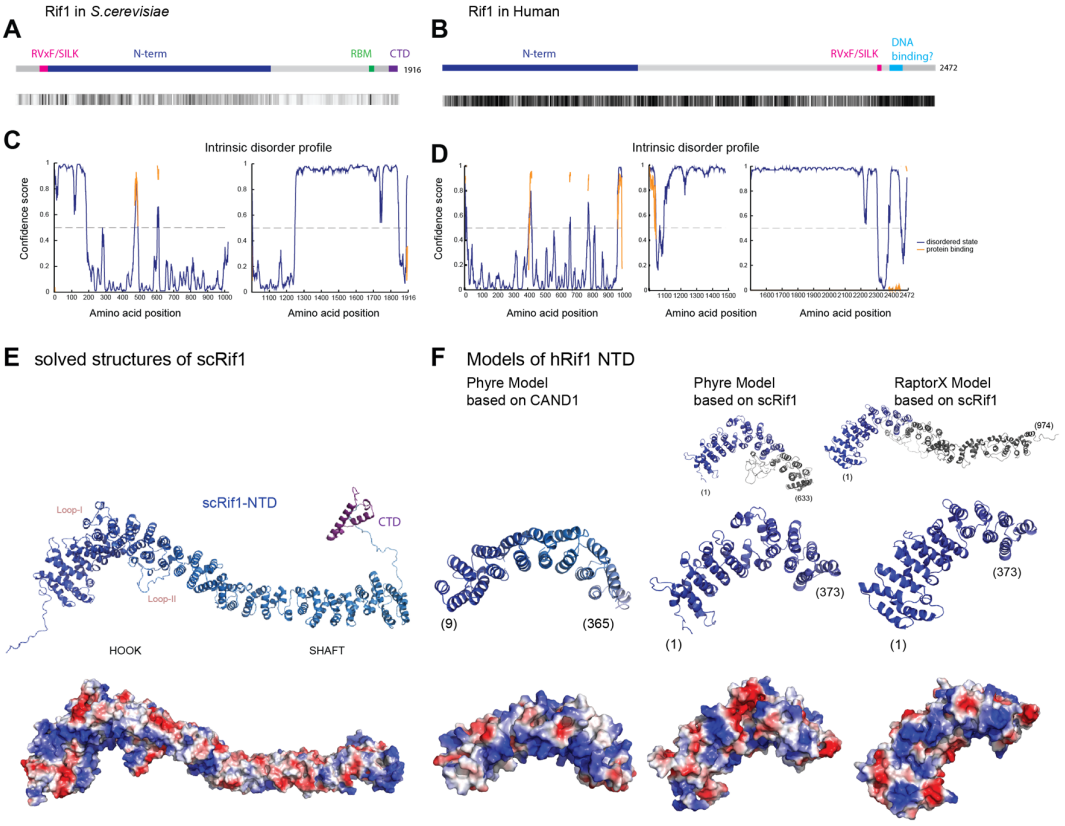

Figure 3.1 – Modeling hRif1. A, B, To scale representation of S.cerevisiae and human Rif1, respectively, and depiction of conservation over the protein using the same parameters (see methods Chapter 4). C, D, Intrinsic disorder analysis of S.cerevisiae and human Rif1, respectively, using DISOPRED. E, Cartoon and electrostatic surface representation of the solved Rif1-NTD and Rif1-CTD structure (CTD from Shi.et al (2013)). F, Structural models of the hRif1-NTD using Phyre² and RaptorX protein structure prediction. Structural models were based on scRif1 or CAND1 (Cullin-Associated and Neddylation-Dissociated 1). All models agree on a Hook like structure of the RIF1-NTD in its N-terminal region up to residue 365.

et al., 2012; Kelley et al., 2015). Both modeling servers calculate models on the basis of the budding yeast Rif1 structure. This raises the question of whether the resulting models are biased. However, when Phyre² bases the structural modeling on the N-terminal HEAT-repeat structure of CAND1 (a key assembly factor of Skp, Cullin, F-box containing E3 ubiquitin ligase complexes), the Hook domain adopts a very similar fold. Thus, based on different templates the N-terminal part of the RIF1-NTD is predicted to also form an alpha-helical repeat analogous to the HEAT-like Rif1 Hook domain.

While the budding yeast Rif1 Hook domain was characterized by a positively charged concave surface lined by 12 lysine, arginine, or histidine residues, it seems that the RIF1-NTD might only have positively charged patches on the concave surface. One explanation could be that RIF1, in contrast to Rif1, does not bind DNA directly but instead binds to a mediator protein. In summary,

structural modeling of RIF1 indicates that the RIF1 also has a structured alpha-helical NTD of the same length as Rif1 containing an N-terminal Hook-like structure.

3.2 The human RIF1-NTD binds directly to a phosphorylated 53BP1 motif

In order for DSBs to be channeled into NHEJ instead of HR, 53BP1 needs to be recruited to the DSBs and co-localize with Rif1. Several groups showed that RIF1 is the key downstream effector of 53BP1 in order to fulfill the decision making step in DSB repair (Chapman et al., 2013; Escribano-Diaz et al., 2013; Zimmermann et al., 2013). U2OS cells readily form 53BP1-Rif1 irradiation induced co-localization foci, and the N-terminal S/T-Q sites of 53BP1, as well as the RIF1-NTD structured part, are required for this co-localization (Escribano-Diaz et al., 2013). However, it is currently not known whether 53BP1 and RIF1 directly interact or whether they need a mediator protein. In order to assess which part of 53BP1 is required for a co-localization and to test whether 53BP1 and RIF1 interact directly, different deletion constructs of 53BP1 were cloned and tested for their ability to co-localize with RIF1. All constructs contained the region critical for 53BP1 focus formation (FFR: Focus formation region consisting of the oligomerization domain (OD), tandem-Tudor domain (Tudor) and the ubiquitin-dependent recruitment motif (UDR)) and a varying region of the N-terminal region (Figure 3.2A). Surprisingly, only a very small motif of 53BP1 (145-182) was required to resemble a RIF1-53BP1 co-localization wild-type phenotype. This motif contains three of the previously published 28 S/T-Q sites (Ser-166, Ser-176, Ser-178). When these three sites (designated 3xAla) were mutated in a fusion construct containing the N-terminal 145-182 peptide and the FFR, co-localization was completely abrogated. By mutating A176S and A178S sites back to the original serine residue, the 53BP1-RIF1 co-localization phenotype is mostly restored to wild-type levels (Figure 3.2B). Followed by a thorough analysis of mutating every residue individually within this peptide, a sequence motif required for the 53BP1-Rif1 focus formation emerged: LxLSQSQ (Figure 3.2C). This implicates that 53BP1 interacts directly or indirectly with RIF1 via this motif.

Figure 3.2

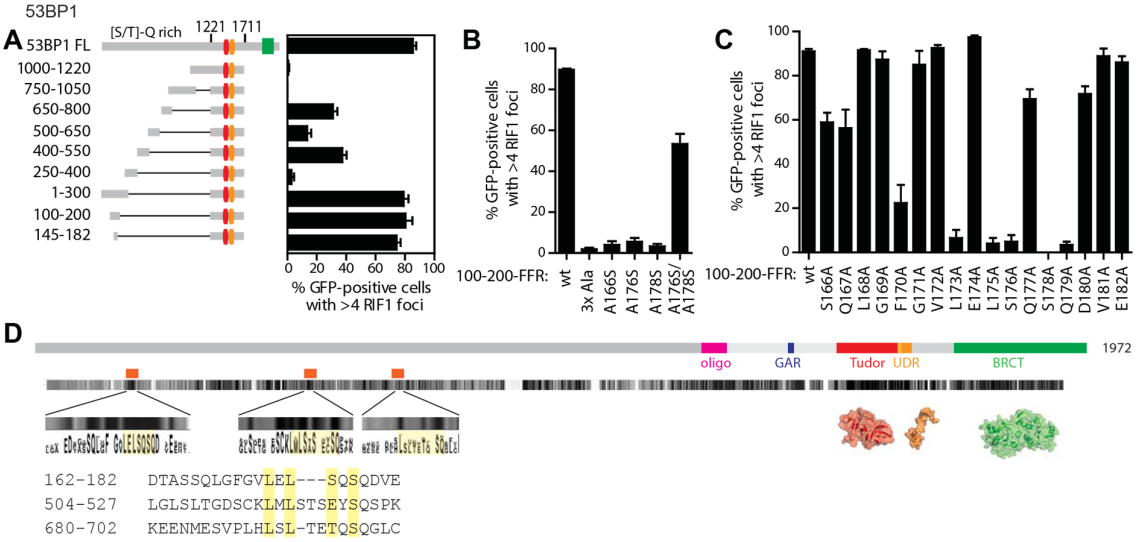

Figure 3.2 – hRif1-NTD is recruited to 53BP1 sequence motif. A, U2OS cells were transfected with siRNA duplex targeting 53BP1. After 24 h cells were transfected with the indicated GFP-tagged siRNA-resistant 53BP1 expression vectors. 24 h post-vector transfection cells were irradiated (10 Gy dose). 1 h post-irradiation cells were fixed and processed for RIF1 immunofluorescence. Data are represented as the mean ± SEM (n=3). B, 53BP1-depleted U2OS cells were transfected with vectors expressing the indicated GFP-53BP1 mutants (100-200 fused to the focus-formation region (FFR; residues 1221-1711) harboring no mutation (wt) or one to three point mutations). 3xAla= S166A, S176A, S178A. 24 h post-vector transfection cells were irradiated (10 Gy) and processed for RIF1 immunofluorescence 1 h post-irradiation. Data are represented as the mean ± SEM (n=3). C, 53BP1-depleted U2OS cells were transfected with vectors expressing the indicated GFP-53BP1 mutants (100-200 fused to the focus-formation region (FFR; residues 1221-1711) harboring no mutation (wt) or one point mutations), irradiated (10 Gy) and processed for RIF1 immunofluorescence. Data are represented as the mean ± SEM (n=3). D, To scale representation of 53BP1 and conservation analysis highlighting three N-terminal motifs. In particular the first motif spanning residues 162-182 is conserved across vertebrate.

53BP1 is conserved among metazoans and a multiple sequence alignment shows that the structured C-terminal domains are more conserved than the unstructured N-terminal part. However, there are some conserved motifs in the N-terminal regions, such as the residues 162-182 (1), which contains the identified LxLSQSQ signature. Analyzing the sequence of 53BP1 further, there are two more regions showing very similar signatures: 504-527 (2) and 680-702 (3) (Figure 3.2D). Since co-localization was found to be dependent on the N-terminal 28 S/T-Q sites of 53BP1 (Di Virgilio et al., 2013; Escribano-Diaz et al., 2013; Zimmermann et al., 2013), we expected that these sites need to be phosphorylated to recruit RIF1 directly or indirectly. To test whether 53BP1 and Rif1 interact directly via this motif and whether phosphorylation is needed for this interaction, we set out to answer this question biochemically.

Figure 3.3

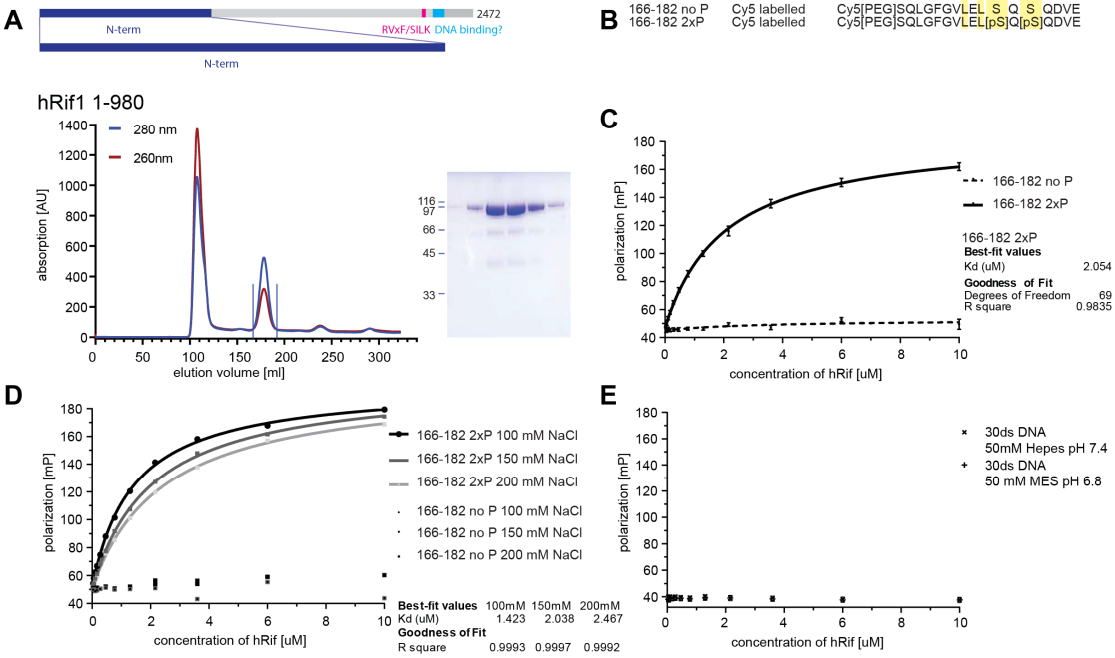

Figure 3.3 – RIF1-NTD binds to 53BP1 phospho-peptide. A, To scale representation of hRif1 highlighting the hRif1-NTD and size exclusion chromatography of purified hRif1-NTD accompanied with SDS-PAGE gel stained with Coomassie blue. B, 53BP1 peptides used for RIF1-NTD binding analysis in C-E. C, hRif1-NTD binds phosphorylated 53BP1 motif specifically. Fluorescent polarization (FP) analysis of fluorescently labeled 53BP1 peptide ± phosphorylation upon addition of RIF1-NTD. Mean values ± s.e.m. are plotted (n = 6). D, hRif1-NTD binding to 53BP1 peptide is salt dependent. FP analysis of fluorescently labeled 53BP1 peptide with phosphorylation upon addition of RIF1-NTD in three different salt concentrations (100 mM 150 mM, 200 mM NaCl), individual values are plotted. E, RIF1 does not bind dsDNA. FP analysis of fluorescently labeled 30bp dsDNA upon addition of RIF1-NTD. Fluorescent polarization. No binding was detected in the different buffers indicated.

The structured part of RIF1 spans from residues 1-980 (RIF1-NTD) and was purified from insect cells (Figure 3.3A). 53BP1 peptides were synthesized commercially with or without two phosphorylation modifications and an N-terminal fluorescent dye (Cy5) (Figure 3.3B). Using fluorescent polarization (FP), the binding of purified RIF1-NTD to 53BP1 peptide was assessed. We could not detect binding of RIF1-NTD towards the non-phosphorylated Cy-5-labelled peptide, whereas RIF1-NTD showed tight binding to the phosphorylated 53BP1 peptide (Kd of 2uM, n=6, R^2=0.984) (Figure 3.3C). This demonstrates that RIF1-NTD binds specifically the 53BP1 sequence signature in its double-phosphorylated form. In order to investigate this interaction further, we also tested whether this interaction is salt dependent. Using the same setup, the affinity between RIF1 and 53BP1 varies between ~1.4 uM and ~2.5 uM with sodium chloride concentrations between 100-200 mM (Figure 3.3D). At the same time, none of these salt concentrations gave rise to hRif1-NTD binding to the unphosphorylated 53BP1 sequence signature. Taken together binding is direct, phosphorylation dependent and on the order of 2 uM.

Having solved the structure of Rif1-NTD in complex with DNA and determined a nanomolar affinity towards different DNA substrates, it remained an open question whether RIF1-NTD also binds DNA directly. Surprisingly, there was no detectable binding of RIF1-NTD to 30bp double-stranded DNA at 150mM NaCl in two different buffers tested (Figure 3.3E). Therefore, we concluded that the NTDs of Rif1 in budding yeast and human probably fulfill the same overall function of blocking DNA-end resection but differ in their interaction partner and mechanism of action. While budding yeast Rif1 interacts directly with DNA, human RIF1 interacts with 53BP1 and functions by being recruited in a phosphorylation-dependent manner.

3.3 The human RIF1-NTD binds to 53BP1 with a positively charged patch

If 53BP1 binds via an N-terminal sequence signature to the RIF1-NTD, it poses the questions, which residues mediate this interaction within the RIF1-NTD. The RIF1 models of the Hook domain show several positively charged patches on the surface (Figure 3.4A–B). Assuming that budding yeast and human Rif1 function analogously, we started to mutate the positively charged patch on the concave surface of the predicted Hook model. We expressed and purified the mutant versions RIF1-NTD^{R283D}, RIF1-NTD$^{K290D/K291D}$, and the combination thereof. Assessing the interaction of RIF1-NTD mutants to the 53BP1 phospho-peptide by FP revealed that there is no detectable binding of the RIF1-NTD$^{K290D/K291D}$ mutant to the 53BP1 phospho-peptide (Figure 3.4C). The RIF1-NTD^{R283D} mutant still binds weakly (Kd of 6uM), accompanied with halved signal intensity (Figure 3.4C). None of the mutants show binding to the non-phosphorylated 53BP1 peptide. This data suggests that the phosphorylated 53BP1 peptide binds to the RIF1-NTD via the positively charged patch on the concave surface of the RIF1 Hook model. This would imply that the budding yeast and human Rif1 Hook domains function in an analogous mode of action using the same structural region, while Rif1 directly interacts with DNA and RIF1 binds to the mediator protein 53BP1.

Figure 3.4

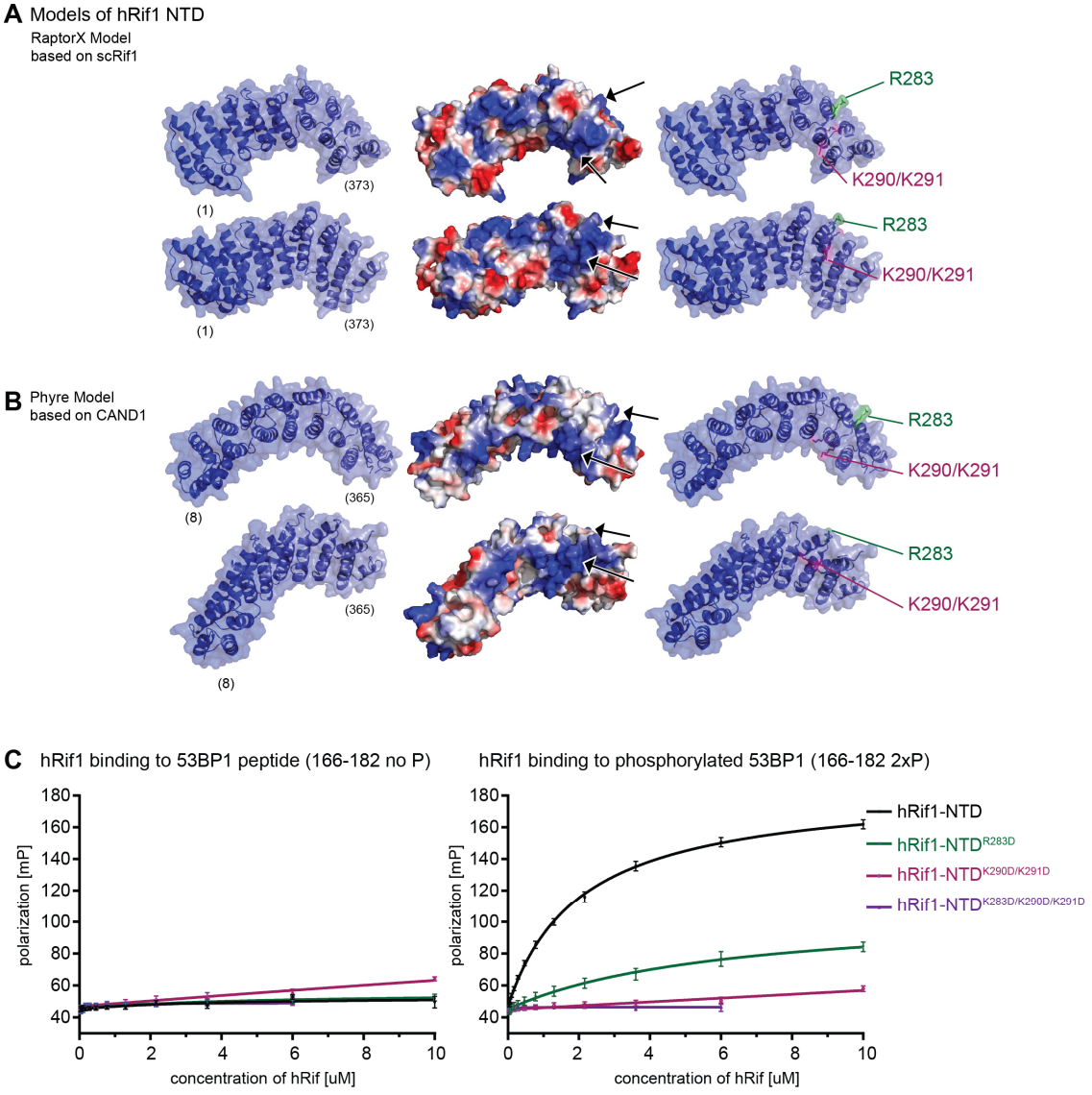

Figure 3.4 – RIF1-NTD binds to phosphorylated 53BP1 peptide N-terminal Hook domain. A, B, Cartoon and surface electrostatic representations of the RIF1 structural models based on the scRif1 structure (A) or CAND1 (B) indicating three positively charged residues. C, Mutating K290/291D on hRif1-NTD abrogates the phospho-specific binding to 53BP1 peptide. FP analysis of fluorescently labelled 53BP1 peptide ± phosphorylation upon addition of hRif1-NTD variants as indicated. Mean values ± s.e.m. are plotted (n = 3).

3.4 Human RIF1 and 53BP1 form a complex

53BP1 is comprised of 1972 amino acids in human and there are structures available for three individual domains: the Tudor domain, the UDR domain and the BRCT domain (depicted in Figure 3.5A). It has also been shown that the UDR domain binds to the acidic patch of the nucleosome upon ubiquitylation of H2AK15 and that the Tudor domain sits on the dimethylated lysine 20 of histone 4 (H4) (Wilson et al., 2016). However, the rest of the 53BP1 structure remains elusive. Interestingly, the N-terminal 1480 are predicted to be unstructured (Figure 3.5A), which puts a particular hurdle to the further structural analysis of the protein. A construct containing the Tudor and UDR domains, the oligomerization domain and the Glycine/Arginine-rich motif (GAR) ($53BP1_{1220\text{-}1631}$) was expressed recombinantly and purified (Figure 3.5B). The construct contained four N-terminal glycines in order to be able to enzymatically link the identified phosphorylated 53BP1 peptide to the $53BP1_{1220\text{-}1631}$ protein. Enzymatic linkage of the peptide was performed using the enzyme sortase, which requires the C-terminal recognition sequence LPETGG and the N-terminal recognition sequence GGGG, so that the enzyme can link the phospho-peptide with purified $53BP1_{1220\text{-}1631}$ (schematic overview in Figure 3.5C adapted to 53BP1) In order to test the efficiency of the sortase linkage reaction, different ratios between peptide and 53BP1 (4x, 8x and 12x excess of peptide) and incubation times (1, 2 and 18 hours) were tested. In order to monitor successful linkage an N-terminal Cy5 labeled peptide was used. As shown in Figure 3.5D all different conditions resulted in a successful linkage of the peptide so that a fluorescent band shift could be detected. In order to get rid of the phosphorylated peptide excess, size-exclusion chromatography (SEC) was performed (Figure 3.5E) and it separated the Cy5-phospho-peptide linked 53BP1 (fractions 2-7), the sortase (fraction 8) and the excess of peptide (fraction 9) (Figure 3.5F).

Figure 3.5

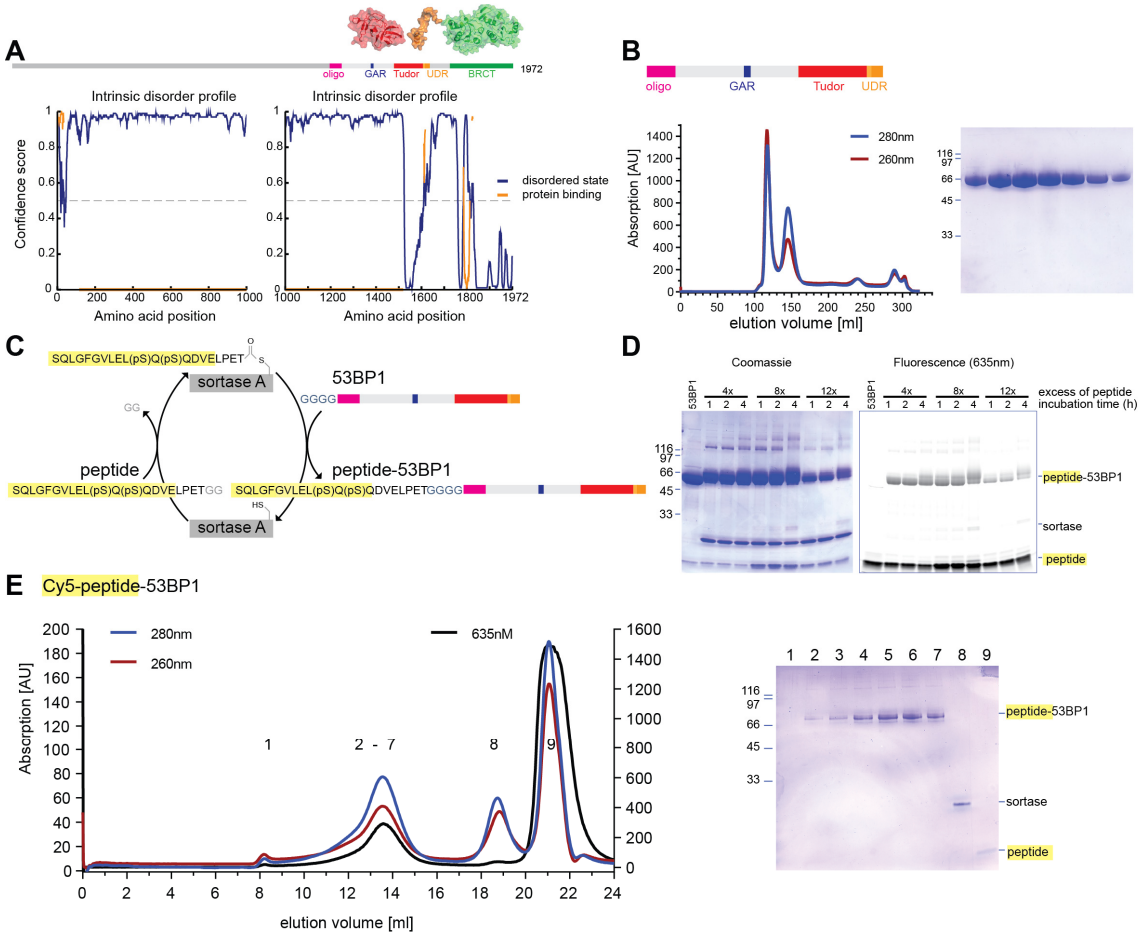

Figure 3.5 – 53BP1 (residues 1220-1631) can be covalently linked to phospho-peptide using sortase. A, To scale representation of 53BP1 and intrinsic disorder analysis using DISOPRED. B, Size exclusion chromatography of purified 53BP1 accompanied with SDS-PAGE gel stained with Coomassie blue. C, Cartoon showing covalent linkage of 53BP1-phospho-peptide to 53BP1 (residues 1220-1631) using the enzyme sortase. D, Phospho-peptide can be covalently linked to 53BP1. Cy5-labeled 53BP1-peptide was incubated with purified 53BP1 (1220-1631) for the indicated time with the indicated excess of peptide over protein. SDS-PAGE gel analysis stained with Coomassie blue or scanned for fluorescent signal at 635nm. E, 53BP1 covalently linked to phospho-peptide can be purified. Size exclusion chromatography of covalently linked Cy5-labeled phospho-peptide to 53BP1 (1220-1631). Indicated fractions were run on a SDS-PAGE gel (right).

To answer the question of whether 53BP1$_{1220\text{-}1631}$ and RIF1_NTD interact and to assess the role of the phospho-peptide in potential complex formation, 53BP1$_{1220\text{-}1631}$ or 53BP1$_{peptide\text{-}1220\text{-}1631}$ were incubated with RIF1-NTD and run over SEC. 53BP1$_{1220\text{-}1631}$ and RIF1_NTD eluted separately, whereas 53BP1$_{peptide\text{-}1220\text{-}1631}$ and RIF1_NTD formed a complex shifting slightly compared to the oligomerized 53BP1$_{1220\text{-}1631}$ (Figure 3.6A). If 53BP1$_{1220\text{-}1631}$ by itself forms an oligomer and each 53BP1 molecule binds to RIF1, the resulting complex should be at least double the size of the 53BP1$_{1220\text{-}1631}$ oligomer and therefore result in a substantial shift in the chromatogram. To gain insight into the size of the individual complexes, SEC in conjunction with multiple angle light scattering was performed (SEC-MALS). RIF1-NTD was shown to be purely monomeric with a measured size of 102 kDa (Figure 3.6B). In contrast, the measured size of 53BP1$_{1220\text{-}1631}$ was 125 kDa, consistent with a trimer. To our surprise, the RIF1-NTD-53BP1$_{peptide\text{-}1220\text{-}1631}$ complex resulted in a measured molecular weight of 157 kDa. This suggests that the 53BP1$_{1220\text{-}1631}$ trimer falls apart when RIF1_NTD is bound. This is unexpected as current models assumed that the oligomerization of 53BP1 is crucial for the assembly of several 53BP1 molecules at the DSB site.

To gain independent validation of the complex formation and to characterize the 53BP1-RIF1 interaction further, cross-linking mass spectrometry was performed. RIF1-NTD and 53BP1$_{1220\text{-}1631}$ in the presence or absence of the linked phospho-peptide were purified over SEC as in Figure 3.6A and cross-linked with the lysine linker DSSO (disuccinimidyl sulfoxide). Six crosslinks could be detected between RIF1-NTD and 53BP1$_{peptide\text{-}1220\text{-}1631}$, whereas no crosslinks were identified between RIF1-NTD and 53BP1$_{1220\text{-}1631}$ (Figure 3.6C). Additionally, more intra-links within 53BP1 were identified when RIF1 and 53BP1 formed a complex suggesting that 53BP1 is less flexible upon binding to RIF1-NTD.

Taken together, this is the first biochemical reconstitution of the 53BP1-RIF1 interactions, which we find depends on phosphorylation of 53BP1. The interaction can be interrupted by mutating two positively charged residues within the predicted RIF1-NTD Hook domain on the concave surface. The alpha-helical repeat is able to distinguish between a phosphorylated and non-phosphorylated motif and to function as the reader of the ATM site. Additionally, our data indicate that the oligomerization of 53BP1 is interrupted upon 53BP1-Rif1 complex formation, which poses new questions on the molecular assembly of 53BP1 and RIF1 at damage sites. This work supplies a good basis for further biochemical and structural studies on the Rif1-53BP1 interplay.

Figure 3.6

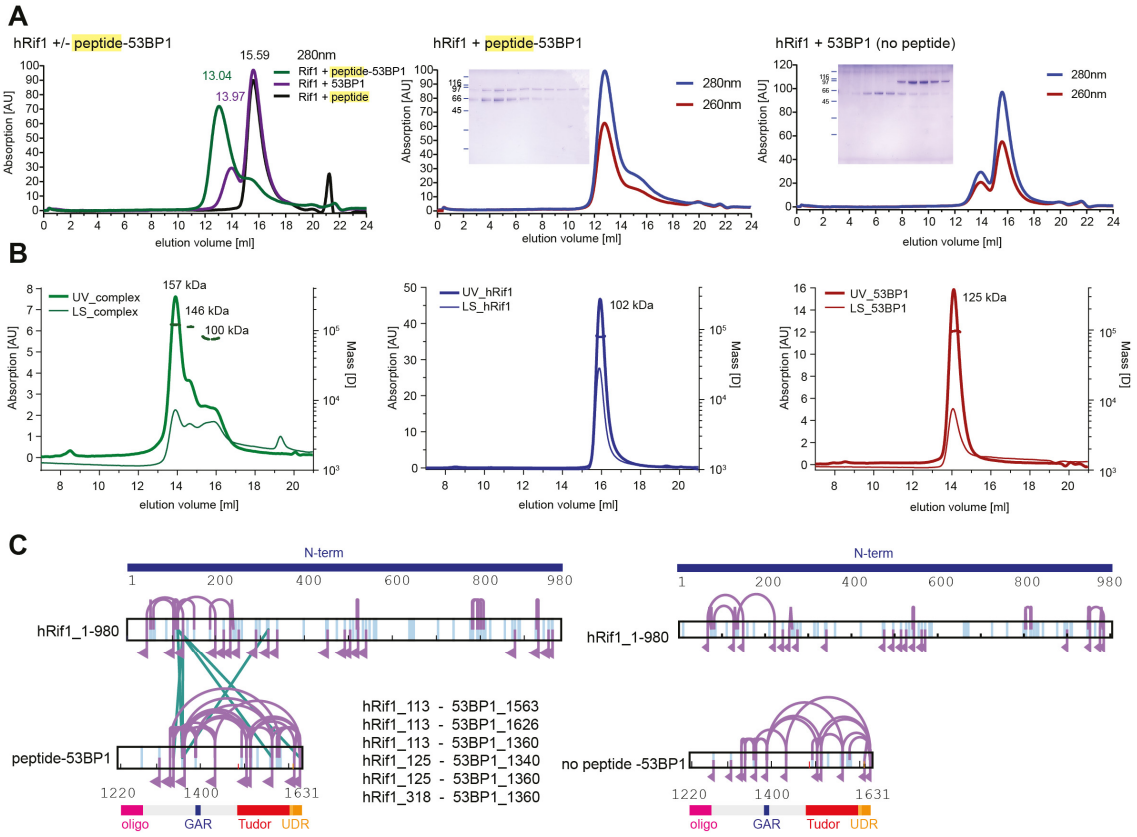

Figure 3.6 – RIF1-NTD-53BP1 forms a complex, which is strictly dependent on the phosphorylated 53BP1 peptide. A, RIF1-NTD and 53BP1 form a complex when the phospho-peptide is present on 53BP1. Size exclusion chromatography of RIF1-NTD incubated with 53BP1 in the presence or absence of covalently linked phospho-peptide. Peak fractions were run on SDS-PAGE stained with Coomassie Blue. Chromatographs were overlaid as indicated and peak volumes are indicated. B, the 53BP1-RIF1 complex abolishes the 53BP1 trimer conformation. SEC-MALS of RIF1-NTD (middle), 53BP1 (1220-1631) (right), and RIF1-NTD incubated with phospho-peptide linked 53BP1 (left). Rif1-NTD is monodisperse (expected: 105kDa, measured: 102kDa), 53BP1 adopts a trimer (expected: 45kDa, measured: 125kDa) and the complex thereof (left) is 157kDa in size; UV (ultraviolet light); LS (light scattering); D (Dalton). C, Crosslinking mass spectrometry of RIF1 incubated with 53BP1 in the presence (left) or absence (right) of covalently linked phospho-peptide. Lysines are indicated as cyan line, purple arcs show self-links within the same protein, purple flags indicate linker modified peptides, and crosslinks between RIF1-NTD and 53BP1 are indicated with green lines. Identified crosslinks are listed. No crosslinks could be detected in the absence of linked phospho-peptide.

4 MATERIALS AND METHODS

4.1 Materials and methods related to Chapter 2

4.1.1 Rif1-NTD protein purification

Saccharomyces cerevisiae Rif1 N-terminal domain (Rif1-NTD) constructs (residues 177-1283 or 100-1322) and mutants were expressed as N-terminal Strep(II)-tag fusions in *Trichoplusia ni* High Five insect cells. Insect cell expression cultures of Rif1 N-terminal domain (Rif1-NTD) constructs (residues 177-1283 or 100-1322) and mutants (residues 100-1322 of $Rif1_{HOOK}$,:K437E, K563E, K570E; $Rif1_{LOOP}$, K691E,K692E) were grown in SF900-II medium (ThermoFisher Scientific) at 27°C and infected at a cell density of 4 x 10^6 cells/mL with 15 mL/L of P2 virus solution. Cells were harvested by centrifugation 48 h after infection and lysed by sonication in 50 mM Tris-HCl pH 8.0, 500 mM NaCl, 1 mM tris(2-carboxyethyl)phosphine (TCEP), 1 mM phenylmethylsulfonyl fluoride, 1× protease inhibitor cocktail (Sigma Aldrich), 5 mM β-mercaptoethanol. After clarification by ultracentrifugation (45,000*g* for 45 min at 4°C), the Rif1-NTD was extracted by Strep-Tactin affinity (Strep-Tactin Sepharose, IBA). The fusion tag was removed by overnight incubation with 5% (w/w) TEV protease. The protein solution was concentrated by ultrafiltration (30 kDa molecular-weight cutoff concentrator; Macrosep, Pall) and separated by size exclusion chromatography (Superdex 200, GE Healthcare) in 50 mM HEPES pH 7.4, 310 mM NaCl, 1 mM TCEP. Purified Rif1-NTD was concentrated by ultrafiltration to 60 µM or 70 µM, flash-frozen in liquid nitrogen and stored at -80°C.

4.1.2 Expression and purification of selenomethionine-labeled Rif1-NTD

Selenomethionine-substituted (SeMet) Rif1-NTD (residues 177-1283) was produced as described previously (Cronin et al., 2007), except that infected High Five cells were cultured in methionine and cysteine-free SF900–II medium supplemented with 2 mM L-glutamine, 2 mM L-cysteine, and 20 mg/L L-selenomethionine, and 8 h post-infection a further 40 mg/L L-selenomethionine was added. SeMet Rif1-NTD (residues 177-1283) was purified in the same manner as the native protein.

4.1.3 Rif1-NTD structure determination

Crystals of Rif1-NTD (residues 177-1283) were grown by hanging-drop vapor diffusion at 22°C from drops prepared by mixing 1µL of protein solution (3.8 mg/ml in storage buffer) with 1 µL of reservoir solution (100 mM Tris-HCl, pH 7.5, 320 mM lithium sulfate, 850 mM potassium sodium tartrate). SeMet-substituted crystals were grown in the same conditions from seeds prepared from native

Rif1-NTD (residues 177-1283) crystals, which were transferred into pre-equilibrated drops (4-16 h) with a cat whisker. Crystals appeared within 4 d and were harvested after two weeks. Prior to X-ray analysis, each crystal was swept briefly through a cryoprotectant solution composed of reservoir solution supplemented with 20% (v/v) ethylene glycol then flash-cooled in liquid nitrogen.

A gold derivative was prepared by soaking a native crystal with 1 mM $KAu(CN)_2$ in a stabilizing solution formulated to reproduce the crystal-growth condition as closely as possible (artificial mother liquor). Crystals were immersed in 4 µL drop of soaking solution and incubated for 1.5 h at 20°C with hanging-drop vapor over a reservoir of stabilizing solution. The crystals were back-soaked for 5 min in a fresh 10 µL drop of stabilizing solution before proceeding to X-ray analysis as for other crystals.

Diffraction data were collected at the Swiss Light Source, Switzerland, from beamline PXII with a Pilatus 6M detector (Dectris) or PXIII with a Pilatus 2M (Dectris) or MarCCD 225 detector (Mar Research).

The data were processed by Richard Bunker (Thomä lab) and the steps of data analysis can be found in Material and Methods section of the published manuscript (Appendix).

4.1.4 Rif1-NTD-DNA structure determination

Rif1-NTD (residues 100-1322) formed crystals with 30 bp dsDNAs bearing a 24 or 30 nt 3' tail (oligonucleotides 1+2 or 18+2 in Table 2.1). The crystals were grown from a mixture of 43.5 µM protein and 65 µM DNA in storage buffer by dehydrating a 1 µL drop of Rif1-NTD–DNA solution by sitting drop vapor diffusion over a reservoir containing 10 mM $NiCl_2$, 100 mM Tris-HCl, pH 8, 20% (w/v) polyethylene glycol MME 2000. Crystals appeared within 3 d and were harvested after 1 week. For cryo-protection, the crystal-growth drop was covered with a thin layer of 25%(v/v) PEG 400 made up in storage buffer, after which a single crystal was quickly removed and flash-cooled in liquid nitrogen.

Diffraction data were collected at the Swiss Light Source, Switzerland, from beamline PXII with a Pilatus 6M detector (Dectris) or PXIII with a Pilatus 2M (Dectris) or MarCCD 225 detector (Mar Research).

The data were processed by Richard Bunker (Thomä lab) and the steps of data analysis can be found in Material and Methods section of the published manuscript (Appendix of this thesis).

Refinement statistics for Rif1-NTD-DNA-II are in Table 2.1. Surface electrostatic potentials were calculated with APBS (Baker et al., 2001). Structural figures were prepared with PyMOL (v. 1.8.2, Schrödinger).

4.1.5 DNA substrates for electromobility shift assays (EMSA)

Polyacrylamide gel electrophoresis (PAGE)-purified DNA oligonucleotides were obtained from Microsynth (Switzerland) (Table 4.1). DNA concentration was measured by UV absorption using a Nanodrop spectrophotometer (ThermoFisher Scientific). For EMSA, oligonucleotides were labeled by T4 polynucleotide kinase (New England Biolabs) and [γ-^{32}P] ATP at 37°C for 1 h. Reactions were stopped by adding 20 mM EDTA. Oligonucleotides were desalted into 10 mM Tris-HCl pH 8.0, 1 mM $MgCl_2$ and 50 mM NaCl using an Illustra MicroSpin G-25 column (GE Healthcare). DNA oligonucleotides at 2 µM were mixed in the combinations listed in Table 4.2 and annealed in 10 mM Tris-HCl pH 8, 1 mM $MgCl_2$, 50 mM NaCl by heating for 5 min to 98°C and cooling at 1°C/min to 4°C to generate the indicated substrates. Annealed DNA substrates were purified by 14% PAGE electrophoresis at 4°C and stored in 10 mM Tris-HCl pH 8.0, 1 mM EDTA at 4°C.

4.1.6 Electromobility shift assays (EMSAs)

Protein concentrations were measured by the Bradford method with a bovine serum albumin (BSA) standard and UV absorption Nanodrop spectrophotometer (ThermoFisher Scientific). EMSAs were performed in a buffer containing 20 mM Tris-HCl pH 8.0, 100 mM NaCl, 2.5 mM $MgCl_2$, 10 mM $CaCl_2$, 0.1 mg/ml BSA, 1 mM TCEP. For simple EMSA titrations (Figures 2.3A-C, 2.4, 2.8D, 2.9E) the labeled DNA at a final concentration of 1 nM was added to the serially diluted protein. The mixture was incubated for 20 min at 20°C prior to gel loading. For equimolar titrations (Figures 2.8A-C, 2.9F), labeled DNA (1 nM final concentration) was added to the protein to obtain the final concentrations indicated. Serially diluted unlabeled DNA was then added to the mixture at the indicated final concentrations. The mixture was incubated for 20 min at 20°C prior to gel loading.

Preincubated protein-DNA solutions were mixed with glycerol at a final concentration of 8% (v/v) and 10 µL samples were separated by 1.2% (w/v) agarose gel electrophoresis in 0.5 × TBE at 4°C for 2 h at 150 V. The gels were dried on DE81 chromatography paper (Whatman), exposed to storage phosphor screens (GE Healthcare), scanned by a Typhoon phosphorimager (GE Healthcare), and quantified (see below).

Table 4.1 – DNA oligonucleotides used for crystallization, negative stain EM, and EMSA

Oligonucleotide	5′ to 3′ sequence
1	ACGCTGCCGAATTCTACCAGTGCCTTGCTAGGACATCTTTGCCCACCTGCAGGTTCACCC
2	TAGCAAGGCACTGGTAGAATTCGGCAGCGT
3	GGGTGAACCTGCAGGTGGGCAAAGATGTCCTAGCAAGGCACTGGTAGAATTCGGCAGCGT
4	ACGCTGCCGAATTCTACCAGTGCCTTGCTA
5	ACGCTGCCGAATTCTACCAGTGCCTTGCTATTTTTTTTTTTTTTTTTTTTTTTTTTTTT
6	ACCAGTGCCTTGCTATTTTTTTTTTTTTTT
7	TAGCAAGGCACTGGT
8	ACCAGTGCCTTGCTA
9	GGGTTTTTTTTTTTTTTTTTTTTTTTTTTTTTTTTTTTTTTTTTTTTTTTTTTTTTT
10	GGGTTTTTTTTTTTTTTTTTTTTTTTTTT
11	GGGTTTTTTTTTTTTTTTT
12	GGGTTTTTTTTTTTT
13	CTGGTGGTGGTGTGTGGTGTGTGGGTGTGT
14	ACACACCCACACACCACACACCACCACCAG
15	ACACACCCACACACC
16	CTGGTGGTGGTGTGT
17	ACACACCACCACCAG
18	ACGCTGCCGAATTCTACCAGTGCCTTGCTAGGACATCTTTGCCCACCTGCAGGT
19	GTGACCGTCTCCCGCACACCCACACACCAGACCCACACCACACCACACCCGACAACCAAC
20	GTTGGTTGTCGGGTGTGGTGTGGTGTGGGT
21	GCGCTACGCGGAATGCCATGACTTCGGACGCTGGTGTGTGGGTGTGCGGGAGACGGTCAC
22	CGTCCGAAGTCATGGCATTCCGCGTAGCGC
23	CGTCTCCGGGAGCTGCATGTGTCAGAGGTTTTCACCGTCATCACCGAAACGCGCGAGACG
24	CGTCTCGCGCGTTTCGGTGATGACGGTGAAAACCTCTGACACATGGCCAGCCCCGACACC
25	GGTGTCGGGGCTGGCCATGTGTCAGAGGTTTTCACCGTCATCACCCGCCGGGCAAGAGCA
26	TGCTCTTGCCCGGCGGGTGATGACGGTGAAAACCTCTGACACATGCAGCTCCCGGAGACG

Table 4.2 – DNA substrate list for EMSA experiments

Substrate list	labeled oligonucleotide	annealed oligonucleotide
15ss	12	
20ss	11	
30ss	10	
60ss	9	
15ds	7	8
30ds	2	4
60ds	1	3
15ds15ss 3'-tailed	6	7
30ds30ss 3-'tailed	5	2
15ss TGseq	16	
30ss TGseq	13	
15ds TGseq	16	17
30ds TGseq	13	14
15ds15ss 3'tailed TGseq	13	17
Fork	19	20, 21, 22
Holliday Junction	23	24, 25, 26

4.1.7 EMSA quantification

EMSA images were analyzed with ImageJ (Schneider et al., 2012), by selecting and blotting individual lanes. Bands were defined across the gel and noise was subtracted. The intensity of the analyzed bands was normalized to the total intensity of the lane. The percentages of intensities were plotted (Figures 2.3C, 2.8A, 2.9E, and F) using GraphPad Prism 6. The K_d was calculated assuming specific binding with a Hill slope ($Y = Bmax*X^h/(Kd^h + X^h)$) (Figure 2.3C). The mean and standard error of the mean were calculated with GraphPad Prism (Figures 2.8A and 2.9F).

4.1.8 Negative stain EM

For negative stain EM without DNA, Rif1-NTD (residues 100-1322) was re-purified by size exclusion chromatography (Superdex 200, GE Healthcare). For EM with DNA, oligonucleotide no. 2 and 5 (Table 4.1) were equilibrated with 50 mM HEPES pH 7.4, 150 mM NaCl, 10 mM $MgCl_2$, 1 mM TCEP and annealed in this buffer by heating for 5 min to 98°C and cooled at 1°C/min to 4°C, forming a 30 bp dsDNA bearing a 30 nt 3′ tail. Different molar ratios of protein to DNA were tested by mixing (1:1, 1:3, 1:5, 1:10). A sample of suitable homogeneity for EM analysis was obtained by mixing Rif1-NTD with a threefold molar excess of 3′-tailed DNA. For EM sample preparation, 20 µM of Rif1-NTD was mixed with 60 µM of annealed DNA and was incubated for 15 min on ice prior to separation in a glycerol gradient (10-20% w/v) by ultracentrifugation for 16 h at 214 000*g* (4°C). Fractions containing Rif1-NTD with or without DNA were diluted to ~0.1 mg/ml and absorbed to glow-discharged Quantifoil grids coated with a continuous thin carbon film (S7/2, Cu 400 mesh, 2 nm carbon film, Quantifoil Micro Tools). A 4 µL sample was applied to a grid and negatively stained with 2% (w/v) uranyl acetate. Data were acquired using a Philips CM200FEG transmission electron microscope operated at 200 kV. Images were recorded in low-dose mode with a TVIPS F416 camera (Tietz Video and Image Processing Systems) at a nominal magnification of 50,000×, resulting in a pixel size of 2.2 Å at the sample. A defocus range -0.5 µm to -5 µm was used for data acquisition.

For Rif1-NTD in isolation, 10 091 particles were manually selected from 100 micrographs using *e2boxer.py* from EMAN2 (Tang et al., 2007) and extracted with a box size of 150 × 150 pixels. For the sample with DNA 39 981 particles were selected from 500 micrographs and extracted with a box size of 180 × 180 pixels. Two dimensional (2D) classifications of the Rif1-NTD dataset without and with DNA were performed by iterative stable alignment and clustering (ISAC) (Yang et al., 2012) with SPARX (Hohn et al., 2007).

The contrast transfer function parameters for each micrograph was estimated using *sxcter.py* from *SPAR*X (Penczek et al., 2014), the particles were phase flipped and rescaled to a box size of 76 × 76 pixels (4.34 Å/pixel). ISAC was run specifying 200 images per group and a pixel error of 7 for 4 (no

DNA) and 10 generations (with DNA), giving 13 stable 2D averages for Rif1-NTD without DNA and 111 stable 2D averages for Rif1-NTD with DNA.

The validated initial three-dimensional (3D) model was calculated from Rif1-NTD with DNA 2D class average representatives using the VIPER procedure in *SPARX* (Hohn et al., 2007) with a low-pass filter frequency of 0.0625. To obtain the final maps, *RELION* (Scheres, 2012) was used for 2D and 3D classification and auto-refinement. Intact particles included in the best 2D classes (4941 particles without DNA and the 17,985 particles with DNA) were pooled and used for iterative cycles of 3D classification with decreasing angular sampling intervals (15º and 7.5º). The initial model obtained with VIPER was used for 3D classification of Rif1-NTD with and without DNA. The models shown in Figures 2.6 were auto-refined by RELION to a maximum resolution of 36 Å Rif1-NTD in isolation and 33 Å for Rif1-NTD+DNA. DNA was not visible, as expected given the resolution and the negative stain conditions.

4.1.9 Differential scanning fluorimetry

The reagents of the Protein Thermal Shift Dye Kit (Applied Biosystems) were used. Protein Thermal Shift Dye was diluted in MilliQ water to a concentration of 4x and 5 ul were pre-dispensed into a non-skirted qPCR 96-well plate. Purified Rif1-NTD (100-1322) and mutants were diluted in 300 mM NaCl, 1mM TCEP and one of the three buffers ((1) 100mM sodium acetate (NaAc) buffer pH5.5, (2) 100mM Bis-Tris pH7, or (3) 100mM Tris-HCl pH8) to the final concentration of 0.1 mg/ml Rif1-NTD and 15ul were added to each well. Each reaction was mixed by pipetting, the plate was sealed and spun at 3500 x g for 5 min. Melting curves were measured using a StepOnePlus Real-Time PCR System (ThermoFisher Scientific). Fluorescence was detected in ROX mode and fluorescence intensity was measured in one-degree increments between 4°C and 99°C. The first derivative of the melting curve, the peak curve, is depicted.

4.1.10 Yeast techniques

All *in vivo* experiments were performed by members of the Shore (University of Geneva) or Rass (FMI, Basel) laboratory and can be found in the published version of the manuscript (Appendix of this manuscript).

4.2 Materials and methods related to Chapter 3

4.2.1 Conservation analysis of 53BP1 and budding yeast and human RIF1

Conservation of Rif1, RIF1, and 53BP1 was analyzed by using the CONSURF server (Ashkenazy et al., 2016; Ashkenazy et al., 2010; Celniker et al., 2013). In order to be able to compare the outcome, all conservations searches were performed with the following parameters: Homolog search algorithm (PSI-BLAST), number of iterations (3), E-value cutoff (0.0001), searching the protein database UNIPROT90. Up to 150 sequences were searched for having a minimal sequence identity of 15% and a maximal sequence identity of 95%. Multiple sequence alignment was performed using the MAFFT-L-INS-i alignment method and a Bayesian Calculation method. Multiple sequence alignments were imported into CLC Genomics Workbench 6.9 and conservation was plotted in a colored-bar (white = 0% conservation; black = 100%conservation) along the sequence. In the sequence logo, the height of the letters directly correlates with the conservation in percent.

4.2.2 Intrinsic disorder analysis of 53BP1, yeast and human RIF1

Intrinsic disorder profiles were generated using the DISOPRED3 (Disorder Prediction) tools within the PSIPRED Protein Sequence Analysis Workbench (Jones and Cozzetto, 2015).

4.2.3 Structural modeling

Structural models of RIF1 were predicted using the Phyre^2 and RaptorX server (Kallberg et al., 2012; Kelley et al., 2015). Phyre^2 model (1) is based on the helical repeat protein CAND1 (PDB:1U6G) and Phyre^2 model (2) and the RaptorX model is based on the Rif1-NTD structure. Due to structural flexibility as of residue 375, all models where cut and only the predicted Hook domain spanning between residue 1-370 is shown.

4.2.4 Protein Expression and Purification

4.2.4.1 RIF1-NTD protein purification

Human RIF1 N-terminal domain (Rif1-NTD) construct (residues 1-980) and mutants (residues 1-980, R283D, K290/291D or R283D_K290/291D) were expressed as N-terminal Strep(II)-tag fusions in *Trichoplusia ni* High Five insect cells (Life Technologies). Bacmids, primary and secondary viruses were produced using the Bac-to-Bac system (Life Technologies) and *Spodoptera frugiperda (Sf9)* insect cells (ThermoFisher Scientific). High Five insect cells were grown in SF900 II medium (Life Technologies) at 27°C and infected at a cell density of 4 x 10^6 mL with 15 mL/L of P2 virus solution. Cells were harvested by centrifugation 48 h after infection and lysed by sonication in 50 mM Tris-

HCl pH 8.0, 500 mM NaCl, 1 mM tris(2 carboxyethyl)phosphine (TCEP), 1 mM phenylmethylsulfonyl fluoride, 1 × protease inhibitor cocktail (Sigma). After clarification by ultracentrifugation (45,000g for 45 min at 4°C), the RIF1-NTD was extracted by Strep-Tactin affinity (Strep-Tactin Sepharose, IBA). The protein solution was concentrated by ultrafiltration (30 kDa molecular-weight cutoff concentrator; Amicon Ultra-15 Centrifugal Filter Units, Millipore) and separated by size exclusion chromatography (Superdex 200, GE Healthcare) in 50 mM HEPES pH 7.4, 250 mM NaCl, 1 mM TCEP (storage buffer). Purified Rif1-NTD was concentrated by ultrafiltration, flash-frozen in liquid nitrogen and stored at -80°C.

4.2.4.2 53BP1 peptides

53BP1 phosphorylated and unphosphorylated peptides were commercially synthesized with or without an N-terminal Cy5 and were more than 95% pure checked by mass spectrometry (New England Peptide, Boston).

4.2.4.3 53BP1 protein purification

53BP1 constructs (residues 703-1631 and 1220-1631) were subcloned into pAC-derived vectors (Abdulrahman et al., 2009) and recombinant proteins expressed as N-terminal Strep(II)-tag-TEV-4xGly fusions in *Trichoplusia ni* High-Five insect cells using the baculovirus expression system (Life Technologies). Primary and secondary viruses were produced in *Spodoptera frugiperda (Sf9*) insect cells (ThermoFisher Scientific). High Five insect cells were grown in SF900 II medium (Life Technologies) at 27°C and infected at a cell density of 4 x 10^6 mL with 15 mL/L of P2 virus solution. Cells were harvested by centrifugation 48 h after infection and lysed by sonication in 50 mM Tris-HCl pH 8.0, 500 mM NaCl, 1 mM tris(2 carboxyethyl)phosphine (TCEP), 1 mM phenylmethylsulfonyl fluoride, 1 × protease inhibitor cocktail (Sigma). After clarification by ultracentrifugation (45,000g for 45 min at 4°C), 53BP1 was extracted by Strep-Tactin affinity (Strep-Tactin Sepharose, IBA). The fusion tag was removed by overnight incubation with 5% (w/w) TEV protease. The protein solution was concentrated by ultrafiltration (30 kDa molecular-weight cutoff concentrator; Amicon Ultra-15 Centrifugal Filter Units, Millipore) and separated by size exclusion chromatography (Superose 6, GE Healthcare) in 50 mM HEPES pH 7.4, 250 mM NaCl, 1 mM TCEP (storage buffer). Purified 53BP1 was concentrated by ultrafiltration (30 kDa molecular-weight cutoff concentrator; Amicon Ultra-15 Centrifugal Filter Units, Millipore), flash-frozen in liquid nitrogen and stored at -80°C.

4.2.5 Fluorescent Polarization

Protein concentrations were measured by the Bradford method with a bovine serum albumin (BSA) standard and UV absorption Nanodrop spectrophotometer (ThermoFisher Scientific). Peptide powders were dissolved in 100% DMSO to gain a 2mM stock. The peptide stock was diluted in

binding buffer (50mM Hepes pH 7.4, 150mM NaCl, 2.5mM $MgCl_2$, 0.25mM TCEP, 50 ug/ml BSA (Sigma) and 0.05 % Tween-20(Sigma)) to a concentration of 200nM in 1%DMSO. RIF1_NTD (WT or mutants) was diluted in the binding buffer to gain a 20uM stock. RIF1_NTD was twelve times serially diluted by a factor of 1.6 in binding buffer. 5ul of each RIF1 and 53BP1 peptide were mixed in a microplate (384 well, small volume, Hibase, Greiner (784076)) and fluorescent polarization was measured with 200 flashes per second over a period of an hour using a Pherastar FS (BMG Labtech).

4.2.6 Statistics for biophysical methods

For analysis, the first 45min of Fluorescent Polarization recordings were used. Polarization data and microscale thermophoresis data was imported into GraphPad Prism (version 7) and analyzed assuming a "One-site Total binding" with no non-specific binding. (Formula: Y=(Bmax*X)/(Kd+X) + Bg; Bmax is the maximum specific binding in the same units as Y; Kd is the equilibrium binding constant, in the same units as X; Bg is the amount of nonspecific binding with no added protein ([RIF1]=0 nM)). If no curve was fitted, individual values are plotted.

The mean and standard error of the mean (SEM) was calculated in GraphPad Prism (version 7) and plotted on the graphs. Goodness of fit is presented with degrees of freedom and with the R^2.

4.2.7 Enzymatic linkage of 53BP1 peptide to 53BP1 construct using sortase labeling

Based on (Theile et al., 2013), a phosphorylated 53BP1 peptide sequence harboring a C-terminal LPETGG was ordered (SQLGFGVLEL(pS)Q(pS)QDVELPETGG, with and without N-terminal Cy5-label) from New England Peptides (Boston) and $53BP1_{1220-1631}$ was expressed with an N-terminal cleavable N-terminal Strep(II)-tag-TEV-4xGly fusion tag as described above. After TEV cleavage, the $53BP1_{1220-1631}$ construct contains four N-terminal glycines, which can be used for N-terminal linkage of a peptide using sortase A (Sarpong and Bose, 2017).

Recombinantly expressed and purified sortase A from S. aureus was a generous gift from A. Potenza (Thomä laboratory). In order to assess the sortase labelling efficiency in a small-scale experiment, purified sortase A at 20.8uM was incubated with $53BP1_{1220-1631}$ at 25uM or 8uM, and 53BP1 peptide at 100 or 200uM to gain 4, 8 or 12.5 fold excess of the peptide compared to $53BP1_{1220-1631}$ in reaction buffer (50mM Hepes pH 7.4, 250 mM NaCl, 0.5 mM TCEP). Mixtures were incubated for one, two or 18 hours at 4°C. Already after one hour and 4 fold excess of peptide, $53BP1_{1220-1631}$ was seen to be fully linked to the phosphorylated peptide on gel electrophoresis by fluorescent detection of the Cy5 dye and by staining with Coomassie blue. The large scale experiment was performed using 12.5 nmoles of $53BP1_{1220-1631}$, 12.5 nmoles of sortase A and 50 nmoles of 53BP1 peptide in a reaction

volume of 500 ul. The peptide-linked $53BP1_{1220-1631}$ ($53BP1_{pept-1220-1631}$) was purified via size exclusion chromatography on a Superose 6 column, and absorption at 260nm, 280nm and 635nm were detected. SDS-PAGE gel electrophoresis was performed on the fractions followed by Coomassie blue staining. Fractions containing $53BP1_{pept-1220-1631}$ were pooled and concentrated by ultrafiltration (30 kDa molecular-weight cutoff concentrator; Amicon Ultra-4 Centrifugal Filter Units, Millipore).

4.2.8 RIF1-$53BP1_{peptide-1220-1631}$ complex formation analysis

Purified RIF1-NTD was incubated with either $53BP1_{pept-1220-1631}$ or $53BP1_{1220-1631}$ with an excess of RIF1 for 1 hour at 4°C in 50mM Hepes pH 7.4, 100mM NaCl and 0.5 mM TCEP. Mixtures were analyzed by size exclusion chromatography (Superose 6), complex formation was assessed by the absorption profile and SDS-PAGE gel electrophoreses followed by Coomassie blue staining.

For size exclusion chromatography followed by multiple angle light scattering (SEC-MALS), RIF1 and $53BP1_{1220-1631}$ were analyzed as single proteins, and as RIF1_NTD $53BP1_{pept-1220-1631}$ complex (preparation as above) using a DAWN HELEOS II, Wyatt instrument.

4.2.9 Crosslinking mass spectrometry (in collaboration with the Protein analysis facility, FMI)

Purified RIF1-NTD was incubated with either $53BP1_{pept-1220-1631}$ or $53BP1_{1220-1631}$ with an excess of RIF1 for 1 hour at 4°C in 50mM Hepes pH 7.4, 100mM NaCl and 0.5 mM TCEP. Mixtures were run on SEC (Superose 6) and all fraction containing protein judged by the absorption profile were pooled and concentrated using an Amicon Ultra-4 Centrifugal Filter Unit, 30 kDa cut-off (Merck). 50 ul of each sample at around 1mg/ml concentration was incubated for 1 hour at a final concentration of 1mM DSSO (disuccinimidyl sulfoxide) followed by quenching with 100mM Tris-HCl, pH8 (final concentration). Samples were further denatured with 8M urea, reduced and alkylated with 5mM TCEP and 10mM chloroacetamide and subsequently digested with Lys-C and trypsin overnight. Samples were dissolved in 10% acetonitrile and LC-MS analysis was performed using an Orbitrap Fusion LUMOS mass spectrometer.

5 DISCUSSION

5.1 Rif1 function at native telomeres

Rif1 is part of the Rif1-Rif2-Rap1 complex covering the double-stranded part of the telomere in budding yeast. Native yeast telomeric repeats are ~300 bp long with an irregular arrangement of Rap1 binding sites, estimated to occur on average every 18 bp (Gilson et al., 1993). Based on this work the molecular architecture of Rif1 supports a twofold mode of interaction with telomeres: protein-protein interactions with Rap1 and direct DNA binding. The Rif1-NTD is tied to the Rap1 binding motifs (CTD and RBM) by a >550 aa linked region (Shi et al., 2013). We suggest that this arrangement provides a high local concentration of Rif1 and sufficient flexibility for Rif1 to engage with accessible DNA in the space between Rap1 binding sites. As Rif1-NTD does not bind to ssDNA of 20 nt in length, we do not expect Rif1 to compete with the CST binding to the short 3' overhangs present outside of S-phase. Thus, the structure and biochemical characterization of the Rif1-NTD presented provides a detailed molecular model of the protein capping architecture at the duplex portion of the yeast telomere. The Rif1-NTD together with the Rap1-Rif1-Rif2 network forming multiple long-range interactions provides a detailed molecular model of a "belts and braces" mechanism to protect the telomere from DNA damage sensors (Figure 5.1).

The telomere elongation phenotype of the *rif1*$_{HOOK}$ mutant supports a previously unknown functional role for Rif1 DNA binding in telomere length regulation. Strikingly, the *rif1*$_{HOOK}$ allele conferred a more severe telomere length defect than the Rap1-binding defective *rif1*$_{RBM}$ allele, while the latter reduces Rif1 occupancy at telomeres more drastically judged by ChIP. Our finding thus supports an effector function of the Rif1-NTD that goes beyond a recruitment role (Figure 5.1A). The ability of Rif1 to directly bind to DNA is thus crucial for telomere homeostasis and it supports a model, in which the Rif1-NTD serves as a downstream effector analogously to mammalian RIF1 at DSBs. The Rif1-NTD DNA binding provides a potential mechanism to directly block access of telomerase, the DNA resection machinery and checkpoint signaling machinery, given the elongated shape and large size of Rif1-NTD (125 kDa, 250 Å long). This in itself could account for the major functions of Rif1 at telomeres.

Chromosome ends in vertebrates form higher-order t-loops as another layer of telomere protection. The telomeric 3'-overhang loops back and invades the duplex telomere DNA, displacing the G-rich strand, and the whole loop is covered by the six-membered shelterin complex. The telomeric repeats are sequence-specifically bound by TRF2 and TRF1 and none of the shelterin complex members form and alpha-helical repeat. In contrast, budding yeast telomeres are

protected by double-strand (Rap1-Rif1-Rif2) and single-strand (Cdc13-Ten1-Stn1) protecting complexes where Rap1 and Cdc13 form sequence-specific DNA-interactions. Budding yeast telomeres are thought to not form t-loops but higher order fold-back structures. In contrast to mammalian t-loops where the single-stranded overhang invades double-stranded telomeric DNA, budding yeast fold-back structures are thought to be mediated by loosely defined protein-protein interactions (de Bruin et al., 2000; de Bruin et al., 2001; Strahl-Bolsinger et al., 1997; Zakian, 2012). The yKu70/80 heterodimer and Rif2 were shown to contribute to telomere folding (Marvin et al., 2009; Poschke et al., 2012). Poschke et al. already noted that a Rif1 deletion causes a defect in fold-back structures of the telomere. However, the authors did not perform further analysis on Rif1 because a Rif1 deletion causes defects on telomere length regulation, telomere capping, and checkpoint regulation. Thus, it is possible that Rif1 mediates the fold-back structures at the budding yeast telomere by engaging dsDNA through both DNA binding channels. In this hypothetical model Rap1 recruits Rif1 and Rif2 through their Rap1 binding motifs, Rif1-NTD interacts with telomeric DNA directly, and Rif1-NTD could mediate fold-back structures through both DNA-binding channels. This model fits with the previously suggested "Velcro" model (Shi et al., 2013) and offers an additional layer of telomere protection.

Another mechanism, which protects telomeres in order not to be mistaken as a DSB, is the transcription of telomeric repeat-containing RNA (TERRA). TERRA is suggested to be conserved from yeast to human (Azzalin et al., 2007; Luke et al., 2008). TERRA elements are transcribed within the telomeric and sub-telomeric region – a tightly regulated process throughout the cell cycle - and TERRA accumulates as telomeres shorten. Rif1 and Rif2 have been shown to repress TERRA transcription in budding yeast (Graf et al., 2017; Iglesias et al., 2011). Even though the exact role of Rif1 in TERRA is not clear, the Rif1 Hook mutant may allow a new handle on the investigation of telomeric repression via TERRA. Rif1 binding affinity to RNA or DNA:RNA hybrids have not been tested in this study but it is likely that Rif1 also shows a high affinity for DNA:RNA hybrids considering the interaction with the Hook domain is mediated by the DNA backbone.

In summary, the Rif1 direct interaction with DNA offers another line of telomere protection, blocks access from other proteins by forming a meshwork, which offers a mechanism to shield telomeric DNA.

Figure 5.1

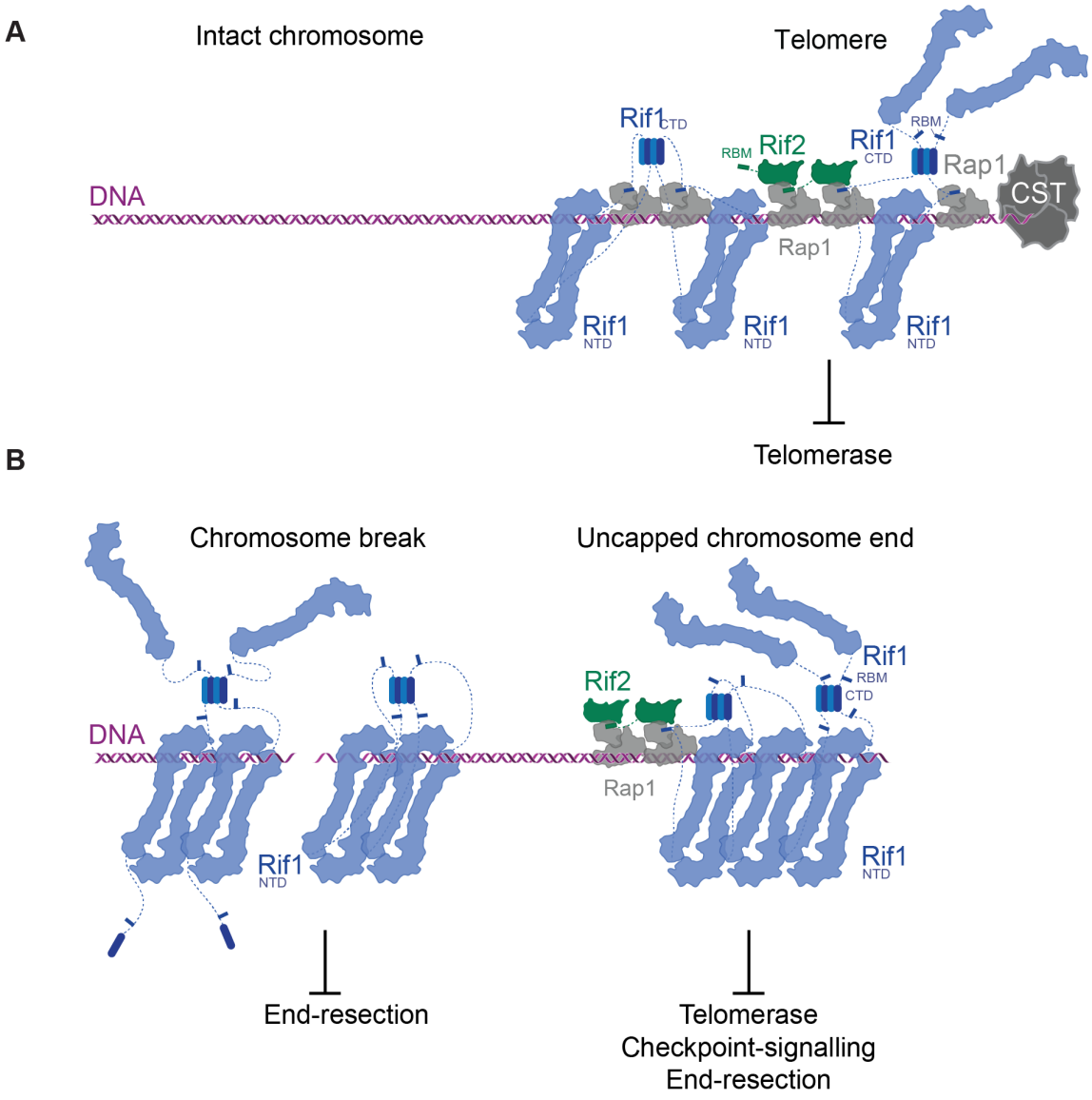

Figure 5.2 – Rif1-NTD controls the fate of DNA ends at telomeres and chromosome breaks. A At native S. cerevisiae telomeres, Rap1 recruits Rif1 and Rif2 to form an intricate protective protein sheath, while Cdc13-Stn1-Ten1 (CST) cover the ssDNA overhang. Telomerase inhibition is dependent on the newly identified Rif1-NTD DNA-binding activity, which may contribute to telomere architecture by engaging unoccupied dsDNA and ssDNA proximal to Rap1 sites. Note that while one dsDNA is shown bound per Rif1-NTD dimer, two DNA molecules could conceivably be bound by each Rif1-NTD dimer, as seen in the crystal structure. A, The Rif1-NTD also engages DNA ends in a Rap1-independent manner, coating ssDNA/dsDNA junctions at chromosome-internal breaks. Rif1-NTD binding DNA at chromosome breaks blocks end-resection, stabilizes DNA ends and facilitates NHEJ. By binding cooperatively, Rif1 is equipped to spread into neighboring DNA regions, insulating the DNA and preventing access of processing factors, a mechanism shared between telomeres and chromosome breaks. Crystallographic models for Rif1-NTD, Rif1-CTD and RBM (blue), Rap1 (light gray), Rif2 (green) and CST (gray) are shown as solid outlines. Dotted lines indicate unstructured parts of Rif1 and Rif2.

5.2 Rif1 at aberrant telomeres and uncapped chromosomes in budding yeast

At uncapped telomeres, the Rif1-NTD DNA-binding domain promotes DNA interactions independent of Rap1 (Xue et al., 2011). Surprisingly, the Rif1-NTD is essential to protect uncapped telomeres in *cdc13-1* cells. A direct role of Rif1 in the inhibition of DNA end resection was shown here using rapid depletion of Rif1 in *cdc13-1* cells and it further demonstrates the protective effect of Rif1 depends on a functional Rif1-NTD DNA-binding domain. Based on its biochemical properties, the Rif1-NTD could in principle bind to 3' overhangs and then nucleate further along the dsDNA. Co-migration of Rif1 with the resection junctions at uncapped *cdc13-1* telomeres has been described (Xue et al., 2011) and would be consistent with our model. While it may be tempting to speculate that direct DNA binding is sufficient to explain Rif1-NTD recruitment to different types of telomeric and non-telomeric breaks *in vivo*, other proteins likely contribute to localization and function of Rif1. For example, Rap1 is also recruiting Rif1 to telomeres and thereby supporting Rif1 functions at the telomere.

In mammalian cells, the shelterin complex protects the telomere. But when TRF2 is deleted, 53BP1 localizes to the telomere and RIF1 blocks hyper-resection of the uncapped telomere. Thus, RIF1 is the key downstream effector of 53BP1 at aberrant telomeres (Zimmermann et al., 2013). RIF1 blocks resection at aberrant telomeres when TRF2 or TPP1/POT1 are deleted in the presence of the other shelterin members (Kibe et al., 2016; Zimmermann et al., 2013). This is remarkable because a deletion of TPP1/POT1 causes unprotected ssDNA, which triggers the activation of the ATR kinase and not the ATM kinase (Kibe et al., 2016). Considering that 53BP1 readily localizes to the aberrant telomeres and RIF1 blocks resection analogously to TRF2 deletion, this suggests that ATR can also phosphorylate 53BP1 by its S/TQ sites so that RIF1 is recruited as the key downstream effector in the same way as it is recruited to DSBs. This shows that even though RIF1 is not part of shelterin in mammalian cells, it still blocks telomere resection in aberrant telomeres in mammalian cells.

5.3 The Rif1-NTD structure in comparison to other structures in DNA repair and telomere biology

The structure of Rif1-NTD reveals a remarkably extended helical architecture with a crook-shaped appearance. It is an irregular alpha-helical repeat fold containing HEAT-like and ARM-like elements. Different crystals showed conformational flexibility of the Shaft domain resulting in different angles of the Shaft domain relative to the Hook domain. The angle between different Shaft domains varied

up to 20 degrees (Figure 2.7B). Helical repeats are often observed to be flexible (Conti et al., 2006; Groves et al.). An example where this has been studied systematically is importin-beta – a HEAT repeat. There are four crystal structures available of importin-beta in complex with different binding partners and every structure shows a different overall conformation with respect to curvature and the opening of the arch (Cingolani et al., 1999; Lee et al., 2005; Lee et al., 2003; Liu and Stewart, 2005). Thus, it is likely that the observed changes in Shaft conformation reflect the flexible nature of the Rif1-NTD.

Rif1 is the only alpha-helical repeat protein at the budding yeast telomere and there is no alpha-helical repeat protein solved or predicted to be part of the human shelterin complex (Figure 1.4). This is remarkable because this poses the question of what the function of the extended helical repeat at the budding yeast telomere is. In fission yeast, Rif1 is also a telomere-associated protein, lacking the C-terminal Rap1 binding motif. Rif1 is recruited to the telomere via the interaction with Taz1 (homolog of TRF1 and TRF2 in human) and not via an interaction with Rap1 (Miller et al., 2005). Similarly to budding yeast, Rif1 in *S.pombe* restricts the elongation of the telomere but, in contrast to budding yeast, in a Rap1 independent way. These observations suggest that the Rif1-NTD might block access of telomerase to the telomere once recruited. Whether the extended helical repeat fulfills this role by the sheer size or whether Rif1 recruits other downstream factors remains elusive.

In contrast, in DSB repair there are several extended alpha-helical repeat proteins. ATM, ATR, and DNA-PKcs all have an enormous extended alpha-helical repeat, which serves as protein-protein interaction surfaces and scaffolding. However, the molecular role of the HEAT repeats within ATM, ATR, and DNA-PKcs is still under investigation and further structural studies on the interaction with their binding partners, including DNA, will elucidate their molecular action in DNA repair (see also 5.5)

5.4 Rif1 helical repeat binds dsDNA with Hook domain

Rif1-NTD appears to be in a monomer/dimer equilibrium, which in the absence of DNA is monomeric and in the presence of DNA is shifted predominantly to a dimeric state judged by negative stain EM. This implies that a DNA bound Rif1 molecule creates a surface attractive for a second Rif1 molecule. In the co-crystal structure, the Shaft domain appears as a lid, closing over the DNA bound Hook of a second Rif1 molecule. However, the Shaft domain of the Rif1 dimer in the co-crystal structure can adopt many different conformations with respect to the Hook domain judged by different crystals. Based on the co-crystal structure, the Rif1 molecules interact mostly via the transition domain of the helical repeat. Limited by resolution of the crystal, one can only guess, which residues are critical for the dimer formation in the transition motif. Interestingly, Cdc13 has

a separate DNA binding and a dimerization domain. Point mutants within the DNA binding motif cause telomere elongation, implying that DNA-binding defective Cdc13 cannot sufficiently block telomerase. In contrast, Cdc13 dimerization mutants showed a decrease in telomere length, which implies a defect in telomerase recruitment to telomeres (Mitchell et al., 2010). These finding can so far not be explained on a molecular level. It would be interesting to study Rif1 mutants defective in dimerization without disrupting the DNA binding, in order to examine whether the disruption in Rif1 dimerization causes a similar telomere shortening effect as in Cdc13.

In the crystal structure, a figure-8-shaped dimer of Rif1 engages 30 bp dsDNA through both channels. Each 30bp dsDNA is covered by two dimers suggesting a DNA length of 15bp dsDNA as the Rif1 binding site. The crystals grew in the presence of 3‘-overhang substrates having a 30bp dsDNA and 30nt or 24nt overhang. The ssDNA cannot be traced in the electron density. By EMSA analysis, Rif1 prefers a 3’-overhang substrate compared to ssDNA and dsDNA substrates of the same length. Rif1 readily binds to ssDNA on EMSA and the binding pattern looks very different implying that different Rif1-DNA conformations are formed causing them to run differently through an agarose gel. While it is unclear how exactly the ssDNA overhang is bound by Rif1, it is possible that the ssDNA is bound by Rif1 with a so far unidentified binding site. Another possibility is that the ssDNA adopts the same overall conformation as dsDNA by following the path of a duplex. If this is the case, the recognition of DNA would be analogous to the RecA helicase where a single-strand DNA also follows the path of ssDNA (Chen et al., 2008c).

In contrast to Rap1 and Cdc13, Rif1 is a sequence-independent binder. Therefore, we do not expect that Rif1 can outcompete Rap1 on telomeric DNA even though Rif1 shows a low nanomolar affinity to DNA. However, Rap1 binds the consensus DNA sequence of 5´-ACACCCATACACC-3´ and is very sensitive to sequence alterations because the CCC core is invariable (Wahlin and Cohn, 2000; Grossi et al., 2001; Graham and Chambers, 1994). Since the budding yeast telomere is comprised of irregular $TG_{1\text{-}3}$ repeats, it is likely that Rif1 can compete with Rap1 at dsDNA, which does not have CCC cores. This encircling of dsDNA by Rif1-NTD and the binding of Rif1 to Rap1 via the Rap1 binding motif provides a protein sheath that shields and protects DNA from being detected by other DNA repair proteins.

The concave surface of the Hook domain of Rif1 contains 12 positively charged residues, which contribute to the DNA binding. While mutating the residues K437E/K563E/K570E (Hook mutant) and K691E/K692E (Loop mutant) resulted in stably recombinantly expressed Rif1 protein and showed an equal expression of the protein in yeast, mutating R401E/K406E/K451E or R401E/K406E/K451E/ K518E/D522A did not result in sufficient expression of Rif1. Additionally, these mutants did not express to wild-type level when integrated into the *S. cerevisiae* genome.

Mutating two or three residues out of the 12 possible in the Hook domain did reduce but not fully abrogate the DNA binding. Analogously, sequence unspecific DNA binders have been shown to require several mutations. The KU70/80 heterodimer is the strongest identified dsDNA end binder and has a measured affinity of around 10nM (Paillard and Strauss, 1991). In order to ablate the DNA binding through the DNA binding channel, six charge reversal mutations are required (Britton et al., 2013). Additionally, an alanine scanning approach on Cdc13 revealed that changing one positively charged residue, which mediates the interaction with the phosphate backbone of the DNA, is tolerated and only shows a minor effect to ssDNA binding (Anderson et al., 2003). Thus, by mutating two or three residues in the Hook domain, Rif1-NTD DNA binding was only reduced biochemically and not fully abrogated. Therefore, the Hook and Loop mutant only hit the DNA binding site partially. However, making the Rif1-NTD DNA binding-deficient is enough to elicit a full phenotype in telomere length regulation and DSB repair showing that a decrease in DNA binding affinity renders the Rif1-NTD incapable to compete with other factors in order to protect DNA-ends *in vivo*.

5.5 The DNA binding of the Rif1 alpha-helical repeat – An emerging mode of DNA binding?

The Rif1-NTD adopts an elongated helical repeat and a DNA duplex is held by the concave face of the Rif1-NTD Hook domain. The Rif1 N-terminal domain is a high-affinity DNA-binding module capable of encircling duplex DNA in a sequence-independent manner. Unexpectedly, Rif1 bound dsDNA directly and this makes Rif1 one of the very few structurally determined helical repeats proteins in complex with DNA. Protein-DNA complexes such as DNA-PKcs-Ku80 were recently structurally analyzed and it is thought that they also directly bind to DNA (Sibanda et al., 2017; Sibanda et al., 2010). Moreover, ATM was recently determined to atomic resolution (Baretic et al., 2017). However, in both cases, the DNA was not part of the electron density so that the authors suggested possible models for DNA binding of the HEAT repeats. Therefore, it is currently not clear how the DNA is held.

Some DNA Glycosylases such as AlkD are HEAT-like repeats and were co-crystallized with dsDNA, forming a positively charged concave surface surrounding nearly one half of the duplex (Rubinson and Eichman, 2012; Rubinson et al., 2010). As well as Rif1-NTD, AlkD was not predicted to directly interact with the DNA and is also lacking a substrate recognition motif. In contrast to sequence-specific binders, the overall arc-shaped conformation of the HEAT-like repeat holds the DNA via electrostatic interactions mediated between positively charged lysines or arginines and the phosphate backbone of the dsDNA. Even though AlkD shows a damage-specific binding to double-

stranded DNA (N3-alkylpurine) and additionally induces a distortion in the DNA helix (Mullins et al., 2015), which we did not detect in our crystals, the overall DNA recognition of Rif1-NTD and AlkD is similar (Figure 5.2A).

More HEAT repeats, which were shown to directly and sequence-independently bind to DNA, are members of the condensin complex. During cell division chromosomes are compacted before chromosomes segregate into daughter cells and condensins mediate the re-organization of chromosome structure during mitosis (Hagstrom and Meyer, 2003). The budding yeast condensin complex consists of a five-membered complex: Smc2, Smc4, Brn1, Ycg1, and Ycs4. While Smc2 and Smc4 are extended antiparallel coiled-coils and are thought to encircle chromatin fibers, Ycg1 and Ycs4 contain one or two HEAT repeats, respectively, and they have been shown to directly bind DNA with a preference for double-stranded DNA in a sequence-independent manner by EMSA and Fluorescent Polarization (Piazza et al., 2014). Very recently the same group published co-crystal structures of the Ycg1 HEAT-repeat, double-stranded DNA, and a Brn1 peptide revealing that an 18 bp double-stranded DNA is bound by the positively charged groove formed by the Ycg1 HEAT-repeat (Figure 5.2A) (Kschonsak et al., 2017). In this co-crystal structure, the double-stranded DNA is also bound by a Brn1 peptide and the authors suggest that Brn1 assists Ycg1-DNA binding. Rif1-NTD is also assisted through the Rap1 interaction to localize to telomeres and it is possible that the Rif1-NTD is supported by a so far uncharacterized interaction to localize to DSBs. Taken together, Rif1-NTD, AlkD, and Ycg1 are all alpha-helical repeats, which directly bind to DNA in a sequence-independent manner via their concave surfaces of the arch-shaped structures (Figure 5.2A).

Another direct nucleic acid binder is Pumilio1, which forms an ARM-like-repeat where the second helix per ARM motif is lining the concave surface of the arch-like architecture. Pumilio binds sequence specifically to 3’ untranslated regions of mRNAs. In contrast to Rif1-NTD, Pumilio was co-crystallized in the presence of different single-stranded RNA substrates and the nucleotide bases are specifically bound (figure 5.2B) (Gupta et al., 2008; Wang et al., 2001).

This illustrates that helical repeats can interact with nucleic acids in different and versatile manners. Due to the low number of co-crystals or atomic resolution cryo-EM maps in complex with DNA, we can

Figure 5.2

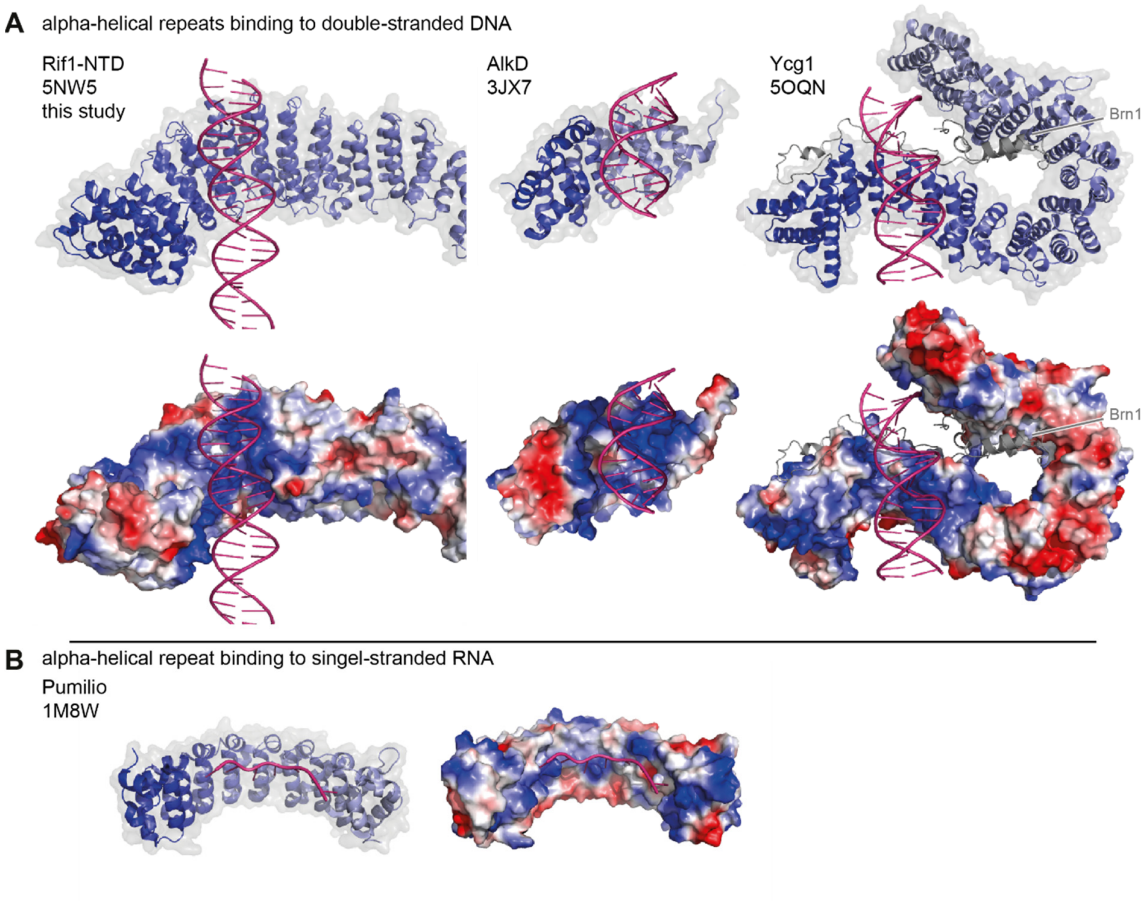

Figure 5.2 – Co-crystal structures of alpha-helical repeats and nucleic acids. A, Alpha-helical repeats proteins, Rif1-NTD, AlkD, and Ycg1 (all blue) in complex with double-stranded DNA (pink) depicted as cartoon representation. Surface electrostatics are depicted underneath. Co-factor (Brn1) is depicted in gray. Structures retrieved from the Protein Data Bank (PDB), PDB codes are listed. B, Pumilio (blue) in complex with single-stranded RNA (pink) depicted as cartoon representation and surface electrostatics, PDB code is listed.

poorly predict the DNA binding ability of alpha-helical repeat proteins and we probably underestimate the number of helical repeats directly interacting with DNA.

5.6 Rif1 at double-strand breaks in yeast and human

Budding yeast Rif1 does not show a preference for telomere sequences but binds to random sequences equally well *in vitro*. Consistently, Rif1 binds to telomeric and non-telomeric induced DSBs *in vivo* assessed by ChIP, which implicates that Rif1-NTD has an intrinsic DNA binding activity strong enough to compete with other DSB factors in the cell. To study the involvement of Rif1 in DNA repair, we used a strain, in which a single DSBs is induced at the MATα locus by HO-endonuclease expression. The concomitant deletion of the silent mating type cassettes *HML* and *HMR* sites, which usually serve as donor templates, ensures that this DSB cannot be repaired by HR,

providing a survival-based assay to directly score NHEJ efficiency (Moore and Haber, 1996). Rif1 deletion causes a 40% drop in survival compared to wild-type strains, indicating that Rif1 is involved in the repair of DSB by NHEJ. Strikingly, the Rif1-NTD DNA-binding deficient mutant (Rif1_Hook), shows the same effect in cell survival compared to the Rif1 deletion, whereas mutating the RVxF/SILK motif did not show an effect. ChIP analyses confirmed that the Rif1_Hook mutations decrease the enrichment of Rif1 in the proximity of the DSB site, providing a rationale to assess putative DNA end-protection roles for the protein. By performing a qPCR-based method designed to quantify the amount of single-stranded DNA produced by end-resection at the MATα locus (Zierhut and Diffley, 2008), we found that cells deleted for Rif1 or expressing the Rif1_Hook mutant show increased levels of ssDNA. These results demonstrate that budding yeast Rif1, like its mammalian counterpart, plays an important role in DSB repair pathway choice. This function strictly depends on the Rif1-NTD and its ability to bind DNA directly in budding yeast. At critically short telomeres, uncapped chromosome ends, and DSBs, the engagement of Rif1 with DNA attenuates DNA end resection, which at DSBs imposes a NHEJ repair bias (Figure 5.1B). Additionally, the observation that Rif1 has a preference for junction DNA provides a mechanism to guide Rif1 to its target sites at both telomeres and DSB ends. Although the Rif1_Hook mutant protein retains residual DNA binding judged by EMSA analyses and by ChIP, their binding defects elicit a severe and a full loss of function phenotype at DSB repair pathway choice.

Human RIF1 recruitment to 53BP1 is strictly dependent on phosphorylated 53BP1 (Rad9 in *S. cerevisiae*) (Chapman et al., 2013; Di Virgilio et al., 2013; Escribano-Diaz et al., 2013; Silverman et al., 2004). Budding yeast Rif1 recruitment to both telomeric and non-telomeric breaks, in contrast, is not dependent on Rad9 but operates through multiple Rap1 interactions at the telomere, or direct DNA binding via the-NTD, respectively (Figure 2.14H and I). This suggests that the overall function of Rif1 in blocking resection at aberrant telomeres and DSBs is conserved from yeast to human, however, the regulation and recruitment of Rif1 likely differ (Escribano-Diaz et al., 2013; Kibe et al., 2016; Mattarocci et al., 2017).

The most conserved Rif1 domain across organisms is the Rif1-NTD, particularly the Hook domain. Modelling human RIF based on the budding yeast template and other helical repeat proteins suggests that the Hook domain in mammals also adopts a HEAT-like repeat. In contrast to the solved structure of Rif1, the model of the RIF1-NTD Hook domain does not show a positively charged concave surface of the arch, and DNA binding residues defined in yeast Rif1 cannot be translated to the human structure. Additionally, RIF1-NTD does not bind DNA by fluorescent polarization, which suggests that RIF1-NTD localizes to DSB in a different way compared to the yeast version, while keeping the effector function and the ability to block of resection. Considering that RIF1

recruitment to DSBs is strictly dependent on 53BP1, mammalian cells have a complex network of players fulfilling regulatory functions and harboring post-translational modification marks. The direct interaction between phosphorylated 53BP1 peptide and hRif1-NTD by fluorescent polarization demonstrates for the first time that RIF1 is conserved in function but different in its regulation and binding partners.

The conserved N-terminal helical repeat was a mystery, particularly in terms of its structure and direct interaction partners. The Rif1-NTD in budding yeast was not predicted to bind to DNA directly, even though it was clear that it is recruited to the budding yeast telomere independently of Rap1 (Xue et al., 2011). Our analysis illustrates that the function of the Rif1-NTD goes beyond a purely structural role of the helical repeat and shows that Rif1-NTD can bind to unpredicted binding partners. The yeast and human Rif1-NTDs selectively bind to DNA or phosphorylated 53BP1, respectively, and thereby both block resection of DNA ends.

5.6.1 The 53BP1-RIF1 interplay and its consequences

Our data shows that the RIF1-NTD directly interacts with phosphorylated 53BP1 peptide in a phosphorylation-dependent manner. Thus, the helical repeat is able to discriminate between the double-phosphorylated and the unphosphorylated peptides. This is a striking finding as this is to our knowledge, the first helical repeat (HEAT or armadillo) shown to specifically bind to a phosphorylated motif. There are other helices domains such as the 14-3-3 proteins consisting of nine antiparallel helices and they specifically bind to phosphorylated serine or threonine residues. 14-3-3 form a concave surface lined by four helices, which mediate the interaction with the phospho-peptide using three positively charged Arginines or Lysines (Reichen et al., 2014; Yaffe et al., 1997; Yaffe and Smerdon, 2001). Another known domain mediating phospho-peptide interactions are BRCT domains (Manke et al., 2003). One example is the BRCT2 domain of 53BP1, which was crystallized in the presence of the H2AX-pS139 phosphorylated peptide (denoted as gamma-H2AX) (Baldock et al., 2015). The crystal showed that the side chain of Lys1814 in 53BP1 interacts with the phospho-Ser139. Analogously to the RIF1-NTD - 53BP1 peptide interaction, the dephosphorylation of the peptide or a single site-directed mutagenesis of Lys1814 abrogated the binding between the BRCT2 domain and the phosphorylated peptide *in vitro* (Baldock et al., 2015). This finding is not just biochemically analogous to the RIF1-53BP1 interaction, but also reveals a more direct role of 53BP1 in DSB detection. The authors showed that 53BP1 can directly bind to gamma-H2AX via its BRCT2 domain, which opens a parallel localization of 53BP1 to DSBs without the presence of MRN, ATM, MDC1, RNF8, and RNF168. The direct interaction between the BRCT2

domain and gamma-H2AX may be a reinforcement mechanisms helping with the recruitment of ATM and MRN, even though it is probably not a major route of recruitment.

A direct interaction of RIF1-NTD with a phosphorylated 53BP1 motif poses the question whether other motifs are used for protein recruitment in DNA repair. The PIKK kinases (ATM, ATR, and DNA-PKcs) have been shown to be recruited to DNA damage via conserved C-terminal peptide sequences of NBS1, ATRIP, and Ku80, respectively (Falck et al., 2005). NBS1, KU80, and ATRIP all contain a C-terminal motif consisting of the minimal consensus $EE(x)_{3-4}DDL$. The C-terminal motif is conserved in metazoans for each protein and NBS1, KU80 and ATRIP show different residues before, between and after the negatively charged glutamic and aspartic acids. Specific interaction between the three PIKK kinases and NBS1, KU80 and ATRIP have been shown by pull-down and mutational analysis of the negatively charged residues (Falck et al., 2005). Interestingly, the authors saw an overlapping recruitment of PIKK kinases to NBS1, KU80, and ATRIP peptides but not the full-length proteins by pull-down assays. The authors suggest that PIKK kinases interact through a larger surface, which also contributes to the discrimination between the adaptor proteins. A similar scenario could be true for the 53BP1-RIF1 interaction. We were able to detect six crosslinks between RIF1-NTD and 53BP1 by mass spectrometry, which were far away from the linked phosphorylated peptide. In contrast, no crosslinks were detected when the phospho-peptide was not linked. This implies that the 53BP1 and RIF1 interaction is induced by the phospho-peptide and further interactions result when the two proteins come closer.

Rif1 blocks resection at aberrant telomeres and DSBs in yeast and human. While this function is strictly dependent on 53BP1 in human, the budding yeast 53BP1 homolog, Rad9, was not detected to play a role in the localization of Rif1 to DSBs (Figure 2.14H and I). RIF1 is the key effector molecule for the promotion of NHEJ and it likely recruits many factors to promote NHEJ, such as MAD2L2, which is also recruited by the RIF1-NTD (Boersma et al., 2015). Considering that a MAD2L2 depletion is only impairing, but not fully abolishing NHEJ at aberrant telomeres, whereas 53BP1 and RIF1 deletions do, it is very likely that there are more downstream factors of RIF1 to be identified.

Another binding partner of 53BP1, which has been identified and may modify the 53BP1-RIF1 interaction, is the association with the LINC complex (Lottersberger et al., 2015). The region spanning between the RIF1-interacting phospho-motifs and the oligomerization domain of 53BP1 has recently been shown to be required for increased mobility of a 53BP1 associated DSB. The increased mobility is also dependent on ATM dependent phosphorylation of S/TQ sites, on the LINC complex association and on microtubule dynamics (Lottersberger et al., 2015). The identified mobility region is predicted to be unstructured and we are so far lacking a molecular understanding

of the interaction. Additionally, the identified mobility region is not overlapping with our identified phospho-sites required for the 53BP1-RIF1 interaction. Further biochemical and structural studies should identify the motifs on 53BP1 required for the LINC association, allowing a separation-of-function understanding of the 53BP1-LINC interaction. Even though the mobility region and the RIF1-interaction motifs are not overlapping, it is possible that the association with the LINC complex modifies the 53BP1-RIF1 interaction.

5.6.2 The oligomeric state of 53BP1 and RIF1

The SEC-MALS results suggest that 53BP1 forms a trimer when expressed recombinantly, but it does not form a trimer conformation when bound to Rif1. The SEC-MALS profile suggests a 1:1 interaction even though the measured mass is ~10kDa too large. This finding would suggest that 53BP1 is recruited as a trimer to chromatin marks, but once RIF1 is bound, the oligomerization is disrupted to lead to a 1:1 binding. In cells, the recruitment of RIF1 and blocking of resection at dysfunctional telomeres is only mildly impaired when the oligomerization is disrupted. This would argue that the oligomerization domain plays a minor role in DSB repair and most breaks can be repaired without it. However, looking at more downstream phenotypes such as class switch recombination efficiency in B-cells, disruption of the oligomerization domain causes a loss of function in B-cells (Lottersberger et al., 2013). The role of the oligomerization of 53BP1 is not clear in CSR and it is possible that 53BP1 helps directly or indirectly to tether the DNA ends together in CSR or even triggers synapsis and the oligomerization domain may play a role in this process (Dong et al., 2015). Mutating the oligomerization domain shows a small reduction in DSB focus formation upon gamma irradiation or when aberrant telomeres are induced. Even though the effect on focus formation and telomere fusion is mild, we may underestimate the consequences of a mild reduction, because successful DSB ligation is not monitored in focus formation analysis. Taken together, 53BP1 and RIF1 work together in DSB pathway choice after exogenous damage as well as in immunoglobulin CSR - a DSB triggered by the cell. Further analysis on the change in oligomeric state upon RIF1 binding is required and should shed light on the functional importance of the oligomerization domain. The RIF1-53BP1 interplay is at the core of DSB pathway choice and it is going to be exciting to get a better biochemical and structural understanding of the 53BP1-RIF1 interaction, particularly to define the interaction surface and potentially elucidate further, whether RIF1 binding and oligomerization are mutually exclusive.

5.6.3 RIF1 – more than a downstream effector?

RIF1 is the key downstream effector of 53BP1, implying a purely sequential role after 53BP1 arrival. However, recent studies showed that Rif1 is not just required to block resection downstream of

53BP1, but also to dissociate the Tudor interacting repair regulator (TIRR) from 53BP1 (Drane et al., 2017). TIRR was identified as a novel binding partner of 53BP1 and was shown to mask the 53BP1 Tudor domain so that it can either bind to H4K20me2 or to TIRR. In order for 53BP1 to dissociate from TIRR, the first 700 residues of 53BP1, ATM, and RIF1 have to be present in human cells (Drane et al., 2017). Considering that all three identified LxL-S/TQ S/TQ motifs are within the first 700 residues of 53BP1 and that the Rif1-NTD mediates the direct interaction with the phosphorylated motif, it suggests that the Rif1-NTD causes the TIRR-53BP1 dissociation. These findings suggest that RIF1 not only has a function downstream of 53BP1 as an effector but also upstream of 53BP1 focus formation to allow TIRR-53BP1 dissociation. A molecular understanding of the RIF1-53BP1 interplay is the basis for further analysis, and a better biochemical and structural understanding of 53BP1-Rif1 complex formation is expected to shed light on the potential role of hRif1 upstream of 53BP1

The Rif1-NTD is the key functional module within the Rif1 protein in yeast and human. The crystal structure of the full helical repeat of Rif1 gives insight into our molecular understanding of the structure and the direct interaction with DNA in budding yeast. Even though 53BP1 has been studied extensively in cells, we are only beginning to understand the 53BP1 interaction partners on a molecular level. This work enables us to start to understand the RIF1-NTD 53BP1 interaction and complex formation. Further structural and biochemical studies on RIF1, its interplay with 53BP1, and possibly other binding partners should inform us about the full RIF1-53BP1 interaction surface and how RIF1 fulfills the effector functions - downstream and upstream of 53BP1. It is currently unclear how RIF1-53BP1 competes with BRCA1-CtIP for access to DSBs and how it is able to block DNA resection in G1 (Escribano-Diaz et al., 2013). A structural approach may elucidate how 53BP1 and RIF1 form a protein-meshwork on nucleosomes, restricting access for BRCA1-CtIP.

5.7 Possible functions of the Rif1-NTD DNA-binding outside of end protection

Although we find that Rif1 has a preference to 3'-tailed DNA junctions compared to ssDNA and dsDNA, the Rif1-NTD exhibits high affinity for diverse DNA substrates including forks and Holliday junctions. It is likely that Rif1-NTD also binds other nucleic acid structures such as G-quadruplexes, RNA, or telomeric RNA/DNA hybrids considering that the protein DNA interaction is mostly electrostatic. Recent findings have implicated *S.pombe* Rif1 in the regulation of late origin firing during DNA replication (Kanoh et al., 2015b). The authors found Rif1 chromatin immuno-precipitated to 35 binding sites within the fission yeast genome and the authors concluded that Rif1 bound to G-quadruplex structures specifically (Kanoh et al., 2015b). The Hook domain would be big

enough to allow a G-quadruplex to bind and it gives an elegant explanation of how Rif1 is recruited to some loci in the genome and not to others, which was so far unanswered. Another study in fission yeast suggested a G-quadruplex-independent recruitment of Rif1 to DNA (Zaaijer et al., 2016). The authors observed Rif1 recruitment to telomere entanglements as well as ultrafine anaphase bridges and showed that Rif1 localization to these DNA substrates is independent of the 53BP1 ortholog, Crb2, in fission yeast. This finding is in line with our findings, that Rif1 is able to interact with DNA ends directly and independently of Rad9, the budding yeast 53BP1 ortholog. Zaaijer et al. speculate that the Rif1 C-terminal DNA binding motif would be responsible for the localization. The DNA binding activity of the Rif1-NTD Hook domain could explain the DNA association they observed, even though there is possibly another factor involved in recruiting Rif1 to telomere entanglements and ultrafine anaphase bridges.

Additionally, RIF1 is recruited to mammalian late origins by a so far undetermined mechanism, which is independent of 53BP1 (Foti et al., 2016). Rif1 not just localizes to late origins, but also associates with lamin B1. When RIF1 is deleted, it causes a loss of spatial chromatin organization followed by a replication-timing disruption. This study suggests a 3D organizational role of Rif1 in mammalian cells. Another study also suggests that Rif1 and Taz1 determine the expression-state boundaries in fission yeast (Toteva et al., 2017). While it seems unlikely that the Rif1-NTD directly interacts with the DNA in mammalian cells, it is possible that the 3D organizational role of Rif1 in fission yeast is also mediated via the DNA binding activity of the Rif1-NTD. Taken together, Rif1 has been found to localize DNA independently of 53BP1 or DNA ends. However, it is so far not clear how Rif1 can localize to these DNA substrates and it is will be interesting to see whether further binding partner will be identified, which assist Rif1 in finding the right genomic localizations.

5.8 Relevance of DSB pathway choice in basic research and beyond

Understanding the 53BP1-RIF1 interplay is a key switch point for DSB pathway choice since the interruption of the interaction leaves cells incapable of blocking resection at DSBs (Di Virgilio et al., 2013; Escribano-Diaz et al., 2013; Zimmermann et al., 2013). Thus, the understanding of this process is a crucial question for biology and genome stability of eukaryotic cells. In addition, DSB pathway choice plays a crucial role in CRISPR-Cas9 genome editing. In CRISPR-Cas9 a genomic sequence is targeted by a complementary RNA sequence and a DSB is introduced by the Cas9 enzyme. However, only if the DSB is repaired by HR and not by NHEJ, the programmable result of gene editing is achieved. The CRISPR-Cas9 technique not just revolutionized laboratory techniques and approaches but may be used soon in the clinic for gene editing, where a reliable targeting is pivotal. Considering that NHEJ is favored in human cells over HR, it may be a future challenge to modify DSB pathway

choice. An endogenously encoded 53BP1 inhibitor, to inhibit NHEJ, has been already identified and it will be interesting to see whether it will be picked up in future clinical studies (Canny et al., 2016). Potentially, a more in-depth understanding of the 53BP1-Rif1 interaction may assist in the design of 53BP1 or hRif1 inhibitors in the future. A molecular understanding of the players involved, as well as the interactions formed, are the basis for future therapeutics.

References

Abdulrahman, W., Uhring, M., Kolb-Cheynel, I., Garnier, J.M., Moras, D., Rochel, N., Busso, D., and Poterszman, A. (2009). A set of baculovirus transfer vectors for screening of affinity tags and parallel expression strategies. Anal Biochem *385*, 383-385.

Acs, K., Luijsterburg, M.S., Ackermann, L., Salomons, F.A., Hoppe, T., and Dantuma, N.P. (2011). The AAA-ATPase VCP/p97 promotes 53BP1 recruitment by removing L3MBTL1 from DNA double-strand breaks. Nat Struct Mol Biol *18*, 1345-1350.

Anand, R., Ranjha, L., Cannavo, E., and Cejka, P. (2016). Phosphorylated CtIP Functions as a Co-factor of the MRE11-RAD50-NBS1 Endonuclease in DNA End Resection. Mol Cell *64*, 940-950.

Anbalagan, S., Bonetti, D., Lucchini, G., and Longhese, M.P. (2011). Rif1 supports the function of the CST complex in yeast telomere capping. PLoS Genet *7*, e1002024.

Anderson, E.M., Halsey, W.A., and Wuttke, D.S. (2003). Site-directed mutagenesis reveals the thermodynamic requirements for single-stranded DNA recognition by the telomere-binding protein Cdc13. Biochemistry *42*, 3751-3758.

Andrade, M.A., Petosa, C., O'Donoghue, S.I., Muller, C.W., and Bork, P. (2001). Comparison of ARM and HEAT protein repeats. J Mol Biol *309*, 1-18.

Ashkenazy, H., Abadi, S., Martz, E., Chay, O., Mayrose, I., Pupko, T., and Ben-Tal, N. (2016). ConSurf 2016: an improved methodology to estimate and visualize evolutionary conservation in macromolecules. Nucleic Acids Res *44*, W344-350.

Ashkenazy, H., Erez, E., Martz, E., Pupko, T., and Ben-Tal, N. (2010). ConSurf 2010: calculating evolutionary conservation in sequence and structure of proteins and nucleic acids. Nucleic Acids Res *38*, W529-533.

Aylon, Y., and Kupiec, M. (2003). The checkpoint protein Rad24 of Saccharomyces cerevisiae is involved in processing double-strand break ends and in recombination partner choice. Molecular and Cellular Biology *23*, 6585-6596.

Aylon, Y., Liefshitz, B., and Kupiec, M. (2004). The CDK regulates repair of double-strand breaks by homologous recombination during the cell cycle. EMBO J *23*, 4868-4875.

Azzalin, C.M., Reichenbach, P., Khoriauli, L., Giulotto, E., and Lingner, J. (2007). Telomeric repeat containing RNA and RNA surveillance factors at mammalian chromosome ends. Science *318*, 798-801.

Baker, N.A., Sept, D., Joseph, S., Holst, M.J., and McCammon, J.A. (2001). Electrostatics of nanosystems: application to microtubules and the ribosome. Proc Natl Acad Sci U S A *98*, 10037-10041.

Baldock, R.A., Day, M., Wilkinson, O.J., Cloney, R., Jeggo, P.A., Oliver, A.W., Watts, F.Z., and Pearl, L.H. (2015). ATM Localization and Heterochromatin Repair Depend on Direct Interaction of the 53BP1-BRCT2 Domain with gammaH2AX. Cell Rep *13*, 2081-2089.

Baretic, D., Pollard, H.K., Fisher, D.I., Johnson, C.M., Santhanam, B., Truman, C.M., Kouba, T., Fersht, A.R., Phillips, C., and Williams, R.L. (2017). Structures of closed and open conformations of dimeric human ATM. Sci Adv *3*, e1700933.

Betermier, M., Bertrand, P., and Lopez, B.S. (2014). Is non-homologous end-joining really an inherently error-prone process? PLoS Genet *10*, e1004086.

Beucher, A., Birraux, J., Tchouandong, L., Barton, O., Shibata, A., Conrad, S., Goodarzi, A.A., Krempler, A., Jeggo, P.A., and Lobrich, M. (2009). ATM and Artemis promote homologous recombination of radiation-induced DNA double-strand breaks in G2. EMBO J *28*, 3413-3427.

Bianchi, A., and Shore, D. (2007). Increased association of telomerase with short telomeres in yeast. Genes Dev *21*, 1726-1730.

Biessmann, H., and Mason, J.M. (1994). Telomeric repeat sequences. Chromosoma *103*, 154-161.

Blackburn, E.H., and Gall, J.G. (1978). A tandemly repeated sequence at the termini of the extrachromosomal ribosomal RNA genes in Tetrahymena. J Mol Biol *120*, 33-53.

Blackburn, E.H., Greider, C.W., and Szostak, J.W. (2006). Telomeres and telomerase: the path from maize, Tetrahymena and yeast to human cancer and aging. Nat Med *12*, 1133-1138.

Blackford, A.N., and Jackson, S.P. (2017). ATM, ATR, and DNA-PK: The Trinity at the Heart of the DNA Damage Response. Mol Cell *66*, 801-817.

Boersma, V., Moatti, N., Segura-Bayona, S., Peuscher, M.H., van der Torre, J., Wevers, B.A., Orthwein, A., Durocher, D., and Jacobs, J.J.L. (2015). MAD2L2 controls DNA repair at telomeres and DNA breaks by inhibiting 5' end resection. Nature *521*, 537-540.

Bonetti, D., Clerici, M., Anbalagan, S., Martina, M., Lucchini, G., and Longhese, M.P. (2010). Shelterin-like proteins and Yku inhibit nucleolytic processing of Saccharomyces cerevisiae telomeres. PLoS Genet *6*, e1000966.

Bothmer, A., Robbiani, D.F., Di Virgilio, M., Bunting, S.F., Klein, I.A., Feldhahn, N., Barlow, J., Chen, H.T., Bosque, D., Callen, E.*, et al.* (2011). Regulation of DNA end joining, resection, and immunoglobulin class switch recombination by 53BP1. Mol Cell *42*, 319-329.

Botuyan, M.V., Lee, J., Ward, I.M., Kim, J.E., Thompson, J.R., Chen, J., and Mer, G. (2006). Structural basis for the methylation state-specific recognition of histone H4-K20 by 53BP1 and Crb2 in DNA repair. Cell *127*, 1361-1373.

Boulton, S.J., and Jackson, S.P. (1996). Identification of a Saccharomyces cerevisiae Ku80 homologue: roles in DNA double strand break rejoining and in telomeric maintenance. Nucleic Acids Res *24*, 4639-4648.

Britton, S., Coates, J., and Jackson, S.P. (2013). A new method for high-resolution imaging of Ku foci to decipher mechanisms of DNA double-strand break repair. J Cell Biol *202*, 579-595.

Brooks, S.C., Adhikary, S., Rubinson, E.H., and Eichman, B.F. (2013). Recent advances in the structural mechanisms of DNA glycosylases. Biochim Biophys Acta *1834*, 247-271.

Brunette, T.J., Parmeggiani, F., Huang, P.S., Bhabha, G., Ekiert, D.C., Tsutakawa, S.E., Hura, G.L., Tainer, J.A., and Baker, D. (2015). Exploring the repeat protein universe through computational protein design. Nature *528*, 580-584.

Bryan, C., Rice, C., Harkisheimer, M., Schultz, D.C., and Skordalakes, E. (2013). Structure of the human telomeric Stn1-Ten1 capping complex. PLoS One *8*, e66756.

Buonomo, S.B., Wu, Y., Ferguson, D., and de Lange, T. (2009). Mammalian Rif1 contributes to replication stress survival and homology-directed repair. J Cell Biol *187*, 385-398.

Callen, E., Di Virgilio, M., Kruhlak, M.J., Nieto-Soler, M., Wong, N., Chen, H.T., Faryabi, R.B., Polato, F., Santos, M., Starnes, L.M.*, et al.* (2013). 53BP1 mediates productive and mutagenic DNA repair through distinct phosphoprotein interactions. Cell *153*, 1266-1280.

Cannavo, E., and Cejka, P. (2014). Sae2 promotes dsDNA endonuclease activity within Mre11-Rad50-Xrs2 to resect DNA breaks. Nature *514*, 122-125.

Canny, M., Wan, L., Fradet-Turcotte, A., Orthwein, A., Moatti, N., Juang, Y.-C., Zhang, W., Noordermeer, S.M., Wilson, M.D., Vorobyov, A.*, et al.* (2016). A genetically encoded inhibitor of 53BP1 to stimulate homology-based gene editing. bioRxiv.

Caron, P., Choudjaye, J., Clouaire, T., Bugler, B., Daburon, V., Aguirrebengoa, M., Mangeat, T., Iacovoni, J.S., Alvarez-Quilon, A., Cortes-Ledesma, F.*, et al.* (2015). Non-redundant Functions of ATM and DNA-PKcs in Response to DNA Double-Strand Breaks. Cell Rep *13*, 1598-1609.

Celniker, G., Nimrod, G., Ashkenazy, H., Glaser, F., Martz, E., Mayrose, I., Pupko, T., and Ben-Tal, N. (2013). ConSurf: Using Evolutionary Data to Raise Testable Hypotheses about Protein Function. Israel Journal of Chemistry *53*, 199-206.

Chang, M., Arneric, M., and Lingner, J. (2007). Telomerase repeat addition processivity is increased at critically short telomeres in a Tel1-dependent manner in Saccharomyces cerevisiae. Genes Dev *21*, 2485-2494.

Chapman, J.R., Barral, P., Vannier, J.B., Borel, V., Steger, M., Tomas-Loba, A., Sartori, A.A., Adams, I.R., Batista, F.D., and Boulton, S.J. (2013). RIF1 is essential for 53BP1-dependent nonhomologous end joining and suppression of DNA double-strand break resection. Mol Cell *49*, 858-871.

Chapman, J.R., Taylor, M.R., and Boulton, S.J. (2012). Playing the end game: DNA double-strand break repair pathway choice. Mol Cell *47*, 497-510.

Chen, C., Gu, P., Wu, J., Chen, X., Niu, S., Sun, H., Wu, L., Li, N., Peng, J., Shi, S.*, et al.* (2017). Structural insights into POT1-TPP1 interaction and POT1 C-terminal mutations in human cancer. Nat Commun *8*, 14929.

Chen, L., Nievera, C.J., Lee, A.Y., and Wu, X. (2008a). Cell cycle-dependent complex formation of BRCA1.CtIP.MRN is important for DNA double-strand break repair. J Biol Chem *283*, 7713-7720.

Chen, L., Trujillo, K., Ramos, W., Sung, P., and Tomkinson, A.E. (2001). Promotion of Dnl4-catalyzed DNA end-joining by the Rad50/Mre11/Xrs2 and Hdf1/Hdf2 complexes. Mol Cell *8*, 1105-1115.

Chen, Y., Yang, Y., van Overbeek, M., Donigian, J.R., Baciu, P., de Lange, T., and Lei, M. (2008b). A shared docking motif in TRF1 and TRF2 used for differential recruitment of telomeric proteins. Science *319*, 1092-1096.

Chen, Z., Yang, H., and Pavletich, N.P. (2008c). Mechanism of homologous recombination from the RecA-ssDNA/dsDNA structures. Nature *453*, 489-484.

Chiruvella, K.K., Liang, Z., and Wilson, T.E. (2013). Repair of double-strand breaks by end joining. Cold Spring Harb Perspect Biol *5*, a012757.

Cingolani, G., Petosa, C., Weis, K., and Muller, C.W. (1999). Structure of importin-beta bound to the IBB domain of importin-alpha. Nature *399*, 221-229.

Clerici, M., Mantiero, D., Guerini, I., Lucchini, G., and Longhese, M.P. (2008). The Yku70-Yku80 complex contributes to regulate double-strand break processing and checkpoint activation during the cell cycle. EMBO Rep *9*, 810-818.

Clikeman, J.A., Khalsa, G.J., Barton, S.L., and Nickoloff, J.A. (2001). Homologous recombinational repair of double-strand breaks in yeast is enhanced by MAT heterozygosity through yKU-dependent and -independent mechanisms. Genetics *157*, 579-589.

Conti, E., Muller, C.W., and Stewart, M. (2006). Karyopherin flexibility in nucleocytoplasmic transport. Curr Opin Struct Biol *16*, 237-244.

Cornacchia, D., Dileep, V., Quivy, J.P., Foti, R., Tili, F., Santarella-Mellwig, R., Antony, C., Almouzni, G., Gilbert, D.M., and Buonomo, S.B. (2012). Mouse Rif1 is a key regulator of the replication-timing programme in mammalian cells. EMBO J *31*, 3678-3690.

Cronin, C.N., Lim, K.B., and Rogers, J. (2007). Production of selenomethionyl-derivatized proteins in baculovirus-infected insect cells. Protein Sci *16*, 2023-2029.

Cuella-Martin, R., Oliveira, C., Lockstone, H.E., Snellenberg, S., Grolmusova, N., and Chapman, J.R. (2016). 53BP1 Integrates DNA Repair and p53-Dependent Cell Fate Decisions via Distinct Mechanisms. Mol Cell *64*, 51-64.

d'Adda di Fagagna, F., Reaper, P.M., Clay-Farrace, L., Fiegler, H., Carr, P., Von Zglinicki, T., Saretzki, G., Carter, N.P., and Jackson, S.P. (2003). A DNA damage checkpoint response in telomere-initiated senescence. Nature *426*, 194-198.

Daley, J.M., and Sung, P. (2014). 53BP1, BRCA1, and the choice between recombination and end joining at DNA double-strand breaks. Mol Cell Biol *34*, 1380-1388.

Dave, A., Cooley, C., Garg, M., and Bianchi, A. (2014). Protein phosphatase 1 recruitment by Rif1 regulates DNA replication origin firing by counteracting DDK activity. Cell Rep *7*, 53-61.

Davis, A.J., and Chen, D.J. (2013). DNA double strand break repair via non-homologous end-joining. Transl Cancer Res *2*, 130-143.

de Bruin, D., Kantrow, S.M., Liberatore, R.A., and Zakian, V.A. (2000). Telomere folding is required for the stable maintenance of telomere position effects in yeast. Mol Cell Biol *20*, 7991-8000.

de Bruin, D., Zaman, Z., Liberatore, R.A., and Ptashne, M. (2001). Telomere looping permits gene activation by a downstream UAS in yeast. Nature *409*, 109-113.

de Lange, T. (2004). T-loops and the origin of telomeres. Nat Rev Mol Cell Biol *5*, 323-329.

de Lange, T. (2009). How telomeres solve the end-protection problem. Science *326*, 948-952.

Di Virgilio, M., Callen, E., Yamane, A., Zhang, W., Jankovic, M., Gitlin, A.D., Feldhahn, N., Resch, W., Oliveira, T.Y., Chait, B.T.*, et al.* (2013). Rif1 prevents resection of DNA breaks and promotes immunoglobulin class switching. Science *339*, 711-715.

Doil, C., Mailand, N., Bekker-Jensen, S., Menard, P., Larsen, D.H., Pepperkok, R., Ellenberg, J., Panier, S., Durocher, D., Bartek, J.*, et al.* (2009). RNF168 binds and amplifies ubiquitin conjugates on damaged chromosomes to allow accumulation of repair proteins. Cell *136*, 435-446.

Dong, J., Panchakshari, R.A., Zhang, T., Zhang, Y., Hu, J., Volpi, S.A., Meyers, R.M., Ho, Y.J., Du, Z., Robbiani, D.F.*, et al.* (2015). Orientation-specific joining of AID-initiated DNA breaks promotes antibody class switching. Nature *525*, 134-139.

Drane, P., Brault, M.E., Cui, G., Meghani, K., Chaubey, S., Detappe, A., Parnandi, N., He, Y., Zheng, X.F., Botuyan, M.V.*, et al.* (2017). TIRR regulates 53BP1 by masking its histone methyl-lysine binding function. Nature *543*, 211-216.

Dudley, D.D., Chaudhuri, J., Bassing, C.H., and Alt, F.W. (2005). Mechanism and Control of V(D)J Recombination versus Class Switch Recombination: Similarities and Differences. In Advances in Immunology, F.W. Alt, ed. (Academic Press), pp. 43-112.

Emerson, C.H., and Bertuch, A.A. (2016). Consider the workhorse: Nonhomologous end-joining in budding yeast. Biochem Cell Biol *94*, 396-406.

Escribano-Diaz, C., Orthwein, A., Fradet-Turcotte, A., Xing, M., Young, J.T., Tkac, J., Cook, M.A., Rosebrock, A.P., Munro, M., Canny, M.D*., et al.* (2013). A cell cycle-dependent regulatory circuit composed of 53BP1-RIF1 and BRCA1-CtIP controls DNA repair pathway choice. Mol Cell *49*, 872-883.

Fairall, L., Chapman, L., Moss, H., de Lange, T., and Rhodes, D. (2001). Structure of the TRFH dimerization domain of the human telomeric proteins TRF1 and TRF2. Mol Cell *8*, 351-361.

Falck, J., Coates, J., and Jackson, S.P. (2005). Conserved modes of recruitment of ATM, ATR and DNA-PKcs to sites of DNA damage. Nature *434*, 605-611.

Falck, J., Forment, J.V., Coates, J., Mistrik, M., Lukas, J., Bartek, J., and Jackson, S.P. (2012). CDK targeting of NBS1 promotes DNA-end resection, replication restart and homologous recombination. EMBO Rep *13*, 561-568.

Feeser, E.A., and Wolberger, C. (2008). Structural and functional studies of the Rap1 C-terminus reveal novel separation-of-function mutants. J Mol Biol *380*, 520-531.

Feng, L., Fong, K.W., Wang, J., Wang, W., and Chen, J. (2013). RIF1 counteracts BRCA1-mediated end resection during DNA repair. J Biol Chem *288*, 11135-11143.

Finn, R.D., Coggill, P., Eberhardt, R.Y., Eddy, S.R., Mistry, J., Mitchell, A.L., Potter, S.C., Punta, M., Qureshi, M., Sangrador-Vegas, A*., et al.* (2016). The Pfam protein families database: towards a more sustainable future. Nucleic Acids Res *44*, D279-285.

Foti, R., Gnan, S., Cornacchia, D., Dileep, V., Bulut-Karslioglu, A., Diehl, S., Buness, A., Klein, F.A., Huber, W., Johnstone, E*., et al.* (2016). Nuclear Architecture Organized by Rif1 Underpins the Replication-Timing Program. Mol Cell *61*, 260-273.

Fradet-Turcotte, A., Canny, M.D., Escribano-Diaz, C., Orthwein, A., Leung, C.C., Huang, H., Landry, M.C., Kitevski-LeBlanc, J., Noordermeer, S.M., Sicheri, F*., et al.* (2013). 53BP1 is a reader of the DNA-damage-induced H2A Lys 15 ubiquitin mark. Nature *499*, 50-54.

Frank-Vaillant, M., and Marcand, S. (2002). Transient stability of DNA ends allows nonhomologous end joining to precede homologous recombination. Mol Cell *10*, 1189-1199.

Garcia, V., Phelps, S.E., Gray, S., and Neale, M.J. (2011). Bidirectional resection of DNA double-strand breaks by Mre11 and Exo1. Nature *479*, 241-244.

Garvik, B., Carson, M., and Hartwell, L. (1995). Single-stranded DNA arising at telomeres in cdc13 mutants may constitute a specific signal for the RAD9 checkpoint. Mol Cell Biol *15*, 6128-6138.

Gelinas, A.D., Paschini, M., Reyes, F.E., Heroux, A., Batey, R.T., Lundblad, V., and Wuttke, D.S. (2009). Telomere capping proteins are structurally related to RPA with an additional telomere-specific domain. Proc Natl Acad Sci U S A *106*, 19298-19303.

Gilson, E., Roberge, M., Giraldo, R., Rhodes, D., and Gasser, S.M. (1993). Distortion of the DNA double helix by RAP1 at silencers and multiple telomeric binding sites. J Mol Biol *231*, 293-310.

Goodarzi, A.A., Noon, A.T., Deckbar, D., Ziv, Y., Shiloh, Y., Lobrich, M., and Jeggo, P.A. (2008). ATM signaling facilitates repair of DNA double-strand breaks associated with heterochromatin. Mol Cell *31*, 167-177.

Graf, M., Bonetti, D., Lockhart, A., Serhal, K., Kellner, V., Maicher, A., Jolivet, P., Teixeira, M.T., and Luke, B. (2017). Telomere Length Determines TERRA and R-Loop Regulation through the Cell Cycle. Cell *170*, 72-85 e14.

Graham, T.G., Walter, J.C., and Loparo, J.J. (2016). Two-Stage Synapsis of DNA Ends during Non-homologous End Joining. Mol Cell *61*, 850-858.

Grandin, N., Damon, C., and Charbonneau, M. (2001). Ten1 functions in telomere end protection and length regulation in association with Stn1 and Cdc13. EMBO J *20*, 1173-1183.

Grandin, N., Reed, S.I., and Charbonneau, M. (1997). Stn1, a new Saccharomyces cerevisiae protein, is implicated in telomere size regulation in association with Cdc13. Genes & Development *11*, 512-527.

Gravel, S., Chapman, J.R., Magill, C., and Jackson, S.P. (2008). DNA helicases Sgs1 and BLM promote DNA double-strand break resection. Genes Dev *22*, 2767-2772.

Gravel, S., Larrivee, M., Labrecque, P., and Wellinger, R.J. (1998). Yeast Ku as a regulator of chromosomal DNA end structure. Science *280*, 741-744.

Greider, C.W., and Blackburn, E.H. (1985). Identification of a specific telomere terminal transferase activity in Tetrahymena extracts. Cell *43*, 405-413.

Greider, C.W., and Blackburn, E.H. (1987). The telomere terminal transferase of Tetrahymena is a ribonucleoprotein enzyme with two kinds of primer specificity. Cell *51*, 887-898.

Griffith, J.D., Comeau, L., Rosenfield, S., Stansel, R.M., Bianchi, A., Moss, H., and de Lange, T. (1999). Mammalian telomeres end in a large duplex loop. Cell *97*, 503-514.

Grob, P., Zhang, T.T., Hannah, R., Yang, H., Hefferin, M.L., Tomkinson, A.E., and Nogales, E. (2012). Electron microscopy visualization of DNA-protein complexes formed by Ku and DNA ligase IV. DNA Repair (Amst) *11*, 74-81.

Groves, M.R., and Barford, D. (1999). Topological characteristics of helical repeat proteins. Curr Opin Struct Biol *9*, 383-389.

Groves, M.R., Hanlon, N., Turowski, P., Hemmings, B.A., and Barford, D. (1999). The structure of the protein phosphatase 2A PR65/A subunit reveals the conformation of its 15 tandemly repeated HEAT motifs. Cell *96*, 99-110.

Gupta, Y.K., Nair, D.T., Wharton, R.P., and Aggarwal, A.K. (2008). Structures of human Pumilio with noncognate RNAs reveal molecular mechanisms for binding promiscuity. Structure *16*, 549-557.

Haber, J.E. (2016). A Life Investigating Pathways That Repair Broken Chromosomes. Annu Rev Genet *50*, 1-28.

Hagstrom, K.A., and Meyer, B.J. (2003). Condensin and cohesin: more than chromosome compactor and glue. Nat Rev Genet *4*, 520-534.

Hardy, C.F., Sussel, L., and Shore, D. (1992). A RAP1-interacting protein involved in transcriptional silencing and telomere length regulation. Genes Dev *6*, 801-814.

Harrison, J.C., and Haber, J.E. (2006). Surviving the breakup: the DNA damage checkpoint. Annu Rev Genet *40*, 209-235.

Hartlerode, A.J., Guan, Y., Rajendran, A., Ura, K., Schotta, G., Xie, A., Shah, J.V., and Scully, R. (2012). Impact of histone H4 lysine 20 methylation on 53BP1 responses to chromosomal double strand breaks. PLoS One *7*, e49211.

Hartlerode, A.J., Morgan, M.J., Wu, Y., Buis, J., and Ferguson, D.O. (2015). Recruitment and activation of the ATM kinase in the absence of DNA-damage sensors. Nat Struct Mol Biol *22*, 736-743.

Hartwell, L.H., and Weinert, T.A. (1989). Checkpoints - Controls That Ensure the Order of Cell-Cycle Events. Science *246*, 629-634.

Haruki, H., Nishikawa, J., and Laemmli, U.K. (2008). The anchor-away technique: rapid, conditional establishment of yeast mutant phenotypes. Mol Cell *31*, 925-932.

Hayano, M., Kanoh, Y., Matsumoto, S., Renard-Guillet, C., Shirahige, K., and Masai, H. (2012). Rif1 is a global regulator of timing of replication origin firing in fission yeast. Genes Dev *26*, 137-150.

Hendrickx, A., Beullens, M., Ceulemans, H., Den Abt, T., Van Eynde, A., Nicolaescu, E., Lesage, B., and Bollen, M. (2009). Docking motif-guided mapping of the interactome of protein phosphatase-1. Chem Biol *16*, 365-371.

Herrmann, G., Lindahl, T., and Schar, P. (1998). Saccharomyces cerevisiae LIF1: a function involved in DNA double-strand break repair related to mammalian XRCC4. EMBO J *17*, 4188-4198.

Hiraga, S., Alvino, G.M., Chang, F., Lian, H.Y., Sridhar, A., Kubota, T., Brewer, B.J., Weinreich, M., Raghuraman, M.K., and Donaldson, A.D. (2014). Rif1 controls DNA replication by directing Protein Phosphatase 1 to reverse Cdc7-mediated phosphorylation of the MCM complex. Genes Dev *28*, 372-383.

Hirano, Y., Fukunaga, K., and Sugimoto, K. (2009). Rif1 and rif2 inhibit localization of tel1 to DNA ends. Mol Cell *33*, 312-322.

Hirano, Y., and Sugimoto, K. (2007). Cdc13 telomere capping decreases Mec1 association but does not affect Tel1 association with DNA ends. Mol Biol Cell *18*, 2026-2036.

Hoeijmakers, J.H. (2009). DNA damage, aging, and cancer. N Engl J Med *361*, 1475-1485.

Hohn, M., Tang, G., Goodyear, G., Baldwin, P.R., Huang, Z., Penczek, P.A., Yang, C., Glaeser, R.M., Adams, P.D., and Ludtke, S.J. (2007). SPARX, a new environment for Cryo-EM image processing. Journal of Structural Biology *157*, 47-55.

Horigome, C., Bustard, D.E., Marcomini, I., Delgoshaie, N., Tsai-Pflugfelder, M., Cobb, J.A., and Gasser, S.M. (2016). PolySUMOylation by Siz2 and Mms21 triggers relocation of DNA breaks to nuclear pores through the Slx5/Slx8 STUbL. Genes Dev *30*, 931-945.

Huen, M.S., Grant, R., Manke, I., Minn, K., Yu, X., Yaffe, M.B., and Chen, J. (2007). RNF8 transduces the DNA-damage signal via histone ubiquitylation and checkpoint protein assembly. Cell *131*, 901-914.

Huen, M.S., Sy, S.M., and Chen, J. (2010). BRCA1 and its toolbox for the maintenance of genome integrity. Nat Rev Mol Cell Biol *11*, 138-148.

Huertas, P., and Jackson, S.P. (2009). Human CtIP mediates cell cycle control of DNA end resection and double strand break repair. J Biol Chem *284*, 9558-9565.

Iglesias, N., Redon, S., Pfeiffer, V., Dees, M., Lingner, J., and Luke, B. (2011). Subtelomeric repetitive elements determine TERRA regulation by Rap1/Rif and Rap1/Sir complexes in yeast. EMBO Rep *12*, 587-593.

Ira, G., Pellicioli, A., Balijja, A., Wang, X., Fiorani, S., Carotenuto, W., Liberi, G., Bressan, D., Wan, L., Hollingsworth, N.M*., et al.* (2004). DNA end resection, homologous recombination and DNA damage checkpoint activation require CDK1. Nature *431*, 1011-1017.

Iyama, T., and Wilson, D.M., 3rd (2013). DNA repair mechanisms in dividing and non-dividing cells. DNA Repair (Amst) *12*, 620-636.

Jackson, S.P., and Bartek, J. (2009). The DNA-damage response in human biology and disease. Nature *461*, 1071-1078.

Jazayeri, A., Falck, J., Lukas, C., Bartek, J., Smith, G.C., Lukas, J., and Jackson, S.P. (2006). ATM- and cell cycle-dependent regulation of ATR in response to DNA double-strand breaks. Nat Cell Biol *8*, 37-45.

Jones, D.T., and Cozzetto, D. (2015). DISOPRED3: precise disordered region predictions with annotated protein-binding activity. Bioinformatics *31*, 857-863.

Joo, W.S., Jeffrey, P.D., Cantor, S.B., Finnin, M.S., Livingston, D.M., and Pavletich, N.P. (2002). Structure of the 53BP1 BRCT region bound to p53 and its comparison to the Brca1 BRCT structure. Genes Dev *16*, 583-593.

Kallberg, M., Wang, H., Wang, S., Peng, J., Wang, Z., Lu, H., and Xu, J. (2012). Template-based protein structure modeling using the RaptorX web server. Nat Protoc *7*, 1511-1522.

Kanoh, Y., Matsumoto, S., Fukatsu, R., Kakusho, N., Kono, N., Renard-Guillet, C., Masuda, K., Iida, K., Nagasawa, K., Shirahige, K.*, et al.* (2015a). Rif1 binds to G quadruplexes and suppresses replication over long distances. Nat Struct Mol Biol *22*, 889-897.

Kanoh, Y., Matsumoto, S., Fukatsu, R., Kakusho, N., Kono, N., Renard-Guillet, C., Masuda, K., Iida, K., Nagasawa, K., Shirahige, K.*, et al.* (2015b). Rif1 binds to G quadruplexes and suppresses replication over long distances. Nat Struct Mol Biol.

Kegel, A., Sjostrand, J.O., and Astrom, S.U. (2001). Nej1p, a cell type-specific regulator of nonhomologous end joining in yeast. Curr Biol *11*, 1611-1617.

Kelley, L.A., Mezulis, S., Yates, C.M., Wass, M.N., and Sternberg, M.J. (2015). The Phyre2 web portal for protein modeling, prediction and analysis. Nat Protoc *10*, 845-858.

Kibe, T., Zimmermann, M., and de Lange, T. (2016). TPP1 Blocks an ATR-Mediated Resection Mechanism at Telomeres. Mol Cell *61*, 236-246.

Kolas, N.K., Chapman, J.R., Nakada, S., Ylanko, J., Chahwan, R., Sweeney, F.D., Panier, S., Mendez, M., Wildenhain, J., Thomson, T.M.*, et al.* (2007). Orchestration of the DNA-damage response by the RNF8 ubiquitin ligase. Science *318*, 1637-1640.

Konig, P., Giraldo, R., Chapman, L., and Rhodes, D. (1996). The crystal structure of the DNA-binding domain of yeast RAP1 in complex with telomeric DNA. Cell *85*, 125-136.

Kramer, K.M., Brock, J.A., Bloom, K., Moore, J.K., and Haber, J.E. (1994). Two different types of double-strand breaks in Saccharomyces cerevisiae are repaired by similar RAD52-independent, nonhomologous recombination events. Mol Cell Biol *14*, 1293-1301.

Krokan, H.E., and Bjoras, M. (2013). Base excision repair. Cold Spring Harb Perspect Biol *5*, a012583.

Kschonsak, M., Merkel, F., Bisht, S., Metz, J., Rybin, V., Hassler, M., and Haering, C.H. (2017). Structural Basis for a Safety-Belt Mechanism That Anchors Condensin to Chromosomes. Cell *171*, 588-600 e524.

Kumar, S., Yoo, H.Y., Kumagai, A., Shevchenko, A., Shevchenko, A., and Dunphy, W.G. (2012). Role for Rif1 in the checkpoint response to damaged DNA in Xenopus egg extracts. Cell Cycle *11*, 1183-1194.

Lacy, E., Roberts, S., Evans, E.P., Burtenshaw, M.D., and Costantini, F.D. (1983). A Foreign Beta-Globin Gene in Transgenic Mice - Integration at Abnormal Chromosomal Positions and Expression in Inappropriate Tissues. Cell *34*, 343-358.

Le Bihan, Y.V., Matot, B., Pietrement, O., Giraud-Panis, M.J., Gasparini, S., Le Cam, E., Gilson, E., Sclavi, B., Miron, S., and Le Du, M.H. (2013). Effect of Rap1 binding on DNA distortion and potassium permanganate hypersensitivity. Acta Crystallogr D Biol Crystallogr *69*, 409-419.

Lee, S.E., Moore, J.K., Holmes, A., Umezu, K., Kolodner, R.D., and Haber, J.E. (1998). Saccharomyces Ku70, mre11/rad50 and RPA proteins regulate adaptation to G2/M arrest after DNA damage. Cell *94*, 399-409.

Lee, S.E., Paques, F., Sylvan, J., and Haber, J.E. (1999). Role of yeast SIR genes and mating type in directing DNA double-strand breaks to homologous and non-homologous repair paths. Curr Biol *9*, 767-770.

Lee, S.J., Matsuura, Y., Liu, S.M., and Stewart, M. (2005). Structural basis for nuclear import complex dissociation by RanGTP. Nature *435*, 693-696.

Lee, S.J., Sekimoto, T., Yamashita, E., Nagoshi, E., Nakagawa, A., Imamoto, N., Yoshimura, M., Sakai, H., Chong, K.T., Tsukihara, T*., et al.* (2003). The structure of importin-beta bound to SREBP-2: nuclear import of a transcription factor. Science *302*, 1571-1575.

Lei, M., Baumann, P., and Cech, T.R. (2002). Cooperative binding of single-stranded telomeric DNA by the Pot1 protein of Schizosaccharomyces pombe. Biochemistry *41*, 14560-14568.

Lei, M., Podell, E.R., Baumann, P., and Cech, T.R. (2003). DNA self-recognition in the structure of Pot1 bound to telomeric single-stranded DNA. Nature *426*, 198-203.

Lengsfeld, B.M., Rattray, A.J., Bhaskara, V., Ghirlando, R., and Paull, T.T. (2007). Sae2 is an endonuclease that processes hairpin DNA cooperatively with the Mre11/Rad50/Xrs2 complex. Mol Cell *28*, 638-651.

Lieber, M.R. (2010). The mechanism of double-strand DNA break repair by the nonhomologous DNA end-joining pathway. Annu Rev Biochem *79*, 181-211.

Lindahl, T. (1993). Instability and decay of the primary structure of DNA. Nature *362*, 709-715.

Lindahl, T., and Barnes, D.E. (2000). Repair of endogenous DNA damage. Cold Spring Harb Symp Quant Biol *65*, 127-133.

Lisby, M., Barlow, J.H., Burgess, R.C., and Rothstein, R. (2004). Choreography of the DNA damage response: spatiotemporal relationships among checkpoint and repair proteins. Cell *118*, 699-713.

Liu, S.M., and Stewart, M. (2005). Structural basis for the high-affinity binding of nucleoporin Nup1p to the Saccharomyces cerevisiae importin-beta homologue, Kap95p. J Mol Biol *349*, 515-525.

Lottersberger, F., Bothmer, A., Robbiani, D.F., Nussenzweig, M.C., and de Lange, T. (2013). Role of 53BP1 oligomerization in regulating double-strand break repair. Proc Natl Acad Sci U S A *110*, 2146-2151.

Lottersberger, F., Karssemeijer, R.A., Dimitrova, N., and de Lange, T. (2015). 53BP1 and the LINC Complex Promote Microtubule-Dependent DSB Mobility and DNA Repair. Cell *163*, 880-893.

Lu, X., Simon, M.D., Chodaparambil, J.V., Hansen, J.C., Shokat, K.M., and Luger, K. (2008). The effect of H3K79 dimethylation and H4K20 trimethylation on nucleosome and chromatin structure. Nat Struct Mol Biol *15*, 1122-1124.

Lukas, J., Lukas, C., and Bartek, J. (2011). More than just a focus: The chromatin response to DNA damage and its role in genome integrity maintenance. Nat Cell Biol *13*, 1161-1169.

Luke, B., Panza, A., Redon, S., Iglesias, N., Li, Z., and Lingner, J. (2008). The Rat1p 5' to 3' exonuclease degrades telomeric repeat-containing RNA and promotes telomere elongation in Saccharomyces cerevisiae. Mol Cell *32*, 465-477.

Mages, G.J., Feldmann, H.M., and Winnacker, E.L. (1996). Involvement of the Saccharomyces cerevisiae HDF1 gene in DNA double-strand break repair and recombination. J Biol Chem *271*, 7910-7915.

Mallette, F.A., Mattiroli, F., Cui, G., Young, L.C., Hendzel, M.J., Mer, G., Sixma, T.K., and Richard, S. (2012). RNF8- and RNF168-dependent degradation of KDM4A/JMJD2A triggers 53BP1 recruitment to DNA damage sites. EMBO J *31*, 1865-1878.

Manke, I.A., Lowery, D.M., Nguyen, A., and Yaffe, M.B. (2003). BRCT repeats as phosphopeptide-binding modules involved in protein targeting. Science *302*, 636-639.

Marcand, S., Pardo, B., Gratias, A., Cahun, S., and Callebaut, I. (2008). Multiple pathways inhibit NHEJ at telomeres. Genes Dev *22*, 1153-1158.

Marcotte, E.M., Pellegrini, M., Yeates, T.O., and Eisenberg, D. (1999). A census of protein repeats. J Mol Biol *293*, 151-160.

Martina, M., Bonetti, D., Villa, M., Lucchini, G., and Longhese, M.P. (2014). Saccharomyces cerevisiae Rif1 cooperates with MRX-Sae2 in promoting DNA-end resection. EMBO Rep *15*, 695-704.

Marvin, M.E., Becker, M.M., Noel, P., Hardy, S., Bertuch, A.A., and Louis, E.J. (2009). The association of yKu with subtelomeric core X sequences prevents recombination involving telomeric sequences. Genetics *183*, 453-467, 451SI-413SI.

Mason, M., Wanat, J.J., Harper, S., Schultz, D.C., Speicher, D.W., Johnson, F.B., and Skordalakes, E. (2013). Cdc13 OB2 dimerization required for productive Stn1 binding and efficient telomere maintenance. Structure *21*, 109-120.

Mattarocci, S., Hafner, L., Lezaja, A., Shyian, M., and Shore, D. (2016). Rif1: A Conserved Regulator of DNA Replication and Repair Hijacked by Telomeres in Yeasts. Front Genet *7*, 45.

Mattarocci, S., Reinert, J.K., Bunker, R.D., Fontana, G.A., Shi, T., Klein, D., Cavadini, S., Faty, M., Shyian, M., Hafner, L.*, et al.* (2017). Rif1 maintains telomeres and mediates DNA repair by encasing DNA ends. Nat Struct Mol Biol *24*, 588-595.

Mattarocci, S., Shyian, M., Lemmens, L., Damay, P., Altintas, D.M., Shi, T., Bartholomew, C.R., Thoma, N.H., Hardy, C.F., and Shore, D. (2014). Rif1 controls DNA replication timing in yeast through the PP1 phosphatase Glc7. Cell Rep *7*, 62-69.

McClintock, B. (1931). Cytological observations of deficiencies involving known genes, translocations and an inversion in Zea mays. Missouri Agr Exp Sta Res Bull *163*, 1-48.

McGee, J.S., Phillips, J.A., Chan, A., Sabourin, M., Paeschke, K., and Zakian, V.A. (2010). Reduced Rif2 and lack of Mec1 target short telomeres for elongation rather than double-strand break repair. Nat Struct Mol Biol *17*, 1438-1445.

Mehta, A., and Haber, J.E. (2014). Sources of DNA double-strand breaks and models of recombinational DNA repair. Cold Spring Harb Perspect Biol *6*, a016428.

Miller, K.M., Ferreira, M.G., and Cooper, J.P. (2005). Taz1, Rap1 and Rif1 act both interdependently and independently to maintain telomeres. EMBO J *24*, 3128-3135.

Mimitou, E.P., and Symington, L.S. (2008). Sae2, Exo1 and Sgs1 collaborate in DNA double-strand break processing. Nature *455*, 770-774.

Mimitou, E.P., and Symington, L.S. (2010). Ku prevents Exo1 and Sgs1-dependent resection of DNA ends in the absence of a functional MRX complex or Sae2. EMBO J *29*, 3358-3369.

Mitchell, M.T., Smith, J.S., Mason, M., Harper, S., Speicher, D.W., Johnson, F.B., and Skordalakes, E. (2010). Cdc13 N-terminal dimerization, DNA binding, and telomere length regulation. Mol Cell Biol *30*, 5325-5334.

Mitton-Fry, R.M., Anderson, E.M., Hughes, T.R., Lundblad, V., and Wuttke, D.S. (2002). Conserved structure for single-stranded telomeric DNA recognition. Science *296*, 145-147.

Mitton-Fry, R.M., Anderson, E.M., Theobald, D.L., Glustrom, L.W., and Wuttke, D.S. (2004). Structural basis for telomeric single-stranded DNA recognition by yeast Cdc13. J Mol Biol *338*, 241-255.

Moore, J.K., and Haber, J.E. (1996). Cell cycle and genetic requirements of two pathways of nonhomologous end-joining repair of double-strand breaks in Saccharomyces cerevisiae. Mol Cell Biol *16*, 2164-2173.

Muller, H.J. (1938). The remaking of chromosomes. Collecting Net *13*, 181-198.

Mullins, E.A., Shi, R., Parsons, Z.D., Yuen, P.K., David, S.S., Igarashi, Y., and Eichman, B.F. (2015). The DNA glycosylase AlkD uses a non-base-flipping mechanism to excise bulky lesions. Nature *527*, 254-258.

Nimonkar, A.V., Ozsoy, A.Z., Genschel, J., Modrich, P., and Kowalczykowski, S.C. (2008). Human exonuclease 1 and BLM helicase interact to resect DNA and initiate DNA repair. Proc Natl Acad Sci U S A *105*, 16906-16911.

Nugent, C.I., Hughes, T.R., Lue, N.F., and Lundblad, V. (1996). Cdc13p: a single-strand telomeric DNA-binding protein with a dual role in yeast telomere maintenance. Science *274*, 249-252.

Ochi, T., Blackford, A.N., Coates, J., Jhujh, S., Mehmood, S., Tamura, N., Travers, J., Wu, Q., Draviam, V.M., Robinson, C.V.*, et al.* (2015). DNA repair. PAXX, a paralog of XRCC4 and XLF, interacts with Ku to promote DNA double-strand break repair. Science *347*, 185-188.

Orr-Weaver, T.L., Szostak, J.W., and Rothstein, R.J. (1981). Yeast transformation: a model system for the study of recombination. Proc Natl Acad Sci U S A *78*, 6354-6358.

Paciotti, V., Clerici, M., Lucchini, G., and Longhese, M.P. (2000). The checkpoint protein Ddc2, functionally related to S. pombe Rad26, interacts with Mec1 and is regulated by Mec1-dependent phosphorylation in budding yeast. Genes & Development *14*, 2046-2059.

Paillard, S., and Strauss, F. (1991). Analysis of the mechanism of interaction of simian Ku protein with DNA. Nucleic Acids Res *19*, 5619-5624.

Paques, F., and Haber, J.E. (1999). Multiple pathways of recombination induced by double-strand breaks in Saccharomyces cerevisiae. Microbiol Mol Biol Rev *63*, 349-404.

Park, J.Y., Zhang, F., and Andreassen, P.R. (2014). PALB2: the hub of a network of tumor suppressors involved in DNA damage responses. Biochim Biophys Acta *1846*, 263-275.

Park, S., Patterson, E.E., Cobb, J., Audhya, A., Gartenberg, M.R., and Fox, C.A. (2011). Palmitoylation controls the dynamics of budding-yeast heterochromatin via the telomere-binding protein Rif1. Proc Natl Acad Sci U S A *108*, 14572-14577.

Peace, J.M., Ter-Zakarian, A., and Aparicio, O.M. (2014). Rif1 regulates initiation timing of late replication origins throughout the S. cerevisiae genome. PLoS One *9*, e98501.

Peifer, M., Berg, S., and Reynolds, A.B. (1994). A repeating amino acid motif shared by proteins with diverse cellular roles. Cell *76*, 789-791.

Penczek, P.A., Fang, J., Li, X., Cheng, Y., Loerke, J., and Spahn, C.M. (2014). CTER-rapid estimation of CTF parameters with error assessment. Ultramicroscopy *140*, 9-19.

Pesavento, J.J., Yang, H., Kelleher, N.L., and Mizzen, C.A. (2008). Certain and progressive methylation of histone H4 at lysine 20 during the cell cycle. Mol Cell Biol *28*, 468-486.

Piazza, I., Rutkowska, A., Ori, A., Walczak, M., Metz, J., Pelechano, V., Beck, M., and Haering, C.H. (2014). Association of condensin with chromosomes depends on DNA binding by its HEAT-repeat subunits. Nat Struct Mol Biol *21*, 560-568.

Polo, S.E., and Jackson, S.P. (2011). Dynamics of DNA damage response proteins at DNA breaks: a focus on protein modifications. Genes Dev *25*, 409-433.

Polotnianka, R.M., Li, J., and Lustig, A.J. (1998). The yeast Ku heterodimer is essential for protection of the telomere against nucleolytic and recombinational activities. Current Biology *8*, 831-834.

Poschke, H., Dees, M., Chang, M., Amberkar, S., Kaderali, L., Rothstein, R., and Luke, B. (2012). Rif2 promotes a telomere fold-back structure through Rpd3L recruitment in budding yeast. PLoS Genet *8*, e1002960.

Ray Chaudhuri, A., Callen, E., Ding, X., Gogola, E., Duarte, A.A., Lee, J.E., Wong, N., Lafarga, V., Calvo, J.A., Panzarino, N.J.*, et al.* (2016). Replication fork stability confers chemoresistance in BRCA-deficient cells. Nature *535*, 382-387.

Reichen, C., Hansen, S., and Pluckthun, A. (2014). Modular peptide binding: from a comparison of natural binders to designed armadillo repeat proteins. J Struct Biol *185*, 147-162.

Ribeyre, C., and Shore, D. (2012). Anticheckpoint pathways at telomeres in yeast. Nat Struct Mol Biol *19*, 307-313.

Robert, T., Vanoli, F., Chiolo, I., Shubassi, G., Bernstein, K.A., Rothstein, R., Botrugno, O.A., Parazzoli, D., Oldani, A., Minucci, S.*, et al.* (2011). HDACs link the DNA damage response, processing of double-strand breaks and autophagy. Nature *471*, 74-79.

Rogakou, E.P., Pilch, D.R., Orr, A.H., Ivanova, V.S., and Bonner, W.M. (1998). DNA double-stranded breaks induce histone H2AX phosphorylation on serine 139. J Biol Chem *273*, 5858-5868.

Rouse, J., and Jackson, S.P. (2002). Lcd1p recruits Mec1p to DNA lesions in vitro and in vivo. Mol Cell *9*, 857-869.

Roy, R., Chun, J., and Powell, S.N. (2011). BRCA1 and BRCA2: different roles in a common pathway of genome protection. Nat Rev Cancer *12*, 68-78.

Rubinson, E.H., and Eichman, B.F. (2012). Nucleic acid recognition by tandem helical repeats. Curr Opin Struct Biol *22*, 101-109.

Rubinson, E.H., Gowda, A.S., Spratt, T.E., Gold, B., and Eichman, B.F. (2010). An unprecedented nucleic acid capture mechanism for excision of DNA damage. Nature *468*, 406-411.

Rubinson, E.H., Metz, A.H., O'Quin, J., and Eichman, B.F. (2008). A new protein architecture for processing alkylation damaged DNA: the crystal structure of DNA glycosylase AlkD. J Mol Biol *381*, 13-23.

Sabourin, M., Tuzon, C.T., and Zakian, V.A. (2007). Telomerase and Tel1p preferentially associate with short telomeres in S. cerevisiae. Mol Cell *27*, 550-561.

Sanchez, Y., Bachant, J., Wang, H., Hu, F.H., Liu, D., Tetzlaff, M., and Elledge, S.J. (1999). Control of the DNA damage checkpoint by Chk1 and Rad53 protein kinases through distinct mechanisms. Science *286*, 1166-1171.

Sandell, L.L., and Zakian, V.A. (1993). Loss of a yeast telomere: arrest, recovery, and chromosome loss. Cell *75*, 729-739.

Sarangi, P., Steinacher, R., Altmannova, V., Fu, Q., Paull, T.T., Krejci, L., Whitby, M.C., and Zhao, X. (2015). Sumoylation influences DNA break repair partly by increasing the solubility of a conserved end resection protein. PLoS Genet *11*, e1004899.

Sarpong, K., and Bose, R. (2017). Efficient sortase-mediated N-terminal labeling of TEV protease cleaved recombinant proteins. Anal Biochem *521*, 55-58.

Sartori, A.A., Lukas, C., Coates, J., Mistrik, M., Fu, S., Bartek, J., Baer, R., Lukas, J., and Jackson, S.P. (2007). Human CtIP promotes DNA end resection. Nature *450*, 509-514.

Scheres, S.H. (2012). RELION: implementation of a Bayesian approach to cryo-EM structure determination. J Struct Biol *180*, 519-530.

Schlegel, B.P., Jodelka, F.M., and Nunez, R. (2006). BRCA1 promotes induction of ssDNA by ionizing radiation. Cancer Res *66*, 5181-5189.

Schneider, C.A., Rasband, W.S., and Eliceiri, K.W. (2012). NIH Image to ImageJ: 25 years of image analysis. Nat Methods *9*, 671-675.

Schotta, G., Sengupta, R., Kubicek, S., Malin, S., Kauer, M., Callen, E., Celeste, A., Pagani, M., Opravil, S., De La Rosa-Velazquez, I.A*., et al.* (2008). A chromatin-wide transition to H4K20 monomethylation impairs genome integrity and programmed DNA rearrangements in the mouse. Genes Dev *22*, 2048-2061.

Seeber, A., Hegnauer, A.M., Hustedt, N., Deshpande, I., Poli, J., Eglinger, J., Pasero, P., Gut, H., Shinohara, M., Hopfner, K.P*., et al.* (2016). RPA Mediates Recruitment of MRX to Forks and Double-Strand Breaks to Hold Sister Chromatids Together. Mol Cell *64*, 951-966.

Shahar, O.D., Raghu Ram, E.V., Shimshoni, E., Hareli, S., Meshorer, E., and Goldberg, M. (2012). Live imaging of induced and controlled DNA double-strand break formation reveals extremely low repair by homologous recombination in human cells. Oncogene *31*, 3495-3504.

Shay, J.W., and Wright, W.E. (2011). Role of telomeres and telomerase in cancer. Semin Cancer Biol *21*, 349-353.

Sheu, Y.J., and Stillman, B. (2006). Cdc7-Dbf4 phosphorylates MCM proteins via a docking site-mediated mechanism to promote S phase progression. Mol Cell *24*, 101-113.

Shi, T., Bunker, R.D., Mattarocci, S., Ribeyre, C., Faty, M., Gut, H., Scrima, A., Rass, U., Rubin, S.M., Shore, D*., et al.* (2013). Rif1 and Rif2 shape telomere function and architecture through multivalent Rap1 interactions. Cell *153*, 1340-1353.

Sibanda, B.L., Chirgadze, D.Y., Ascher, D.B., and Blundell, T.L. (2017). DNA-PKcs structure suggests an allosteric mechanism modulating DNA double-strand break repair. Science *355*, 520-524.

Sibanda, B.L., Chirgadze, D.Y., and Blundell, T.L. (2010). Crystal structure of DNA-PKcs reveals a large open-ring cradle comprised of HEAT repeats. Nature *463*, 118-121.

Siede, W., Friedl, A.A., Dianova, I., Eckardt-Schupp, F., and Friedberg, E.C. (1996). The Saccharomyces cerevisiae Ku autoantigen homologue affects radiosensitivity only in the absence of homologous recombination. Genetics *142*, 91-102.

Silverman, J., Takai, H., Buonomo, S.B., Eisenhaber, F., and de Lange, T. (2004). Human Rif1, ortholog of a yeast telomeric protein, is regulated by ATM and 53BP1 and functions in the S-phase checkpoint. Genes Dev *18*, 2108-2119.

Soudet, J., Jolivet, P., and Teixeira, M.T. (2014). Elucidation of the DNA end-replication problem in Saccharomyces cerevisiae. Mol Cell *53*, 954-964.

Sreesankar, E., Senthilkumar, R., Bharathi, V., Mishra, R.K., and Mishra, K. (2012). Functional diversification of yeast telomere associated protein, Rif1, in higher eukaryotes. BMC Genomics *13*, 255.

Stewart, S.A., and Weinberg, R.A. (2006). Telomeres: cancer to human aging. Annu Rev Cell Dev Biol *22*, 531-557.

Strahl-Bolsinger, S., Hecht, A., Luo, K., and Grunstein, M. (1997). SIR2 and SIR4 interactions differ in core and extended telomeric heterochromatin in yeast. Genes Dev *11*, 83-93.

Stucki, M., Clapperton, J.A., Mohammad, D., Yaffe, M.B., Smerdon, S.J., and Jackson, S.P. (2005). MDC1 directly binds phosphorylated histone H2AX to regulate cellular responses to DNA double-strand breaks. Cell *123*, 1213-1226.

Sturzenegger, A., Burdova, K., Kanagaraj, R., Levikova, M., Pinto, C., Cejka, P., and Janscak, P. (2014). DNA2 cooperates with the WRN and BLM RecQ helicases to mediate long-range DNA end resection in human cells. J Biol Chem *289*, 27314-27326.

Sukackaite, R., Jensen, M.R., Mas, P.J., Blackledge, M., Buonomo, S.B., and Hart, D.J. (2014). Structural and biophysical characterization of murine rif1 C terminus reveals high specificity for DNA cruciform structures. J Biol Chem *289*, 13903-13911.

Sun, J., Lee, K.J., Davis, A.J., and Chen, D.J. (2012). Human Ku70/80 protein blocks exonuclease 1-mediated DNA resection in the presence of human Mre11 or Mre11/Rad50 protein complex. J Biol Chem *287*, 4936-4945.

Sun, J., Yang, Y., Wan, K., Mao, N., Yu, T.Y., Lin, Y.C., DeZwaan, D.C., Freeman, B.C., Lin, J.J., Lue, N.F., *et al.* (2011). Structural bases of dimerization of yeast telomere protein Cdc13 and its interaction with the catalytic subunit of DNA polymerase alpha. Cell Res *21*, 258-274.

Sun, J., Yu, E.Y., Yang, Y., Confer, L.A., Sun, S.H., Wan, K., Lue, N.F., and Lei, M. (2009). Stn1-Ten1 is an Rpa2-Rpa3-like complex at telomeres. Genes Dev *23*, 2900-2914.

Sun, Z., Hsiao, J., Fay, D.S., and Stern, D.F. (1998). Rad53 FHA domain associated with phosphorylated Rad9 in the DNA damage checkpoint. Science *281*, 272-274.

Syeda, A.H., Hawkins, M., and McGlynn, P. (2014). Recombination and replication. Cold Spring Harb Perspect Biol *6*, a016550.

Szostak, J.W., and Blackburn, E.H. (1982). Cloning yeast telomeres on linear plasmid vectors. Cell *29*, 245-255.

Tang, G., Peng, L., Baldwin, P.R., Mann, D.S., Jiang, W., Rees, I., and Ludtke, S.J. (2007). EMAN2: an extensible image processing suite for electron microscopy. J Struct Biol *157*, 38-46.

Teixeira, M.T., Arneric, M., Sperisen, P., and Lingner, J. (2004). Telomere length homeostasis is achieved via a switch between telomerase- extendible and -nonextendible states. Cell *117*, 323-335.

Teo, S.H., and Jackson, S.P. (2000). Lif1p targets the DNA ligase Lig4p to sites of DNA double-strand breaks. Curr Biol *10*, 165-168.

Tewari, R., Bailes, E., Bunting, K.A., and Coates, J.C. (2010). Armadillo-repeat protein functions: questions for little creatures. Trends Cell Biol *20*, 470-481.

Theile, C.S., Witte, M.D., Blom, A.E., Kundrat, L., Ploegh, H.L., and Guimaraes, C.P. (2013). Site-specific N-terminal labeling of proteins using sortase-mediated reactions. Nat Protoc *8*, 1800-1807.

Thorslund, T., Ripplinger, A., Hoffmann, S., Wild, T., Uckelmann, M., Villumsen, B., Narita, T., Sixma, T.K., Choudhary, C., Bekker-Jensen, S., *et al.* (2015). Histone H1 couples initiation and amplification of ubiquitin signalling after DNA damage. Nature *527*, 389-393.

Tomimatsu, N., Mukherjee, B., Catherine Hardebeck, M., Ilcheva, M., Vanessa Camacho, C., Louise Harris, J., Porteus, M., Llorente, B., Khanna, K.K., and Burma, S. (2014). Phosphorylation of EXO1 by CDKs 1 and 2 regulates DNA end resection and repair pathway choice. Nat Commun *5*, 3561.

Toteva, T., Mason, B., Kanoh, Y., Brogger, P., Green, D., Verhein-Hansen, J., Masai, H., and Thon, G. (2017). Establishment of expression-state boundaries by Rif1 and Taz1 in fission yeast. Proc Natl Acad Sci U S A *114*, 1093-1098.

Uhlmann, F., Lottspeich, F., and Nasmyth, K. (1999). Sister-chromatid separation at anaphase onset is promoted by cleavage of the cohesin subunit Scc1. Nature *400*, 37-42.

Usui, T., Foster, S.S., and Petrini, J.H. (2009). Maintenance of the DNA-damage checkpoint requires DNA-damage-induced mediator protein oligomerization. Mol Cell *33*, 147-159.

Valencia, M., Bentele, M., Vaze, M.B., Herrmann, G., Kraus, E., Lee, S.E., Schar, P., and Haber, J.E. (2001). NEJ1 controls non-homologous end joining in Saccharomyces cerevisiae. Nature *414*, 666-669.

Wake, C.T., Gudewicz, T., Porter, T., White, A., and Wilson, J.H. (1984). How damaged is the biologically active subpopulation of transfected DNA? Molecular and Cellular Biology *4*, 387-398.

Walker, J.R., Corpina, R.A., and Goldberg, J. (2001). Structure of the Ku heterodimer bound to DNA and its implications for double-strand break repair. Nature *412*, 607-614.

Wang, F., Podell, E.R., Zaug, A.J., Yang, Y., Baciu, P., Cech, T.R., and Lei, M. (2007). The POT1-TPP1 telomere complex is a telomerase processivity factor. Nature *445*, 506-510.

Wang, X., Zamore, P.D., and Hall, T.M. (2001). Crystal structure of a Pumilio homology domain. Mol Cell *7*, 855-865.

Ward, J.F. (1988). DNA damage produced by ionizing radiation in mammalian cells: identities, mechanisms of formation, and reparability. Prog Nucleic Acid Res Mol Biol *35*, 95-125.

Weinert, T.A., and Hartwell, L.H. (1988). The RAD9 gene controls the cell cycle response to DNA damage in Saccharomyces cerevisiae. Science *241*, 317-322.

Wellinger, R.J., and Zakian, V.A. (2012). Everything you ever wanted to know about Saccharomyces cerevisiae telomeres: beginning to end. Genetics *191*, 1073-1105.

Williams, R.S., Dodson, G.E., Limbo, O., Yamada, Y., Williams, J.S., Guenther, G., Classen, S., Glover, J.N., Iwasaki, H., Russell, P.*, et al.* (2009). Nbs1 flexibly tethers Ctp1 and Mre11-Rad50 to coordinate DNA double-strand break processing and repair. Cell *139*, 87-99.

Wilson, M.D., Benlekbir, S., Fradet-Turcotte, A., Sherker, A., Julien, J.P., McEwan, A., Noordermeer, S.M., Sicheri, F., Rubinstein, J.L., and Durocher, D. (2016). The structural basis of modified nucleosome recognition by 53BP1. Nature *536*, 100-103.

Wilson, T.E., Grawunder, U., and Lieber, M.R. (1997). Yeast DNA ligase IV mediates non-homologous DNA end joining. Nature *388*, 495-498.

Wohlbold, L., Merrick, K.A., De, S., Amat, R., Kim, J.H., Larochelle, S., Allen, J.J., Zhang, C., Shokat, K.M., Petrini, J.H.*, et al.* (2012). Chemical genetics reveals a specific requirement for Cdk2 activity in the DNA damage response and identifies Nbs1 as a Cdk2 substrate in human cells. PLoS Genet *8*, e1002935.

Wotton, D., and Shore, D. (1997). A novel Rap1p-interacting factor, Rif2p, cooperates with Rif1p to regulate telomere length in Saccharomyces cerevisiae. Genes Dev *11*, 748-760.

Xu, D., Muniandy, P., Leo, E., Yin, J., Thangavel, S., Shen, X., Ii, M., Agama, K., Guo, R., Fox, D., 3rd, *et al.* (2010). Rif1 provides a new DNA-binding interface for the Bloom syndrome complex to maintain normal replication. EMBO J *29*, 3140-3155.

Xue, Y., Rushton, M.D., and Maringele, L. (2011). A novel checkpoint and RPA inhibitory pathway regulated by Rif1. PLoS Genet *7*, e1002417.

Yaffe, M.B., Rittinger, K., Volinia, S., Caron, P.R., Aitken, A., Leffers, H., Gamblin, S.J., Smerdon, S.J., and Cantley, L.C. (1997). The structural basis for 14-3-3:phosphopeptide binding specificity. Cell *91*, 961-971.

Yaffe, M.B., and Smerdon, S.J. (2001). PhosphoSerine/threonine binding domains: you can't pSERious? Structure *9*, R33-38.

Yamazaki, S., Hayano, M., and Masai, H. (2013). Replication timing regulation of eukaryotic replicons: Rif1 as a global regulator of replication timing. Trends Genet *29*, 449-460.

Yamazaki, S., Ishii, A., Kanoh, Y., Oda, M., Nishito, Y., and Masai, H. (2012). Rif1 regulates the replication timing domains on the human genome. EMBO J *31*, 3667-3677.

Yang, J., Yan, R., Roy, A., Xu, D., Poisson, J., and Zhang, Y. (2015). The I-TASSER Suite: protein structure and function prediction. Nat Methods *12*, 7-8.

Yang, Z., Fang, J., Chittuluru, J., Asturias, F.J., and Penczek, P.A. (2012). Iterative stable alignment and clustering of 2D transmission electron microscope images. Structure *20*, 237-247.

Yoshimura, S.H., and Hirano, T. (2016). HEAT repeats - versatile arrays of amphiphilic helices working in crowded environments? J Cell Sci *129*, 3963-3970.

Yu, E.Y., Sun, J., Lei, M., and Lue, N.F. (2012). Analyses of Candida Cdc13 orthologues revealed a novel OB fold dimer arrangement, dimerization-assisted DNA binding, and substantial structural differences between Cdc13 and RPA70. Mol Cell Biol *32*, 186-198.

Yun, M.H., and Hiom, K. (2009). CtIP-BRCA1 modulates the choice of DNA double-strand-break repair pathway throughout the cell cycle. Nature *459*, 460-463.

Zaaijer, S., Shaikh, N., Nageshan, R.K., and Cooper, J.P. (2016). Rif1 Regulates the Fate of DNA Entanglements during Mitosis. Cell reports.

Zakian, V.A. (1989). Structure and function of telomeres. Annu Rev Genet *23*, 579-604.

Zakian, V.A. (2012). Telomeres: the beginnings and ends of eukaryotic chromosomes. Exp Cell Res *318*, 1456-1460.

Zgheib, O., Pataky, K., Brugger, J., and Halazonetis, T.D. (2009). An oligomerized 53BP1 tudor domain suffices for recognition of DNA double-strand breaks. Mol Cell Biol *29*, 1050-1058.

Zhang, W., Zhang, J., Zhang, X., Xu, C., and Tu, X. (2011). Solution structure of Rap1 BRCT domain from Saccharomyces cerevisiae reveals a novel fold. Biochem Biophys Res Commun *404*, 1055-1059.

Zhang, Y., Hefferin, M.L., Chen, L., Shim, E.Y., Tseng, H.M., Kwon, Y., Sung, P., Lee, S.E., and Tomkinson, A.E. (2007). Role of Dnl4-Lif1 in nonhomologous end-joining repair complex assembly and suppression of homologous recombination. Nat Struct Mol Biol *14*, 639-646.

Zhu, X.D., Kuster, B., Mann, M., Petrini, J.H., and de Lange, T. (2000). Cell-cycle-regulated association of RAD50/MRE11/NBS1 with TRF2 and human telomeres. Nat Genet *25*, 347-352.

Zhu, Z., Chung, W.H., Shim, E.Y., Lee, S.E., and Ira, G. (2008). Sgs1 helicase and two nucleases Dna2 and Exo1 resect DNA double-strand break ends. Cell *134*, 981-994.

Zierhut, C., and Diffley, J.F. (2008). Break dosage, cell cycle stage and DNA replication influence DNA double strand break response. EMBO J *27*, 1875-1885.

Zimmermann, M., Lottersberger, F., Buonomo, S.B., Sfeir, A., and de Lange, T. (2013). 53BP1 regulates DSB repair using Rif1 to control 5' end resection. Science *339*, 700-704.

Zou, L., and Elledge, S.J. (2003). Sensing DNA damage through ATRIP recognition of RPA-ssDNA complexes. Science *300*, 1542-1548.

Zubko, M.K., Guillard, S., and Lydall, D. (2004). Exo1 and Rad24 differentially regulate generation of ssDNA at telomeres of Saccharomyces cerevisiae cdc13-1 mutants. Genetics *168*, 103-115.

List of Abbreviations

14-3-3 protein	name based in migration pattern on DEAE-cellulosechromatography, phosphoserine/threonine-binding protein
53BP1	p53 binding protein
alt-NHEJ	altenative non-homologous end-joining
Arg	Arginine
ARM	armadillo repeat
ATM	Ataxia-telangiectasia mutated kinase
ATR	Ataxia telangiectasia and Rad3-related protein
BLM	Bloom syndrome protein; DNA helicase, RecQ-like type 2
bp	base pair
BRCA1	Breast Cancer 1, early onset gene
BRCA2	Breast Cancer gene 2
BRCT	BRCA1 C Terminus domain
ChIP	Chromatin immunoprecipitation
c-NHEJ	classical/canonical non-homologous end-joining
Co-IP	Co-immunoprecipitation
CSR	immunoglobulin class-switch recombination
CST	Cdc13-Stn1-Ten1 complex
CTD	C-terminal domain
DNA2	DNA replication ATP-dependent helicase/nuclease DNA2
DNA-PK	DNA-dependent protein kinase
DNA-PKcs	DNA-dependent protein kinase, catalytic subunit
Dnl4 (Lig4)	DNA ligase 4
DSB	DNA double-strand break
dsDNA	double-stranded DNA
EM	electron microscopy
EMSA	Electrophoretic Mobility Shift Assay
EXO1	Exonuclease 1
FP	Fluorescent Polarization
gamma-H2AX	histone variant H2AX phosphorylation on serine 139
Gln	Glutamine
H2AK15ub	ubiquitylated Lysine position 15 of histone 2A
H4K20me2	dimethylated Lysine position 20 of histone 4
HEAT	Huntingtin, elongation factor 3, the A subunit of protein phosphatase 2A (PP2A), signaling kinase TOR1
HJ	holliday junction
HR	homologous recombination
HU	hydroxyurea
Kd	dissociation constant
KU70/80	heterodimer of Ku70 (X-ray repair cross-complementing protein 6) and Ku80 (X-ray repair cross-complementing protein 5)
LC8	8-kDa light chain of dynein
Lif1	Ligase-interacting factor 1
LINC	linker of nucleoskeleton and cytoskeleton
Lys	Lysine
MAT	mating-type locus
MDC1	Mediator of DNA damage checkpoint protein 1
Mec1	Mitosis entry checkpoint protein 1
MEF	Mouse embryonic fibroblasts

MRN	MRE11-RAD50-NBS1 complex
MRX	Mre11-Rad50-Xrs2 complex
Nej1	Non-homologous end-joining protein 1
NHEJ	non-homologous end-joining
nt	nucleotide
NTD	N-terminal domain
OD	oligomerization domain
PALB2	Partner and localizer of BRCA2
PIKK	Phosphatidylinositol 3-kinase-related kinase
PTIP	PAX (paired box) interacting protein 1
RBM	Rap1 binding motif
RIF1	Rap1 interacting factor
RNF168	Ring finger protein 168, E3 ubiquitin ligase
RNF8	Ring finger protein 8, E3 ubiquitin ligase
RPA	Replication protein A
S.cerevisiae	*Saccharomyces cerevisiae*
S.pombe	*Schizosaccharomyces pombe*
S/TQ	Serine or Threonine followed by a Glutamine (Ser/Thr-Gln)
Sae2	Sporulation in the absence of SPO11 protein 2, DNA endonuclease
Ser	Serine
ssDNA	single-stranded DNA
TCEP	Tris(2-carboxyethyl)phosphin
Tel1	Telomere length regulation protein 1
TERRA	Telomeric repeat-containing RNA
TG80	80-bp tract of TG1-3 telomeric DNA
Thr	Threonine
UDR	ubiquitylation-dependent recruitment motif
XLF	XRCC4-like factor
XRCC4	X-ray repair cross-complementing protein 4

Acknowledgements

This thesis would not have been possible without the support and guidance of Nicolas H. Thomä over the past four years. When Nico proposed to work on Rif1 to me I was fascinated, and I am very grateful for the opportunity to work on these very exciting projects. I am particularly thankful for the freedom to develop my own ideas while being provided support and re-focusing whenever needed.

I would like to thank my thesis committee members Susan M. Gasser and Wei Yang for being happy to accept the roles as faculty representative and external advisor. Both have been helpful, supportive and encouraging during Committee meetings and at international conferences.

I would also like to thank the whole Thomä group (past and present members) for many useful discussions, help and critical input. It has been a great time and a pleasant working atmosphere. In particular, I am thankful to Tianlai Shi who worked on Rif1 before and performed the initial experiments on Rif1-NTD. I am grateful to Kerstin Böhm, who taught me a lot of protein biochemistry in the first year of my Ph.D. Moreover, I am very grateful to Susanne Kassube who was always happy to offer her outstanding scientific advice. Additionally, I would like to thank Mahamadou Faty for helping me with protein purifications. I am also very grateful to Richard Bunker, without whose scientific excellence and experience we would have never found the DNA in the co-crystals. Many thanks also go to Simone Cavadini and Andreas Schenk for their input on negative stain data processing.

I am also very grateful to Ulrich Rass for all the time and effort spent during critical discussions, improving the EMSA results, and writing of the paper manuscript. He has always been supportive and always believed in the significance of the Rif1 story. I am also thankful to Dominique Klein, with whom I performed a lot of EMSAs. It was always a pleasure to work with him. I am also very thankful to Gabriele Fontana because working with him is the definition of a fruitful and pleasant collaboration, and to whom I owe a debt of thanks for providing comments on the thesis.

I would also like to thank David Shore, Stefano Mattarocci, Maksym Shyian, and Lukas Hafner for a great and long-lasting collaboration. David and Stefano have been very helpful and I appreciate their patience and productive exchange of ideas throughout the project.

I am also thankful to Daniel Durocher, Marcus Wilson, and Cristina Escribano-Diaz for welcoming me for a month in Toronto. I very much appreciate Daniel‘s thorough and critical mind. Marcus has been an excellent teacher; Cristina and I shared a lot of ideas on human RIF1 – Thank you both!

Many thanks also go to the outstanding facility platforms at the FMI. Firstly, I would like to thank Heinz Gut and Jeremy Keusch, who both supplied scientific input whenever needed. I am very grateful that they run their facility so smoothly and that hiccups with instruments are dealt with swiftly and efficiently. Secondly, I would like to thank Daniel Hess, Vytautas Iesmantavicius, and Jan Seebacher for their helpful discussions and mass spectrometry analysis. Thirdly, I would like to thank Christel Genoud and Alexandra Graff-Meyer for the assistance with negative stain EM. Alex was a very patient teacher and I am grateful for all the hours she spent with me on sample optimization and collection.

I would also like to thank Elida Keller and Piera Cicchetti for answering every question and for their advice. Their friendly and open nature is a great help to Ph.D. student life at the FMI.

Many thanks go to Böhringer-Ingelheim Fonds (BIF) who financially supported a large part of my Ph.D. and traveling to a conference in Mexico. I am grateful to be part of this amazing network and it has always been very stimulating to attend their seminars.

Last but not least, I would like to thank my family and friends for their continuous support. I would like to thank Peter and Jan for playing Squash with me - it has always been good fun. I am also grateful to Lucia, Sofia, and Hanna for keeping my thoughts off the lab from afar. I am deeply grateful to Susanne and David for their constant support, for refreshing discussions and for comments on my thesis. I am also profoundly thankful to my parents for all the encouragement and for grounding me. Finally, special recognition goes to Andrew, who always listens to me, cares for me, and believes in me.

Appendix

Published Manuscript (pages 132-160)

Mattarocci, S.*, Reinert, J.K.*, Bunker, R.D.*, Fontana, G.A.*, Shi, T., Klein, D., Cavadini, S., Faty, M., Shyian, M., Hafner, L., Shore D., Thomä N.H., Rass U. (2017). **Rif1 maintains telomeres and mediates DNA repair by encasing DNA ends.** Nat Struct Mol Biol *24*, 588-595. *equal contribution